AD-E476 450

LEVEL III

AD B.S.

CONTRACT REPORT ARBRL-CR-00427

THE ROLE OF OXYGEN IN GUN BARREL EROSION AND CRACKING

A Shock Tube Gun Investigation

Prepared by

Calspan Corporation
P. O. Box 400
Buffalo, NY 14225

April 1980

US ARMY ARMAMENT RESEARCH AND DEVELOPMENT COMMAND
BALLISTIC RESEARCH LABORATORY
ABERDEEN PROVING GROUND, MARYLAND

DTIC
ELECTED
JUN 20 1980
S
D
D

80 6 6 019

REPORT DOCUMENTATION PAGE	READ INSTRUCTIONS BEFORE COMPLETING FORM
1. REPORT NUMBER 2. GOVT ACCESSION NO. 3. RECIPIENT'S CATALOG NUMBER CONTRACT REPORT ARBRL-CR- 00427	
4. TITLE (and Subtitle) THE ROLE OF OXYGEN IN GUN BARREL EROSION AND CRACKING A Shock Tube Gun Investigation	5. TYPE OF REPORT & PERIOD COVERED Final Report-21 June 1978 7 November 1978 6. PERFORMING ORG. REPORT NUMBER 6343-D-1
7. AUTHOR(s) E.B. Fisher C.C. Morphy	8. CONTRACT OR GRANT NUMBER(s) DAAK11-78-C-0070
9. PERFORMING ORGANIZATION NAME AND ADDRESS Calspan Corporation P.O. Box 400 Buffalo, NY 14225	10. PROGRAM ELEMENT, PROJECT, TASK AREA & WORK UNIT NUMBERS
11. CONTROLLING OFFICE NAME AND ADDRESS ARRADCOM, Procurement Directorate Chemical/Ballistic Procurement Division Aberdeen Proving Ground, MD 21005	12. REPORT DATE April 1980 13. NUMBER OF PAGES 91
14. MONITORING AGENCY NAME & ADDRESS(if different from Controlling Office) US Army Armament Research & Development Command US Army Ballistic Research Laboratory ATTN: DRDAR-BL Aberdeen Proving Ground, MD 21005	15. SECURITY CLASS. (of this report) UNCLASSIFIED 15a. DECLASSIFICATION/DOWNGRADING SCHEDULE

16. DISTRIBUTION STATEMENT (of this Report)

Approved for public release, Distribution unlimited.

17. DISTRIBUTION STATEMENT (of the abstract entered in Block 20, if different from Report)

18. SUPPLEMENTARY NOTES

19. KEY WORDS (Continue on reverse side if necessary and identify by block number)

Wear	Heat Transfer
Erosion	Gun Barrel
Shock Tube Gun	Oxidation

20. ABSTRACT (Continue on reverse side if necessary and identify by block number)

The subject program is part of an on-going effort to determine the individual contributors to gun barrel erosion. The chemical contribution in an oxidizing atmosphere was the main topic for investigation during this program. Experiments were conducted in the Shock Tube Gun (STG), a ballistic compressor, designed and developed by Calspan Corporation. This facility can compress mixtures of pure gases and can generate flow conditions and cycle times similar to those experienced in large caliber guns.

(cont'd)

DD FORM 1473 1 JAN 73 EDITION OF 1 NOV 65 IS OBSOLETE

(cont'd)

    Tests were conducted with a mixture of argon and nitrogen to define the threshold of melting erosion for an inert baseline. Small concentrations of oxygen were substituted for nitrogen in the mix to quantify the oxidation effect. Subsequently, tests were conducted with various gas mixtures containing carbon dioxide, which dissociates to produce oxygen when compressed to high temperatures.

    The basic oxidation effect was observed to be a nearly linear increase in erosion with oxygen concentration. A corresponding shift in the erosion threshold to less severe convective heating conditions was observed in response to surface chemistry. A similar effect was observed for carbon dioxide mixture where erosion was correlated in terms of the equilibrium concentration of oxygen at peak pressure. Surface cracking was observed and found to be most severe near the erosion threshold where the oxide layer was thickest. A white layer was observed in tests with oxygen in the absence of carbon dioxide.

Accession For		
NTIS GRA&I		☒
DDC TAB		☐
Unannounced		☐
Justification		
By		
Distribution/		
Availability Codes		
Dist.	Avail and/or special	
A		

TABLE OF CONTENTS

LIST OF FIGURES

LIST OF FIGURES (cont.)

LIST OF TABLES

I. INTRODUCTION

In combustion testing, it has been difficult to evaluate the mechanisms of erosion because of an inability to separate the effects of pure forced convective heating of the bore from combined thermochemical effects. Use of propellants containing carbon and oxygen as a means of providing bore surface heating and erosion is clearly in conflict with the desire for separation of effects, but has until now been the only means by which heating conditions of sufficient magnitude could be produced. With the introduction of the Shock Tube Gun (STG), described in this report, Calspan has provided a tool which overcomes the limitations of the combustion approach to erosion testing, and can permit examination of the thermochemical nature of erosion in the near melting range.

Prior research[1] developed the measurement techniques, for use with the STG, which permit accurate determination of material loss and heating. Concurrent formulation of a computer code which translated ballistic and gross heating data into bore surface temperature histories and melting rates, predicted the heating conditions required to produce pure melting of steel in the STG. Testing corroborated the melting predictions of the code and thus, the primary objective of the previous study was achieved. However, computer, STG test analysis, and 60mm firing tests[2] conducted at Calspan have indicated that significant erosion and cracking may be caused by chemical reactions in propellants. This report describes the results of ongoing research to identify and quantify the thermochemically induced erosion and cracking in gun barrels.

The primary objective of this study was to quantify the erosion of a typical gun steel, SAE 4340, in a gun-like environment using gas mixtures that varied in their _oxidizing_ potential. Therefore, the amount of material loss for given test gas conditions was a primary measurement of causality in the role that oxygen plays in gun barrel erosion and cracking. This primary objective has been largely achieved.

A secondary objective was to develop the capability of predicting erosion in terms of measurable test quantities. A predictive computer code was developed which simulates the thermodynamic mechanism and governing relationships in the Shock Tube Gun during a test. Ultimately, this code will provide, in correlation with empirical findings of the STG, a model of propellant erosivity and the ability to minimize erosion features in future propellant formulations. Presently, this portion of the study requires refinement and remains an area for further research.

1.   F.A. Vassallo, W.R. Brown, "Shock Tube Gun Melting Erosion Study," USA Ballistic Research Laboratory, ARRADCOM, Contract Report ARBRL-CR-00406, January 1979. (AD#A076219)

2.   F.A. Vassallo, "Study of Wear and Erosion in the 60mm MC-AAAC Gun," Calspan Monthly Reports to ARRADCOM, Nos. 1 through 12, to 1 October 1978.

II. SHOCK TUBE GUN FACILITY

2.1 STG Concept

Calspan has developed a unique variable gun system, the operation of which is based upon shock tube principles (Shock Tube Gun). In contrast to measuring erosion that results from firing a vast number of combustion rounds, the facility is designed to be used as a developmental tool for propellant formulation changes and to assure an approach to optimal propellant-tube interfaces. In achieving this goal, tests in the Shock Tube Gun are supported by special erosion and thermal sensors, metallurgical analysis, and ballistic measurements. Briefly, the STG generates a high pressure, high-temperature test gas by an adiabatic compression process. As shown in Figure 1, the facility consists of a driver chamber, driven tube, a flying piston, a gas collection chamber and an instrumented gun tube containing a projectile. Compression of the test gas (the counterpart to the propellant gas in an actual gun) within the driven tube is accomplished by motion of the flying piston contained within this tube. Motion of the piston is the result of force applied by the pressure of the driver gas. As the piston approaches the collection chamber, the test gas pressure and temperature rapidly increase in a time history representative of actual gun firings. A projectile contained at the start of the gun tube is acted upon by this collected gas. Suitable means are provided in the facility to allow regulation of shot start pressure on the projectile. Once released, the projectile is accelerated along the tube in a ballistic cycle dependent upon selected input factors. Data regarding pressure, velocity, heating, and erosion are collected through measurements in the instrumented test barrel.

With suitable variation in parameters, factors affecting erosion such as pressure history, propellant gas velocity, gas temperature, gas composition, tube composition, and propellant additives may be investigated. The compression ratio, driven gas composition and its initial conditions essentially govern the peak temperature and pressure; piston motion, influenced by its mass, and projectile movement effectively govern the pressure pulse duration. Variation of piston mass, initial conditions, and compression ratio then permit independent change in peak temperature and pressure as well as time. Obviously, effects due to variation of driven gas composition may be tested under controlled interior ballistic conditions. This is a most powerful experimental mode of operation of the facility, and the principal mode used in this study.

2.2 Design and Construction

The Shock Tube Gun is designed to adequately represent predicted ballistic conditions within guns as large as the eight-inch howitzer, requiring peak test chamber pressures up to 300 MPa and projectile velocities up to 800 m/sec. Table 1 lists the present structural makeup of the Shock Tube Gun. These values were established through the use of a preliminary
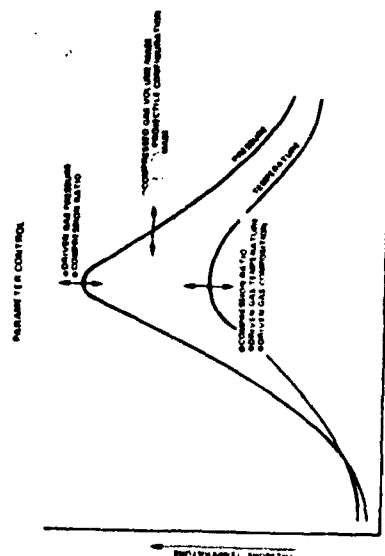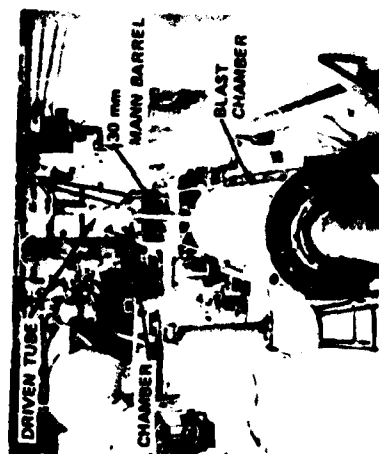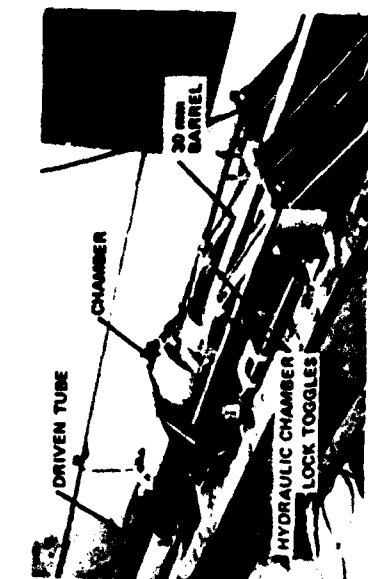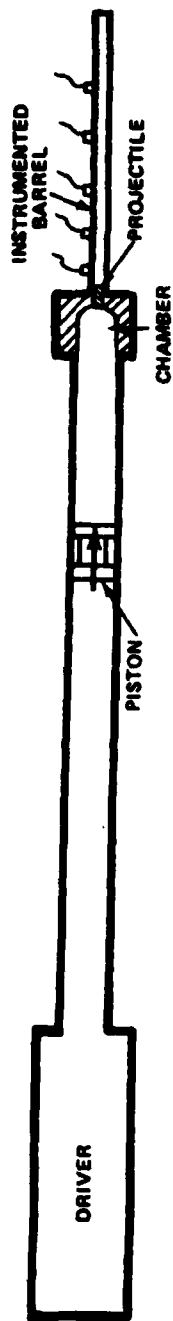
Figure 1 SHOCK TUBE GUN

11

mathematical model of piston action based upon adiabatic compression. Through exercise of the model, approximate size requirements were established with final selection of sizes dictated by available engineering materials. The photographs of Figure 1 illustrate the resulting Shock Tube Gun assembly as well as its individual components. As shown, the projectile launch components consist of the driven tube, chamber and 30mm smooth bore barrel. These are supported on a carriage which is free to move on tracks in the direction of piston motion, during the extreme impulse loads imposed by the unbalanced chamber pressure during test gas compression. This maintains the integrity of the supporting base structure. The floating mount system requires use of a pneumatic brake on the driven tube for safety.

The projectile capture components consist of a telescoping tube coupled to the barrel, a blast chamber, and a sand filled tube to decelerate the projectile (impact zone). The blast chamber, the purpose of which is to reduce the noise and pressure levels at projectile exit of the tube, also contains an internal provision for measurement of projectile velocity using velocity screens. The telescoping tube allows motion of the carriage independent of the blast chamber.

Also shown in Figure 1 are views of the chamber and toggle restraint system needed to contain the high chamber pressures and associated axial loads. Chamber pressures are sensed using piezoelectric pressure transducers. The entrance region of the launch tube can accommodate pressure, heat flux, and erosion sensing devices. The launch tube itself is a 30mm smooth bore barrel, 4.57 meters long.

Another essential component of the facility is the brake area at the upstream end of the driven tube. This brake limits the maximum permissible axial load on the driven tube during the rapid piston deceleration period. Without it, loads could exceed the axial strength capability of the tube. In essence, load is limited by slippage in the brake at a preselected load below the failure strength of the tube. The brake is air actuated and thus may be adjusted according to the amount of slippage desired up to the strength limit of the tube. The brake is presently used at only about one-half capacity without excessive slippage. Hence, much greater maximum chamber pressures than presently produced can be accommodated.

The piston which is used to compress test gas in the driven tube is made from 4340 steel and weighs 68 kg. inc` `ing the release catch at its rear end. Gas seal is obtained using "T" rings at the front and rear of the piston. Three brass wear rings are used to prevent metal-to-metal contact between piston and tube. A buffer projection on the face of the piston and a complementary close-fitting port at the end of the driven tube entering the chamber preclude direct impact of the piston with the end of the driven tube in the event that driven gas is exhausted too rapidly, as by a failure in the chamber. The buffer projection is necessitated by the presence of the chamber volume at the end of the driven tube which can permit piston contact at the driven

12

tube end with insufficient chamber pressure development. Metal-to-metal impact, if allowed to take place, could cause damage to the piston and/or tube face. The buffer prevents this occurrence.

For any particular combination of driven (test) gases and desired ballistic result, Shock Tube Gun settings, namely: driver pressure, piston and projectile weights, and driven gas initial pressure are determined using a computer code which models the dynamic conditions within the gun. The computer code was validated in early developmental testing of the STG whereby piston position, chamber pressure, and projectile velocity were measured and compared with those predicted. Using the computer code, STG input factors can be chosen to result in preselected test conditions of pressure, temperature, gas velocity and gas activity at the entrance of the launch tube. These represent parameters which are important in tube heating and erosion.

Table 1.   Shock Tube Gun Characteristics

Configuration Data:

Driven Tube I.D.	0.191m	(7.5 in.)
Driven Tube Length	24.6m	(970 in.)
Piston Area	$0.0285m^2$	(44.179 sq. in.)
Piston Mass	Up to 91 kg.	(200 lb.)
Projectile Diameter	30mm	(1.181 in.)
Projectile Area	$706mm^2$	(1.095 sq. in.)
Projectile Mass	Up to .91 kg	(2 lb.)
Driver Volume	$0.885m^3$	(54,000 cu. in.)
Chamber Volume	$2140mm^3$	(130.8 cu. in.)
Pressure - at release of projectile	Variable	
Tube Length	4.57m	(180 in.)

13

III. TEST PREPARATIONS

3.1 Specimen Selection and Installation

The chief objective of this work is to determine propellant gas conditions which lead to possible oxidation and/or cracking of the bore surface, resulting in material loss and fatigue. To do this effectively, test bore specimens amenable to analysis had to be uniform in shape and composition, to eliminate these variables in the testing, and representative of a conventional gun steel. 4340 steel, which has been increasingly used in gun barrel applications since the early 1950's, was chosen as the test bore material. The physical properties of 4340 steel are listed in Table 2 . Tests conducted with 4340 in the previous program[1] failed to create a melting condition. Therefore, the test sample was altered by decreasing its bore diameter from 20mm to 12.7mm (0.5 inches). This flow channel reduction creates a sonic flow condition which elevates the surface heat flux. The test sample design is shown in Figure 2. Also shown in the figure are the ports for in-wall thermocouples which are used to determine the integrated heat input.

The erosion test section within the chamber of the Shock Tube Gun is as shown in Figure 3. Each test specimen is fabricated in the form of a cylindrical nozzle and placed downstream from the entrance throat. The outer diameter of the specimens was selected to be 31.75mm and each was 38.1mm long. Samples of this size fit on the specimen stage of Calspan's Etec Autoscan Scanning Electron Microscope (SEM) such that "before and after" examination of the bore surface can be conducted without recourse to replicas.

Each test specimen was characterized with regard to mass and bore diameter before testing. Specimens were weighed using an analytical balance so that mass changes of a fraction of a milligram could be readily determined. The bore diameter was measured to within 10^{-4}mm at four specific axial locations as measured from the leading edge of the sample: 6.35, 18.4, 27.3, 37.8mm (0.25, 0.725, 1.075, 1.49 inches).

3.2 Heat Transfer Instrumentation

A primary measurement of the study is the amount of bore heating associated with each test. For this measurement, in-depth thermocouples were installed in selected samples. These in-depth thermocouples were placed at distances approximately 0.5mm from the bore surface. The method of installation is as shown in Figure 4. Each of these thermocouples independently may be used to determine net heating to the bore. Total heat input is calculated from the in-wall thermocouples output by use of methods developed and

14
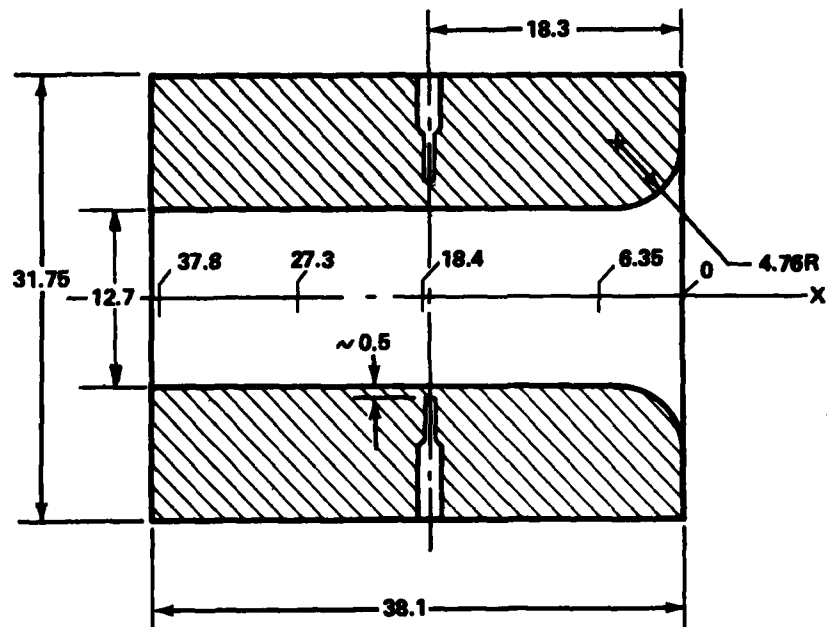
Figure 2 SHOCK TUBE GUN TEST SAMPLE

15
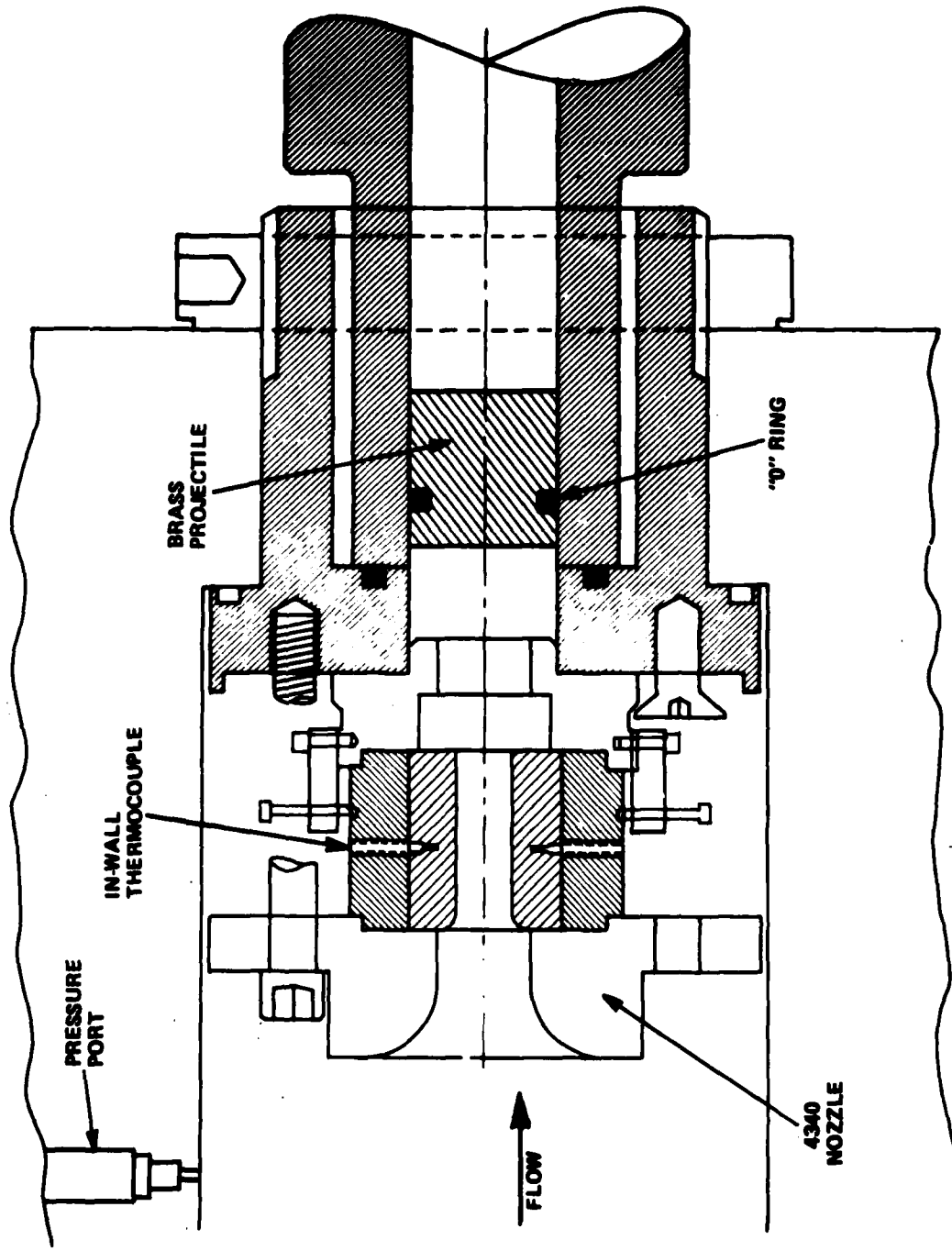
Figure 3 SHOCK TUBE GUN TEST SECTION

BRASS PROJECTILE

"O" RING

IN-WALL THERMOCOUPLE

PRESSURE PORT

4340 NOZZLE

FLOW

16

SILICONE GREASE

STAINLESS SHEATH

MgO INSULATION

THERMOCOUPLE WIRES (40 GAGE) CHROMEL-ALUMEL

1.041 DIA.

0.5

10-32 SCREW

SPRING LOAD

SPECIMEN HOUSING

TEST SPECIMEN

BORE SURFACE
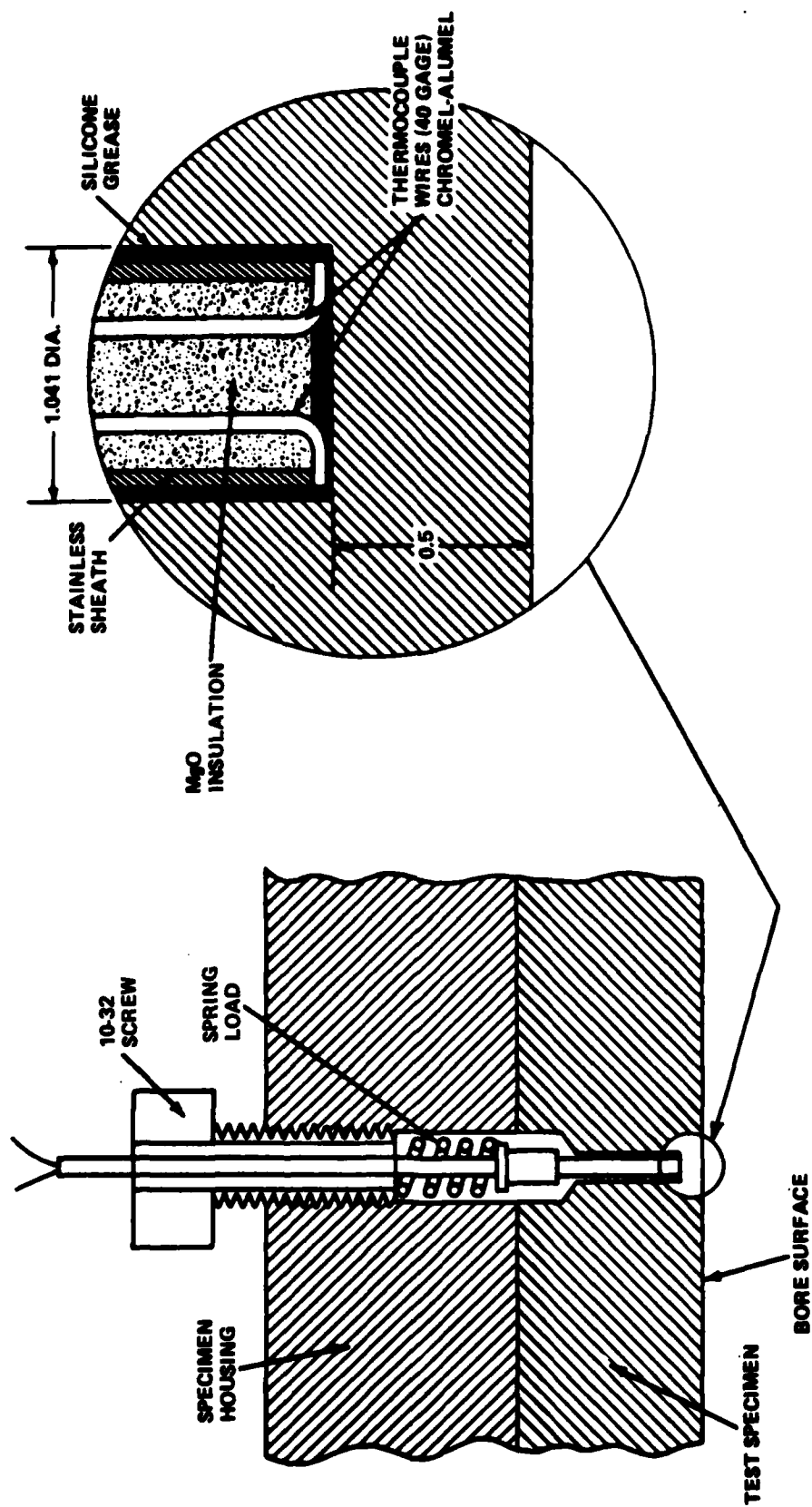
Figure 4 IN-WALL THERMOCOUPLE INSTALLATION

17

reported by Calspan.[3] Briefly, conversion of in-wall thermocouple outputs (millivolts vs. time) to total net heat input per unit area is made by use of the relation

$$Q(t) = \Delta T(t) \sqrt{\pi k c_\rho t} \tag{1}$$

where Q(t) is the net bore heat input

$\Delta T(t)$ is the indicated change in in-wall temperature as a function of time

k is the thermal conductivity

c_ρ is the heat capacity per unit volume

t is the time after start of heating.

Data reduction procedure is simply to apply Equation (1) at successive time intervals (e.g., 0.05, 0.1, 0.15 sec, etc.) resulting in a plot of Q(t) vs. t. The curve thus produced will be asymptotic to the desired heat input.

3.3 Selection of Test Conditions

The program objective was to experimentally characterize the role of oxidation in gun barrel erosion. Oxidation reactions in guns are produced by carbon dioxide and water vapor. These reactions are suppressed by the presence of carbon monoxide. It is believed that the neutral point occurs when the ratio CO/CO_2 equals 3.[4] The combustion products of energetic double and triple-base propellant fall into the oxidation regime according to this criterion.

A preliminary test matrix was devised to examine oxidation effects on 4340 barrel steel, the primary material used in the manufacture of gun barrels. The combination of test configuration and gas conditions required to achieve the melting threshold for 4340 steel was to be established during the initial test series. This threshold condition was not achieved previously and a test configuration with increased heating, namely the aforementioned reduction in flow passage diameter, was instituted. A requirement for these and subsequent tests was obtaining gas pressures and temperatures of the magnitude generally obtained in large caliber weapons. A fundamental property of the test gas mixture which governs the pressure/temperatures produced in the shock tube compression process is its ratio of specific heats, γ_m. The previous study concluded that the optimum γ_m for the facility was 1.53. Therefore the initial "inert" tests were conducted with a 45.5% nitrogen

3. F.A. Vassallo, "Mathematical Models and Computer Routines Used in Evaluation of Caseless Ammunition Heat Transfer," Calspan Report No. GM-2948-Z-1, June 1971.

4. ASM Committee on Furnace Atmospheres, "Furnace Atmosphere and Carbon Control," ASM 1964, pg. 2.

18

54.4% argon mix yielding a 1.5 specific heat ratio, and the reactive gas mixture tests that followed were designed to be within similar proximity of the optimum γ_m value.

The second test series was intended to quantify the contribution of oxidation by varying the oxygen concentration at the 4340 melting threshold gas conditions and by varying gas conditions with a constant oxygen concentration. These tests were designed to determine erosion augmentation as a function of oxygen concentration, determine whether or not melting is a prior condition for increased erosivity, and determine the effective heat addition from oxidation. The basic philosophy behind these tests was to make only small changes in a basic gas mixture. In this way, test conditions would be nearly constant so that the true oxidation influence would be readily apparent. Furthermore, small increments in oxygen made it possible to generate the empirical results that are useful in guns while large concentrations create spectacular but less useful results.

A third series replaced oxygen with carbon dioxide. These tests were designed to explore oxidation as it actually occurs in guns. Dissociated carbon dioxide is believed to provide a major source of oxygen for reaction with barrel steel during the ballistic cycle. Therefore, carbon dioxide was introduced into the test gas in the amount normally present in propellant gas. Gas temperatures were varied over the range experienced by various propellants of interest. The object of these experiments was to determine whether or not an atmosphere rich in carbon dioxide would enhance barrel erosion above the level attributed to pure melting, and to quantify the erosion in terms of an equivalent amount of oxygen for a given concentration of carbon dioxide, test conditions and test material. This is the first step in relating chemical erosion in a gun to laboratory conditions.

Future research could make use of gas mixtures containing both carbon dioxide and carbon monoxide to more closely investigate the neutral point region, i.e., CO/CO_2 ~3, where oxidation may give way to other erosive thermochemical reactions.[2] A study of CO/CO_2 ratios in excess of the neutral point logically extends into a subsequent program dealing with carburization.

Table 2 .   Physical Properties of 4340 Steel

Density (ρ)	7850 kg/m^3	(490 lbm/ft^3)
Specific Heat (c)	181 J/kg-°K	(0.14 Btu/lbm-°R)
Thermal Conductivity (k)	10.47 J/m-sec-°K	(19.6 Btu/ft-hr-°R)
Solidus/Liquidus	1720/1770 °K	(2640/2720 °F)
Latent Heat	232,600 J/kg	(100 Btu/lbm)

19

IV.   TEST PROCEDURE AND RESULTS

4.1   Test Procedures

Collection of test data regarding ballistics, heating, and erosion followed a set procedure. First, all important components of the facility were inspected for attrition due to the previous firing. Expendable items such as "O" rings and other seals were replaced. The driven tube, chamber, and piston were carefully cleaned to avoid the presence of contaminants. The piston was then fixed in position at the upstream end of the driven tube. The projectile was inserted into the barrel.

Specimens were characterized prior to testing using an analytical balance for initial mass, and then installed within the chamber. M-11 pressure gauges were also installed in the chamber for a redundant measure of pressure. All required instrumentation including pressure transducers, thermocouples and velocity screens were connected to suitable recording devices: the piezoelectric pressure output was recorded on a Bell and Howell tape recorder at a speed of .76 meters per second (30 inches per second) to minimize tape flutter and pulse response rise time; thermocouple output was recorded directly on a CEC oscillograph at a paper speed of 5 inches per second; the projectile transit time between velocity screens was recorded by use of a Tektronix oscilloscope for 1 millisecond per division. The Tektronix scope was also used to record the pressure signal playback from the tape which was performed at a tape speed of .76 meters per second, the same speed used for recording. Matching the playback and recording speeds eliminated hysteretic pulsing of the tape heads.

After installation of the projectile and specimens, the entire driver tube including the chamber was evacuated to a pressure level of less than 2.0 millimeters of mercury. The chamber was then purged by filling with pure argon. It was again evacuated and filled to the required partial pressures with the gases selected for the test mix. These partial pressures are dependent upon the mix ratio desired.

Equations for establishing partial pressure settings were derived from the Dalton model of ideal gas mixtures, which assumes the following:

1.   The moles of mixture, n, equals the sum of the moles of the component gases, $n_A + n_N + n_O$, where A, N and O are subscripts referring to argon, nitrogen and oxygen, respectively.

2.   Each component gas in the mixture occupies the entire mixture volume, V, which in this case is the volume of the driven tube.

20

3. The temperature, T, of the components before and after mixing remains constant.

4. The mixture pressure, P, in this case, 1 atmosphere, is reasonably low, to assure near ideal gas behavior.

For the components: $P_A V = n_A \bar{R} T$.

$$P_N V = n_N \bar{R} T$$

$$P_O V = n_O \bar{R} T$$

For the mixture: $PV = n\bar{R}T$

Since $V/\bar{R}T$ is a constant in all the equations:

$$\frac{P_A}{n_A} = \frac{P_N}{n_N} = \frac{P_O}{n_O} = \frac{P}{n}$$

Rewriting:

$$\frac{P_A}{P} = \frac{n_A}{n}$$

$$\frac{P_N}{P} = \frac{n_N}{n}$$

$$\frac{P_O}{P} = \frac{n_O}{n}$$

That is, for each component of a mixture of ideal gases, the mole fraction and the ratio of the partial pressure to the total pressure are equal.

Following these test preparations, the driver tube was pressurized to the desired level, recording devices were activated and the piston was released.

After exhausting residual driver pressure, specimens were removed and hard copy was made of the test data. Specimens were inspected, weighed and measured diametrally at the aforementioned axial locations. Photographs were taken of a sample when deemed appropriate.

21

4.2   Text Matrix

A total of 31 tests were conducted during this program. A summary of the test conditions, the weight loss, the recession measurements along the length of the test sample are given in Table 3. The initial driver pressure required to achieve the test conditions, the peak pressure, projectile velocity that was obtained during the test and bulk heating, as measured by the in-wall thermocouples, are presented in Table 4.

The test matrix was divided into essentially eight areas. The first area involves establishing a baseline with inert tests. The test gas composition for these tests was 45 1/2 percent nitrogen and 54 1/2 percent argon. This mixture, when compressed to a pressure of 275 MPa, generated a test gas temperature in the vicinity of 3700°K. This gas temperature is quite similar to that of a hot double-base propellant such as M8. After establishment of the inert baseline conditions, three series of tests were conducted with small concentrations of oxygen to define the effects of oxidation in erosion of barrel steel. During these tests, the concentrations of oxygen were maintained at a low level to minimize the impact of gas mixture variation on gas temperature and pressure. With this approach, the effects that were observed during these tests, when compared to the inert baseline, were due to solely the oxygen content rather than changes in test conditions. This permitted direct assessment of the impact of oxidation. Gas mixtures with oxygen levels of 1, 2.5 and 5 percent of the total mixture were incorporated during this phase of the test program.

Following oxygen tests, carbon dioxide was used as a gas constituent in place of oxygen, once at 5 percent concentration and the remaining nine runs at 10 percent. Variations of the fraction of argon and nitrogen were made to achieve a variety of test gas temperatures, pressures, and equilibrium gas constituents. The dissociation of carbon dioxide creates free oxygen at the higher gas temperatures, which can promote oxidation-type reactions. The amount of oxygen available at peak conditions from dissociation of carbon dioxide is used as a means to interpret the erosion due to carbon dioxide in terms of the oxygen content of the previous runs where oxygen was introduced as a primary constituent.

Finally, two short series of tests were conducted whereby concentrations of 5 and 10 percent hydrogen were introduced with 10 percent carbon dioxide. This created a gas condition more nearly like that in propellant gases, and provided metallographic data for comparison of the "cracking" potential of CO_2-H_2 and straight CO_2 gas mixtures.

Adiabatic compression of the test gas is the mechanism by which the temperature and pressure profile is generated. The test gas composition alters the relationship between the gas temperature and pressure for a given compression ratio. This relationship is shown in Figure 5 for all of the gas compositions used during this series of tests. The individual points for the runs are shown on Figure 6, as well as the previous figure, so that the level of temperature and pressure is indicated as well as the potential latitude that can be achieved in the Shock Tube Gun.

22

TABLE 3. OXIDATION TEST RESULTS -- SPECIMEN CHARACTERISTICS

Test No.	Specimen No.	Active Gas** Constituent (%)	Peak Gas Pressure (MPa)	Peak Gas Temperature (°K)	Mass Loss* (mg)	Diametral Recession*				Martensite Thickness (mm)
						A (mm)	B (mm)	C (mm)	D (mm)	
31	1	Inert — 45.5 N_2	295	3717	---	---	---	---	---	---
32	1	Inert — 45.5 N_2	281	3666	52	.076	.008	.000	.005	.099
33	2	5 O_2 — 40.5 N_2	283	3516	714	.071	.084	.064	.058	.093
34	3	2.5 O_2 — 43 N_2	174	3112	(1)	(.008)	(.010)	(.013)	(.013)	---
35	4	2.5 O_2 — 43 N_2	95	2625	---	---	---	---	---	---
36	4	2.5 O_2 — 43 N_2	103	2681	---	---	---	---	---	---
37	4	2.5 O_2 — 43 N_2	108	2723	1	.003	.000	(.005)	(.008)	---
38	5	2.5 O_2 — 43 N_2	280	3555	309	.094	.046	.041	.020	.096
39	5	1 O_2 — 44.5 N_2	293	3648	306	.074	.048	.036	.015	.100
40	6	2.5 O_2 — 43 N_2	232	3372	100	.018	(.013)	(.013)	(.003)	.073
41	7	2.5 O_2 — 43 N_2	200	3237	15	(.010)	(.013)	(.015)	(.008)	.094
42	8	1.2 O_2 — 44.3 N_2	277	3584	165	.030	.020	.003	(.008)	---
43	9	5 O_2 — 40.5 N_2	267	3460	672	.097	.089	.086	.061	---
44	10	1 O_2 — 44.5 N_2	285	3617	188	.056	.124	.015	(.020)	.101
45	11	2.5 O_2 — 43 N_2	254	3465	241	.066	.023	.015	.013	.091
46	12	Inert — 44.5 N_2	194	3285	(3)	(.008)	(.008)	(.003)	(.008)	.075
47	13	5 CO_2 — 40.5 N_2	317	3326	2	(.010)	(.008)	(.018)	(.005)	.076
48	14	5 CO_2 — 35.5 N_2	306	3055	7	(.005)	.000	.000	(.008)	.080
49	16	10 CO_2 — 20 He	217	3756	164	.053	.013	.010	.015	.108
50	15	10 CO_2 — N_2	270	3947	416	.094	.061	.043	.018	.095
51	17	10 CO_2 — 5 N_2	285	3817	453	.132	.079	.053	.030	.096
52	18	10 CO_2 — 20 N_2	302	3422	155	.053	.030	.015	.005	.095
53	19	10 CO_2 — 10 N_2	257	3568	291	.099	.033	.010	.000	.094
54	20	10 CO_2 — 22 N_2	308	3373	153	.058	.028	.050	(.003)	.092
55	21	10 CO_2 — 30 N_2	330	3239	68	(.005)	.003	.013	.003	.086
56	22	10 CO_2 — 50 N_2	276	2692	5	(.008)	(.010)	.000	.003	.064
57	23	10 CO_2-10 H_2- 10 N_2	246	2450	13	.003	(.008)	(.003)	.000	.083
58	24	10 CO_2-10 H_2- 5 N_2	223	2487	4	---	---	---	---	.089
59	25	10 CO_2-10 H_2	179	2427	3	(.010)	(.005)	(.025)	(.025)	.079
60	26	10 CO_2- 5 H_2	210	3316	2	.000	(.005)	.000	(.018)	.088
61	27	Inert — 45.5 N_2	272	3611	169	.030	.023	.010	.005	.095
62	28	10 CO_2- 5 H_2- 10 N_2	223	3056	0	(.010)	(.005)	(.005)	(.010)	.072

* Parenthesis indicates weight gain, or material buildup.
** The remaining percentage of the mixture is argon.

23

TABLE 4. HEATING/BALLISTIC TEST RESULTS - SHOCK TUBE GUN

Test No.	Y	Driver Pressure MPa	Driver Pressure psi	Chamber Pressure MPa	Chamber Pressure psi	Projectile Velocity m/sec	Projectile Velocity ft/sec	Heat Input J/mm²	Heat Input Btu/ft²
31	1.49	4.48	650	295	42800	625	2050	---	---
32				281	40800	685	2250	.96	85
33				283	41100	---	---	.97	86
34		→	→	174	25200	520	1700	---	---
35		2.69	390	95	13800	---	---	.82	73
36		2.90	420	103	14900	520	1700		
37		4.48	650	108	15700	---	---		
38		→	→	280	40600	580	1900	1.07	95
39				293	42500	550	1800	.99	88
40		4.14	600	232	33600	---	---	1.03	92
41		3.79	550	200	29000	---	---	1.09	96
42		4.48	650	277	40200	365	1200	.96	85
43		→	→	267	38700	520	1700	1.19	105
44				285	41300	550	1800	---	---
45				254	37000	520	1700	1.06	94
46		3.79	550	194	28100	260	850	1.04	92
47	1.48	4.48	650	317	45900	---	---	1.01	89
48	1.47	4.41	640	306	44400	580	1900	.99	87
49	1.63	4.55	660	217	31500	335	1100	1.17	103
50	1.59	4.93	715	270	39100	---	---	1.14	100
51	1.57	→	→	285	41300	305	1000	1.07	94
52	1.51	4.58	665	302	43800	520	1700	1.19	105
53	1.55	→	→	257	37200	335	1100	---	---
54	1.51			308	44700	425	1400	.91	80
55	1.51			330	47900	625	2050	---	---
56	1.49	4.21	610	276	40000	440	1450	.89	78
57	1.44	→	→	246	35600	730	2400	1.02	90
58				223	32300	760	2500	.99	88
59	1.45	→	→	179	25900	655	2150	.96	85
60	1.48	4.34	630	210	30400	185	600	1.04	92
61	1.49	4.48	650	272	39400	---	---	1.01	98
62	1.46	4.21	610	223	32300	---	---	1.06	93

NOTE: Dashed lines indicate lost data due to instrumentation malfunction.

Figure 5 ISENTROPES FOR TEST GAS MIXTURES UNDERGOING ADIABATIC COMPRESSION

25
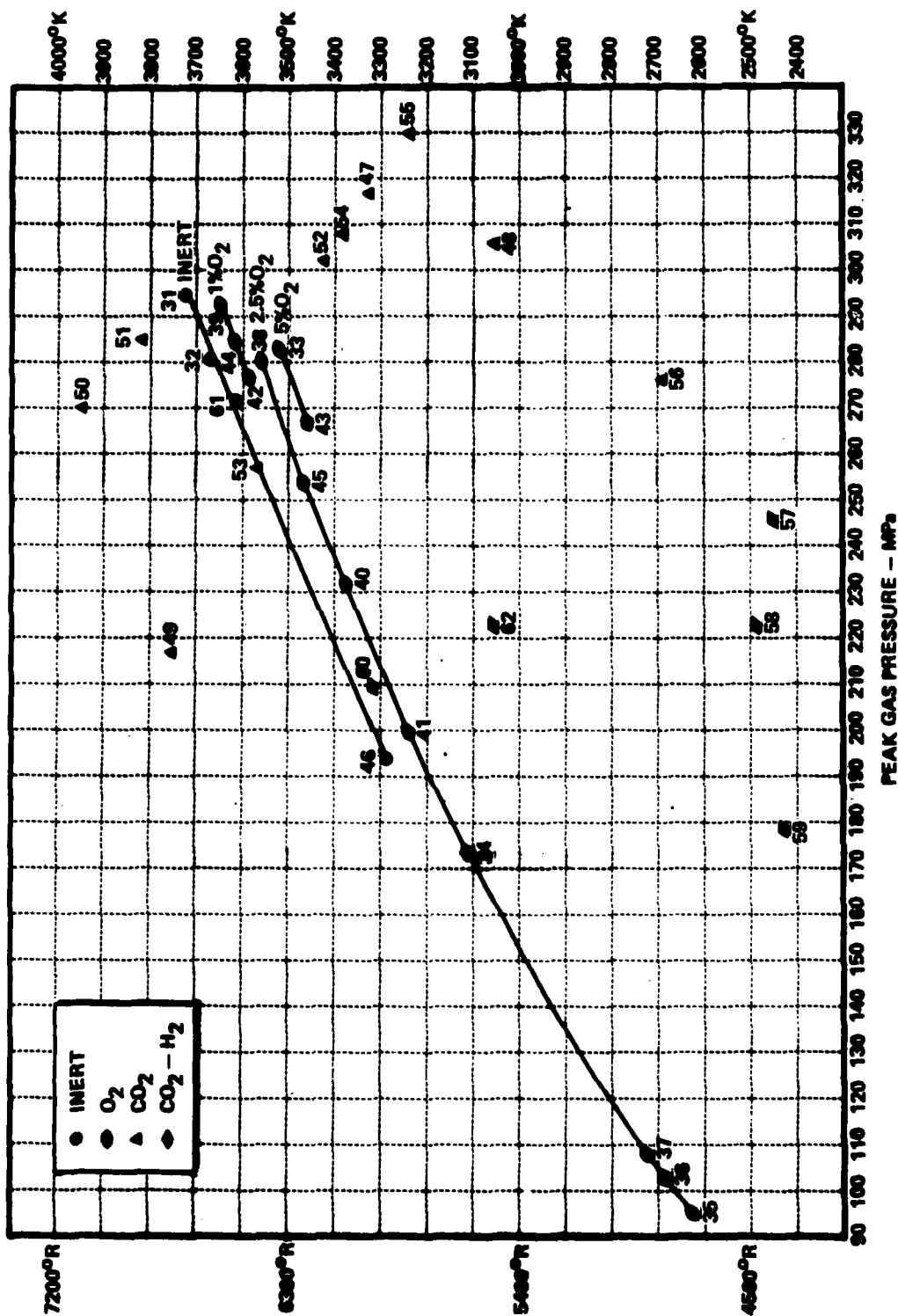
Figure 6 PEAK TEST GAS PRESSURE VS PEAK TEST GAS TEMPERATURE

26

Test conditions along the isentrope were computed by an equilibrium combustion program. Appendix II contains a brief description of the code and a sample printout. This program was also used to determine the equilibrium composition of the gas mixture. In this way, with a specified gas mixture and measured pressure, the temperature and gas constituents generated as a result of the dissociation and chemical reactions were determined for the compression cycle.

The equilibrium-gas-mixture mole fractions of the most significant constituents are shown in Table 5. Table 5 lists the active constituents by mole fraction of each test gas mixture, both at ambient, pre-test conditions and at the "equilibrium," maximum pressure and temperature test conditions. Nitrogen, though classified as "inert" when not in the presence of oxygen or carbon dioxide, has been included in the Table to illustrate its potential for forming oxides, acids, and cyanides with active mixture components during a test. These nitrogen compounds, all gaseous byproducts, contribute little to direct barrel wear and erosion. The significant role they do play is in limiting the oxidizing potential of the truly reactive components in the mixture. Argon has been excluded from the table since it truly is "inert." However, since the mole fraction of Argon was not constant for all tests, the mole fractions of the remaining constituents have not been normalized to equal one. This practice would be misleading, particularly in the CO_2 tests where the total mole fraction of active constituents was, for the majority of runs, lower than in the oxygen tests. In particular, the mole fraction of oxygen molecules is given on this table. It is significant that during tests with CO_2 and nitrogen as the main reacting gas species, significant oxygen was developed. However, with the addition of hydrogen into the mixture, oxygen was consumed by formation of water and the amount of free oxygen available in the stream at peak conditions was reduced substantially. This has a significant impact on the overall results of this program which will be discussed in Section V.

27

TABLE 5.   TEST GAS MIXTURE COMPOSITION

Test No.	Ambient Gas Mixture mole fraction				"Equilibrium" Gas Mixture mole fraction					
	CO_2	H_2	N_2	O_2	CO	CO_2	H_2	H_2O	N_2	O_2
31	---	---	.455	---	---	---	---	---	.455	---
32	---	---	.455	---	---	---	---	---	.455	---
33	---	---	.405	.05	---	---	---	---	.3922	.0364
34	---	---	.43	.025	---	---	---	---	.4237	.0186
35	---	---	.43	.025	---	---	---	---	.4265	.0214
36	---	---	.43	.025	---	---	---	---	.4262	.0211
37	---	---	.43	.025	---	---	---	---	.4259	.0208
38	---	---	.43	.025	---	---	---	---	.4210	.0156
39	---	---	.445	.01	---	---	---	---	.440	.0044
40	---	---	.43	.025	---	---	---	---	.4221	.0167
41	---	---	.43	.025	---	---	---	---	.4229	.0176
42	---	---	.443	.012	---	---	---	---	.4372	.0059
43	---	---	.405	.05	---	---	---	---	.3926	.0370
44	---	---	.445	.01	---	---	---	---	.440	.0045
45	---	---	.43	.025	---	---	---	---	.4216	.0162
46	.05	---	.455	---	---	.0377	---	---	.455	---
47	.10	---	.405	---	.0120	.0888	---	---	.3996	.0029
48	.10	---	.355	---	.0111	.0651	---	---	.3507	.0033
49	.10	---	.20 He	---	.0329	.0594	---	---	---	.0154
50	.10	---	---	---	.0385	.0632	---	---	---	.0175
51	.10	---	.05	---	.0349	.0776	---	---	.0458	.0131
52	.10	---	.20	---	.0214	.0717	---	---	.1943	.0069
53	.10	---	.10	---	.0269	.0792	---	---	.0953	.0096
54	.10	---	.22	---	.0197	.0837	---	---	.2144	.0063
55	.10	---	.30	---	.0156	.0950	---	---	.2947	.0047
56	.10	---	.50	---	.0048		---	---	.4978	.0013
57	.10	.10	.10	---	.0709	.0291	.0290	.0709	.0999	TRACE
58	.10	.10	.05	---	.0710	.0289	.0288	.0710	.0500	TRACE
59	.10	.10	---	---	.0707	.0292	.0292	.0707	---	TRACE
60	.10	.05	---	---	.0467	.0529	.0049	.0436	---	.0005
61	---	---	.455	---	---	---	---	---	.455	---
62	.10	.05	.10	---	.0458	.0541	.0051	.0443	.0997	.0001

28

V. DISCUSSION AND CORRELATION OF RESULTS

5.1 Correlation of Erosion Data

5.1.1 Oxidation Effects

A series of tests was conducted to quantify erosion due to oxidation of 4340 steel as described previously. The primary variables in these tests were oxygen concentration of the test gas and the compression ratio which determined pressure and temperature. A baseline test mixture of 54 1/2 percent argon and 45 1/2 percent nitrogen was selected during the previous program.[1] This baseline mixture was modified to include oxygen by replacing nitrogen with oxygen. The total oxygen concentration for the test was kept relatively low in order to maintain nearly constant gas temperature and pressure conditions for the different concentrations and also to keep the net oxidation level at an order of magnitude that might be expected in a gun. The test series included oxygen concentrations of 0, 1 percent, 2 1/2 percent, and 5 percent, and pressure levels from 100 MPa to a nominal maximum level of 280 MPa.

The role of oxidation on surface erosion is readily shown in Figure 7 where weight loss is shown as a function of initial oxygen concentration at the maximum nominal pressure of 280 MPa. The convective heating is sufficiently high to cause significant material loss by pure melting with no oxygen. Weight loss increases rapidly from this initial level with increasing oxygen concentration. The nearly linear dependence of weight loss on oxygen content indicates a situation where the rate of oxidation is diffusion controlled. That is, the oxidation is limited by the number of oxygen molecules coming in contact with the sample surface rather than the rate at which the reaction occurs.

The variation of weight loss with flow conditions, as specified by pressure, for gas mixtures containing zero and 2 1/2 percent oxygen is shown in Figure 8. Additional inert data presented in this figure and others were obtained during testing subsequent to this program.[5] The threshold at which sample weight loss is first observed occurs at 194 MPa for a gas mixture containing 2 1/2 percent oxygen and approximately 250 MPa for a mixture with no oxygen. Weight loss increases as pressure increases beyond the threshold level. At pressures in the vicinity of and below the threshold level, samples tested with the 2 1/2 percent oxygen mixture exhibited little weight change but the diametral surface measurements indicated an oxide buildup. The oxide buildup at low pressures gives way to surface recession at high pressures.

The shift in the erosion threshold is an indication that melting is not a prior requisite for the onset of oxidation and that surface reactions are the mechanism by which oxidation of steel enhances material loss. The erosion versus pressure curves shown in Figure 8 are roughly parallel to each other which indicates that the effects of oxidation represent a constant input rather than a driving force that would further enhance erosion. The situation

---

5. "Investigation of the Role of Carburization in Gun Barrel Erosion and Cracking," Bimonthly Progress Report No. 3, ARRADCOM Contract DAAK11-79-C-0049, November 1979.
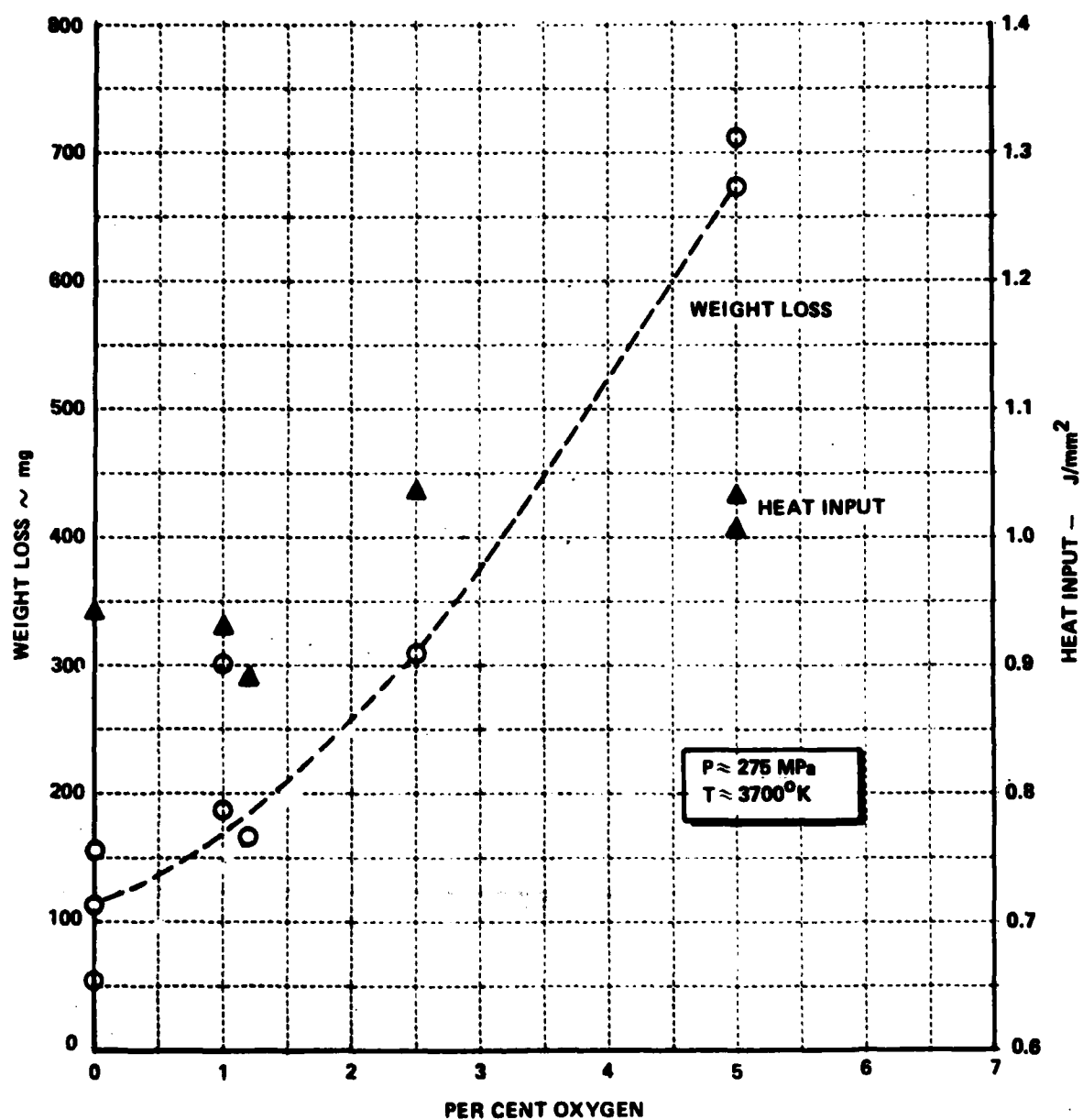
Figure 7 VARIATION OF WEIGHT LOSS AND HEAT INPUT AS A FUNCTION OF OXYGEN CONCENTRATION
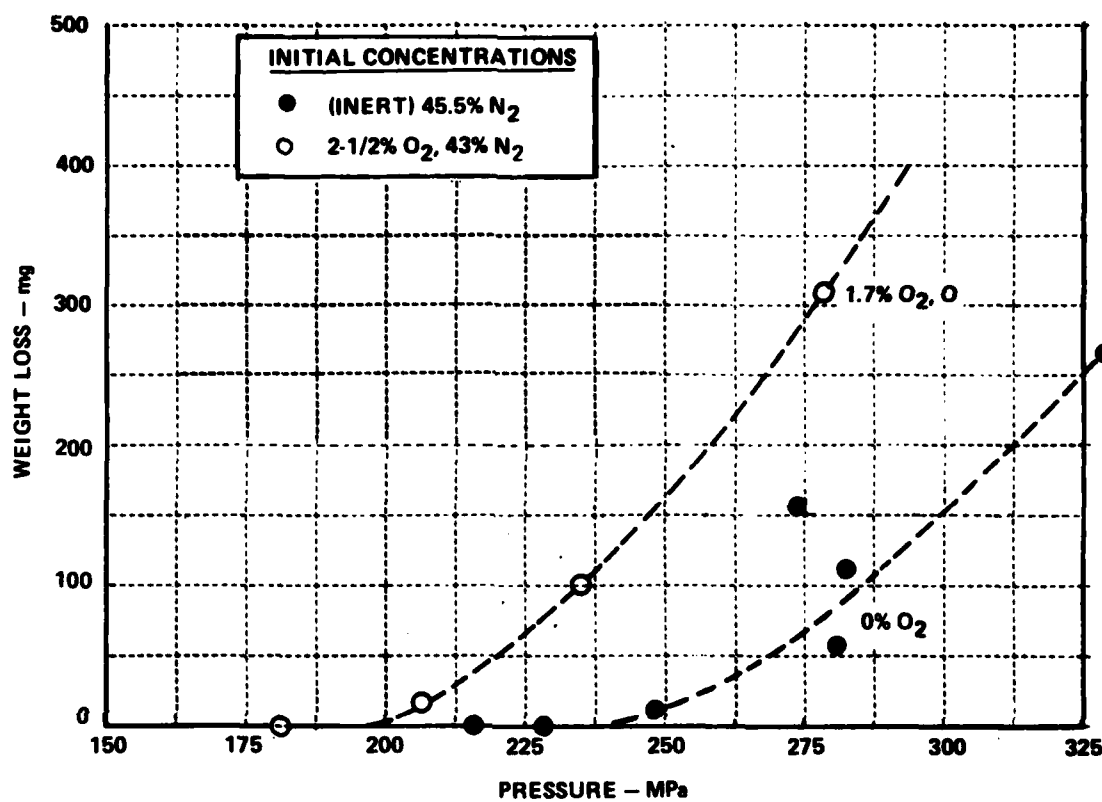
Figure 8   WEIGHT LOSS AND HEAT INPUT FOR VARIABLE TEST CONDITIONS AND
2-1/2% OXYGEN CONCENTRATION

31

where combustion in the boundary layer causes catastrophic material erosion was observed in the case of aluminum[6,7] which has roughly an order-of-magnitude greater heat of combustion. In this instance, catastrophic erosion resulted after initial melting took place. Such does not appear to be the case with 4340 steel, but rather, the surface reaction tends to serve as a constant heat flux increment to the convective term.

5.1.2 Erosion With Mixtures Containing Carbon Dioxide

Oxidation in combustion gases is believed to occur when the ratio of carbon monoxide to carbon dioxide is less than the 3.0.[4] A series of tests was conducted in this program whereby a gas mixture consisting of nitrogen, carbon dioxide and argon was compressed to temperatures and pressures experienced in guns. The equilibrium concentration ratio of carbon monoxide to carbon dioxide was considerably less than 3.0 for these runs. In many cases, the equilibrium oxygen concentration at peak pressure was at levels similar to those of tests where oxygen was introduced initially as a gas constituent.

The initial tests involving carbon dioxide were conducted under the same philosophy as those involving oxygen with only a small concentration of carbon dioxide being introduced in order to cause only a small perturbation to the test conditions. However, very little erosion was observed during these initial tests, and also it was found that carbon dioxide, being significantly different from nitrogen, caused significant changes in the relationship between gas temperature and pressure as shown previously in Figure 5. Therefore, the initial concentration of argon was increased in order to increase the gas temperature level and to increase the level of material erosion. This change in test conditions made pressure alone an unsuitable parameter for correlating all erosion data.

Convective hot wall heat flux is the driving potential for melting erosion once the melting temperature is achieved. Thus, it follows that convective heat flux to a hot surface is a natural parameter for correlating simple melting erosion data resulting from similar heating cycles. Similarity of heating cycles is important because the heat flux history determines the surface temperature. The flow conditions for each test were computed with a combination of two computer programs and experimentally measured pressure. The model of the STG cycle (Appendix I) was used to create the proper pressure profile. Also included in this particular code is a representation of the flow through the test sample and calculation of the convective heat flux using the empirical equation for turbulent flow over a flat plate. The gas conditions of temperature, density and

---

6. Summerfield, et. al., "Erosion of Aluminum by High Pressure Propellant Gases," 10th JANNAF Combustion Meeting, CPIA Publication No. 243, August 1973.

7. Fisher and Cytron, "Influence of Combustion on Aluminum Cartridge Case Burnthrough," 10th JANNAF Combustion Meeting, CPIA Publication No. 243, August 1973.

velocity are evaluated in this code. The local hot wall heat flux is computed and a running summation of the heat input to the wall is evaluated. The computed total heat input was compared with the experimentally determined value for the input gas mixture. A factor was applied to the heat flux calculation to bring the total heat input into agreement with the experimentally determined value. In this manner, the instantaneous value of convective heating, as determined by the flow conditions and exclusive of chemical heating, is believed to be reasonably correct for tests with inert and low-oxygen-concentration gas mixtures.

The gas temperature as determined by the STG model in its current state of development is only an approximate calculation. A more accurate temperature calculation is provided by the equilibrium combustion code that is described briefly in Appendix II. This code computes an isentropic compression of gases beginning with an arbitrary mixture. In addition to determining the temperature and pressure, the concentration of the various chemical species formed during the equilibrium combustion process are also determined. Thus, the mole fraction of free oxygen formed by compression of gas mixtures containing carbon dioxide is evaluated.

An approximate technique was used to correct the heat flux calculated by the STG model to the more accurate temperature conditions of the equilibrium combustion code. The heat flux to a surface is equal to the product of a coefficient and the temperature difference between the gas and the surface,

$$q = h \ (T_O - T_W).$$

For the heat flux to a flat plate in turbulent flow, the coefficient is functionally proportional to the gas density, velocity and viscosity,

$$h \sim (\rho u)^{0.8} \ \mu^{0.2}$$

These gas parameters can be expressed in terms of temperature as follows:

$$\rho \sim T^{-1}$$ through the perfect gas equation of state

$$u \sim T^{1/2}$$ through the energy equation,

and $$\mu \sim T^{1/2}$$ from molecular transport theory.

Thus, the approximate dependence of h on the gas temperature is

$$h \sim (T^{-1} \cdot T^{1/2})^{0.8} \ (T^{1/2})^{0.2} = T^{-.4}$$

The convective hot wall heat flux computed by the STG code is

$$q_s \sim T_{gs}^{-0.4} (T_{gs} - T_{ws})$$

where T_{gs} and T_{ws} are the respective peak values for gas and surface temperatures. Similarly, the convective heat flux to a melting steel surface is

$$q_{hw} \sim T_{ge}^{-0.4} (T_{ge} - T_{wm})$$

where T_{ge} is the gas temperature calculated by the equilibrium combustion code and T_{wm} is the solidus temperature of barrel steel, 1720°K. The corrected value for heat flux, q_{hw}, is

$$q_{hw} = q_s \frac{T_{ge}}{T_{gs}}^{-0.4} \frac{T_{ge} - T_{wm}}{T_{gs} - T_{ws}}$$

This represents an approximate value of convective heat flux to a melting surface and was used in subsequent correlation of erosion data.

A graph showing the correlation of weight loss with convective hot wall heating is shown in Figure 9. All test gases containing oxygen initially are shown with clear symbols while gas mixtures containing carbon dioxide are shown with filled symbols. The inert as well as the 2 1/2 percent oxygen tests are fairly well established curves that show the shift in erosion threshold due to the addition of oxygen. It is noted that test sequences for mixtures containing 1 percent oxygen and 5 percent oxygen are not sufficiently complete to define the onset of erosion, however, the points from those curves fall in proper sequence with respect to the inert and 2 1/2 percent oxygen curves so that at any point there is nearly a linear increase in erosion with increasing oxygen as noted earlier in Figure 7.

The data for CO_2 runs show that, in some cases, carbon dioxide tends to enhance erosion, while in others, the erosion is about the same as for the inert gas mixture. It is interesting to note that the amount of erosion above that for the inert gas can be correlated reasonably well with the amount of free oxygen at peak conditions. In particular, tests 50, 51 and 53 all contain approximately 1 percent or more free oxygen at peak conditions. The points from these tests all fall above the curve for 2 1/2 percent oxygen. Tests 52 and 54, contain 0.6 and 0.7 percent free oxygen, respectively, and these points fall above the curve for 1 percent oxygen. Finally, the weight loss experienced during run 55, which contained 0.5 percent free oxygen at peak conditions is slightly below the values for 1 percent oxygen. Thus, there appears to be twice the erosion for these runs than for runs with an equivalent amount of oxygen. This trend was broken by run 47 from which there was no measurable erosion and, yet, it contained 0.3 percent free oxygen. The point fell slightly below the inert curve, very close to the threshold of erosion.

SYM	RUN(S)	% GAS MIXTURE				% FREE O_2 AT PEAK COND.
		N_2	O_2	CO_2	H_2	
○	32, 46, 61	45.5	0	0	0	0
△	33, 43	40.5	5	0	0	3.6
□	34, 37, 38, 40, 41, 45	43	2.5	0	0	1.7
◖	39, 42, 44	44.5	1	0	0	0.5
◀	47	40.5	0	5	0	0.3
●	48	36.5	0	10	0	0.3
■	50	0	0	10	0	1.8
◖	51	5	0	10	0	1.3
◆	52	20	0	10	0	0.7
◆	53	10	0	10	0	1.0
◤	54	22	0	10	0	0.6
◆	55	30	0	10	0	0.5
✕	56	50	0	10	0	0.1
●	57	10	0	10	10	<0.1
◤	58	5	0	10	10	<0.1
▲	59	0	0	10	10	<0.1
■	60	0	0	10	5	0.1
◣	62	10	0	10	5	<0.1

CONVECTIVE HOT WALL HEAT FLUX ~ J/mm^2-Sec
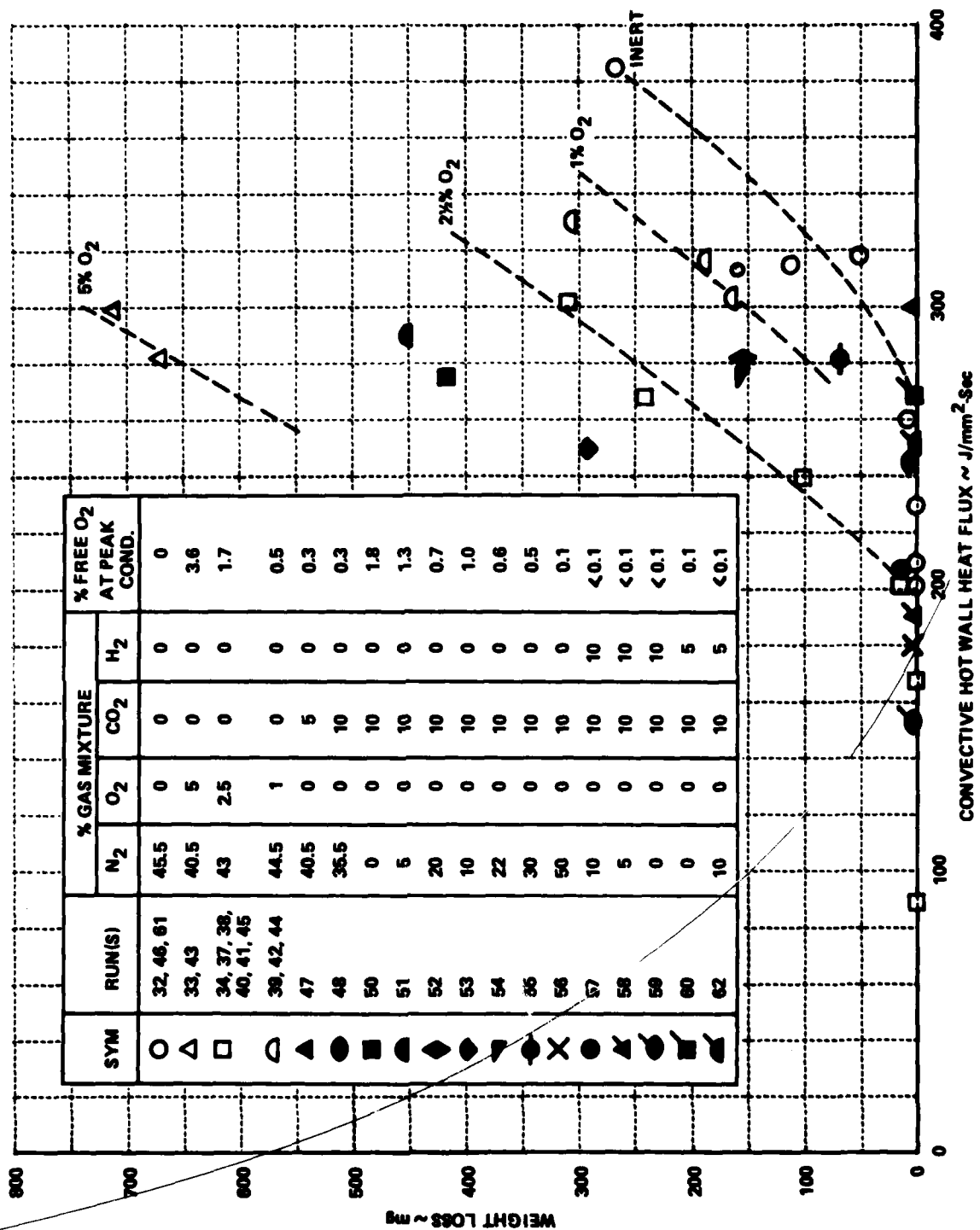
WEIGHT LOSS ~ mg

Figure 9 INFLUENCE OF CONVECTIVE HEATING AND OXIDATION-TYPE REACTIONS ON EROSION OF 4340 STEEL

35

If one examines this figure, it is apparent that most of the tests with CO_2 that experienced erosion in excess of the inert case fell either on or very close to the line of constant heat flux at the 280 joules per square millimeter per second. The weight loss versus equilibrium oxygen concentration at this heating level for both the tests with oxygen and with carbon dioxide is plotted in Figure 10. In this figure, the augmentation of erosion due to carbon dioxide over that of an equivalent amount of oxygen becomes readily apparent. It is evident from these two figures that the equilibrium concentration of oxygen in the stream is an indicator of erosion enhancement over the inert case.

The enhanced erosion observed during tests with carbon dioxide over those during tests with oxygen-nitrogen mixtures suggests the existence of an erosion mechanism other than oxidation. One might postulate that oxidation occurring initially at the surface might cause depleted oxygen in that region which would promote formation of carbides. Carbon-rich steels and carbides have lower melting temperatures than pure steels or oxides as shown in Figure 11, which suggests one mechanism by which enhanced erosion in the presence of CO_2 might occur. 4340 steel melts at approximately 1700°K, while iron carbide is believed to melt in the vicinity of 1440°K. The term "melting" is used loosely here to mean the solidus point or onset of the mushy state indicated in Figure 11. It is assumed that shear and deformation by high pressure gas flow removes the material at this temperature. For the case of run 51, just this change in melting temperature could account for a 13 percent increase in material loss rate. As the carbon content increases in steel, its thermal conductivity decreases, so that for a given heat flux to the surface, one might expect accelerated removal. Such mechanisms represent only conjecture at this point. Future analyses of test samples, however, may indicate an elevated carbon content at the surface which would support the argument.

Part of the enhanced CO_2 erosion indicated by Figure 10 may be attributed to differences in the ballistic cycle. The amount of material removal is not only a function of the convective hot wall heat flux, but on its entire heating history. Both the time at the high heating rate and the dynamic heat conduction processes are important. The measured total heat input represents the integrated convective and chemical heat flux to the sample and is an indicator of differences in ballistic cycle time between tests with equal levels of hot wall heat flux in a similar chemical environment.

The measured total heat input is given in Table 4. This represents the residual heat in the sample at the end of the test. This quantity is in error for samples experiencing large erosion because the act of material removal also removes heat from the location of the heat sensor. Therefore, a correction factor was added to the heat input data for the purpose of correlating weight loss measurements. The factor is based on the assumptions that the material removed was at 1720°K and that the material was sloughed away before the latent heat was absorbed. The correction factor is

$$\Delta Q = \rho c \Delta x \ \Delta T = 3.30 \ \Delta x \ J/mm^2$$

which is simply added to the heat input given in Table 4 to form Q_{corr}. The value of Δx is the diametral recession under column B, which represents the

location of the heat sensor. If the latent heat term were included, the correction factor, ΔQ, would be increased by 0.91 Δx.

The correlation of weight loss with the corrected heat input is shown in Figure 12. With the exception of a few "flyers," the dotted line connects the points in a reasonable fashion. The weight loss remains at zero with increasing heat input until the combination of heat input and peak hot wall heating is sufficiently high to cause material removal. It is noted that several samples experienced total heating in excess of the apparent threshold but did not lose material. During these tests, the ballistic cycle was long which gave a high total heat input, but the peak hot wall heat flux was below the level required to achieve melting conditions. Of greater significance, however, is the observation that data from runs 50 and 51 appear to have higher weight loss than those tests with a gas containing 2-1/2 percent oxygen because the total heat input is higher. The cause of the elevated heat input is not clear at present. Measured pressure curves indicated the ballistic cycle for tests with carbon dioxide were nearly 10 percent shorter in duration than for the tests with oxygen. The increased total heating is likely a combined effect of surface chemistry, convective heat transfer coefficient, and accumulated low level heating before a measurable pressure was reached. Clearly, this is an area that requires additional investigation.

It has been shown, however, that some gas mixtures containing carbon dioxide are more erosive than an inert gas at similar heating environments and that the level of erosivity appears to correlate with the equilibrium level of free oxygen in the gas at peak conditions. This is in contrast to the work of Caveny[8] where no enhanced erosion in an atmosphere of carbon dioxide without water was observed. The current result may be attributed to the factor-of-four longer test times of the STG over Caveny's ballistic compressor.

If hydrogen is added to the gas, the amount of free oxygen is decreased substantially due to formation of water. In the situations tested, no erosion was observed in excess of the inert erosion for gases containing mixtures of carbon dioxide and hydrogen. Tests were only conducted up to the threshold of erosion of an inert gas mixture. Additional tests are required to extend the data base to higher heating conditions for hydrogen-carbon dioxide mixtures.

5.2   Erosion Distribution

The distribution of surface erosion along the length of the test sample is shown in Figure 13 for gas mixtures with 0, 2-1/2 percent, and 5 percent oxygen. The pressures and temperatures were approximately the same for each of the tests so differences between the three curves are primarily due to the oxygen concentration. It is noted that the data for 0 percent oxygen show moderately high erosion at the first point of measurement. The amount of erosion decreases rapidly until there is essentially no erosion at the third and fourth points of measurement, which are representative of the downstream half of the test sample.

---

8.   Caveny, L., "Erosion of Steel by Combustion Gases," presented at ARO-sponsored Workshop II on Mechanisms of Erosion in Hot Flowing Media, 9-12 October 1979.

800

CARBON DIOXIDE-NITROGEN GAS MIXTURE

OXYGEN-NITROGEN GAS MIXTURE

SAMPLE WEIGHT LOSS

600

400

200

0

0   1   2   3   4   5

% EQUILIBRIUM O_2 CONCENTRATION
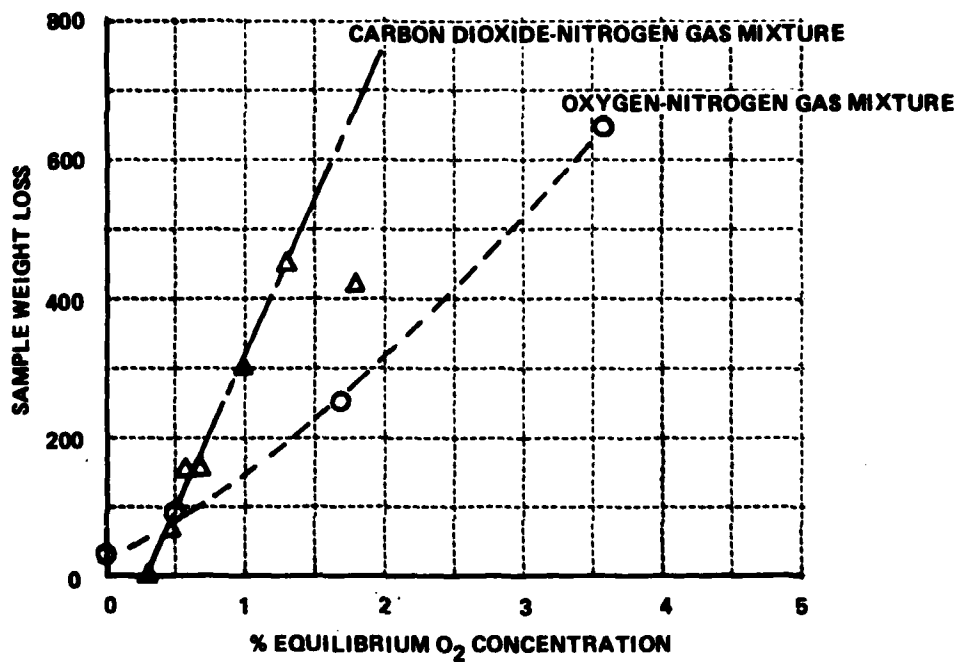
Figure 10 CORRELATION OF WEIGHT LOSS OF 4340 STEEL WITH TEST GAS
EQUILIBRIUM CONCENTRATION OF OXYGEN AT A PEAK CONVECTIVE
HOT WALL HEATING RATE OF 280 J/mm^2-sec
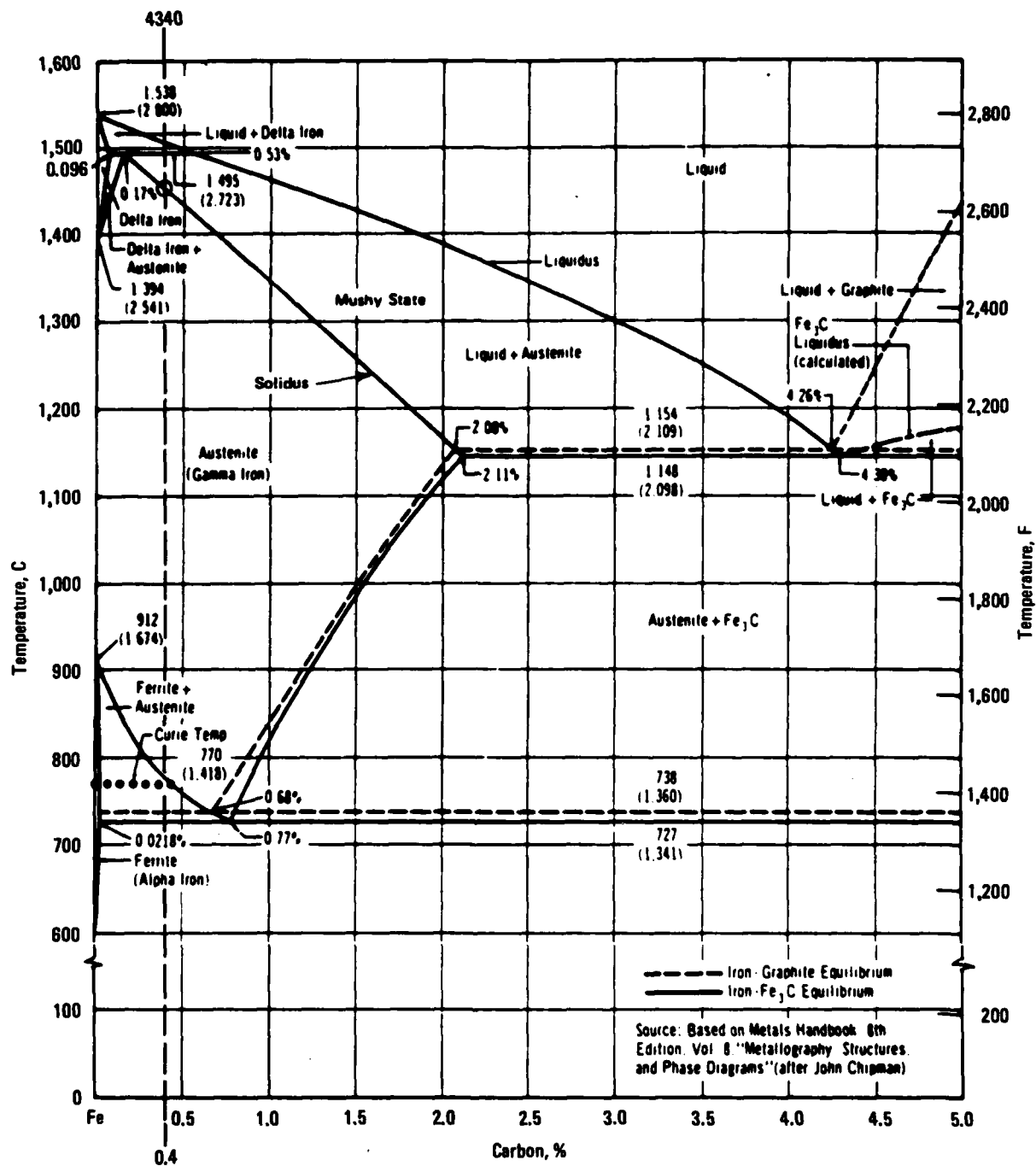
Figure 11 IRON-CARBON EQUILIBRIUM DIAGRAM

39

SYM	RUN(S)	% GAS MIXTURE				% FREE O_2 AT PEAK COND.
		N_2	O_2	CO_2	H_2	
O	32, 46, 61	45.5	0	0	0	0
△	33, 43	40.5	5	0	0	3.6
□	34, 37, 38, 40, 41, 45	43	2.5	0	0	1.7
◁	39, 42, 44	44.5	1	0	0	0.5
◀	47	35.5	0	10	0	0.3
●	48	35.5	0	10	0	0.3
■	50	0	0	10	0	1.8
◖	51	5	0	10	0	1.3
◆	52	20	0	10	0	0.7
▼	54	22	0	10	0	0.6
X	56	50	0	10	0	0.1
●	57	10	0	10	10	<0.1
◤	58	5	0	10	10	<0.1
◗	59	0	0	10	10	<0.1
◼	60	0	0	10	5	0.1
◣	62	10	0	10	5	<0.1

CORRECTED TOTAL HEAT INPUT, Q_{CORR} — J/mm^2
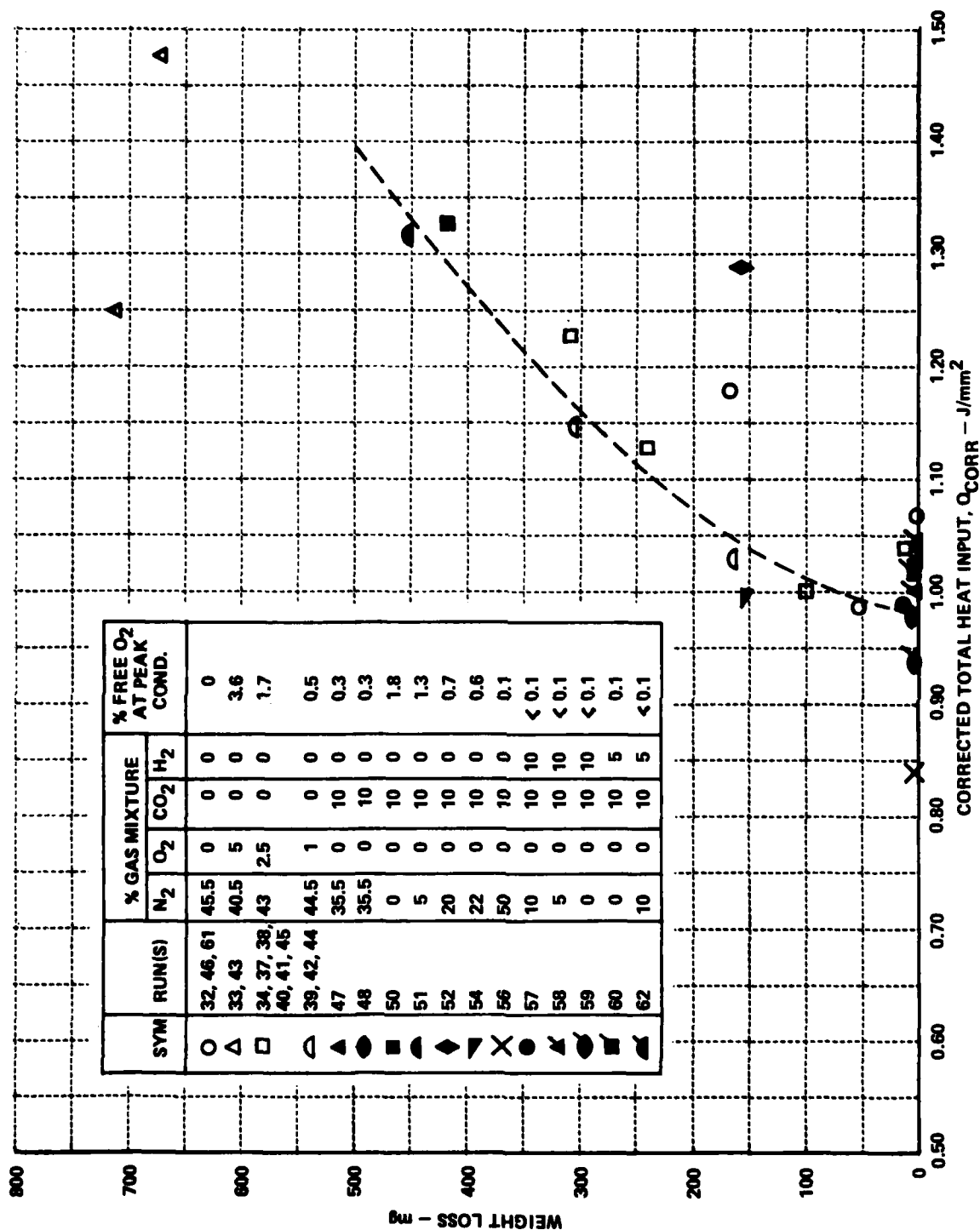
WEIGHT LOSS — mg

Figure 12 CORRELATION OF 4340 SAMPLE WEIGHT LOSS WITH MEASURED TOTAL HEAT INPUT CORRECTED FOR LOCAL HEAT LOST BY MATERIAL REMOVAL

40
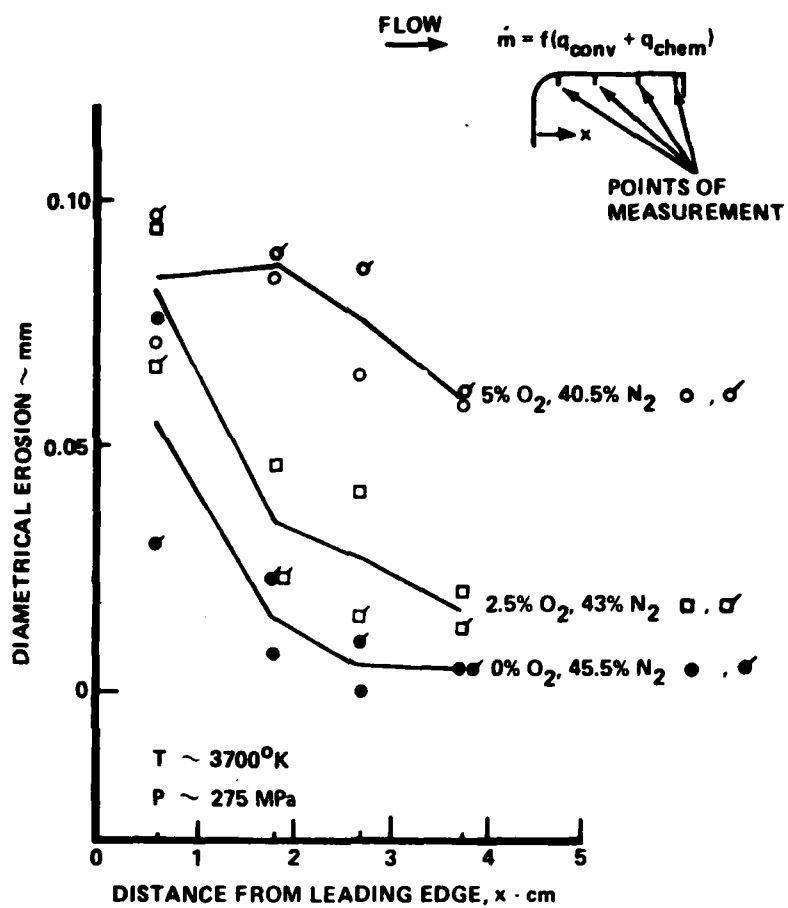
Figure 13 INFLUENCE OF OXIDATION ON SURFACE RECESSION

41

The data from the sample tested at a 2 1/2 percent concentration of oxygen show a somewhat higher erosion at the first measurement point but the same basic distribution over the length of the sample as for the inert gas mixture. The erosion at the flow exit point was very small. For a 5 percent oxygen mixture, the sample experienced a heavy erosion over its entire length with the erosion at the first three stations being nearly the same and dropping off only slightly at the flow exit point.

These observations are interpreted with the help of Figure 14. Here, characteristic heat flux distributions are shown plotted versus distance from the sample stagnation point. The distribution of heating over the curved portion of the sample to the sonic point, which is denoted by S*, is approximated on the basis of melting patterns observed near the melting threshold. From that point, the sample is assumed to be subjected to a distribution of heat flux that is analogous to the heat flux to a flat plate in turbulent boundary layer flow. The inert heating profile was arbitrarily established for melting to occur at the leading edge.

Several assumptions can be made as to the impact of oxygen on the distribution of erosion. It was observed previously, that the presence of oxygen in the gas mixture caused a shift in the threshold of erosion. This indicates that oxidation increases the effective level of total heating which causes the melting threshold to occur at a lower level of convective heating and less severe flow conditions. At downstream locations on the test sample, the surface-chemistry-effect might be expected to elevate the heat flux level by an increment as illustrated conceptually in Figure 14.

Once the level of heating required to achieve melting is reached, the rate at which material removal occurs at a given location is greatly accelerated by any additional heating. Therefore, most of the difference in surface recession between the 5 and 2 1/2 percent oxygen tests can be attributed to an increase in chemical heating at downstream locations from threshold to levels substantially in excess of the threshold. The percentage increase in heating in excess of that required for melting is much less at the forward stations so changes there are not as dramatic.

Melting in the forward portion of the sample and subsequent combustion results in addition of heat to the boundary layer, which increases the effective gas temperature. This augments the convective heating, in addition to local heating due to surface chemistry at downstream locations. The magnitude of this effect is governed by the heat released during the oxidation process and the distribution of this energy in the stream. This was found to be a dominant factor for aluminum cartridge case burn-through[6] because aluminum has a high heat of reaction with oxygen. FeO has a heat of formation only 15 percent that of aluminum oxide and effects of combustion in the boundary layer are believed to be correspondingly small.

42
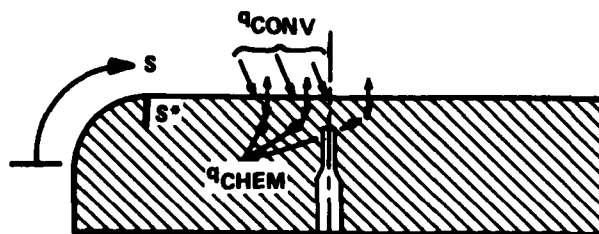
$$\dot{q}_{TOT} = \dot{q}_{CONV} + \dot{q}_{CHEM}$$
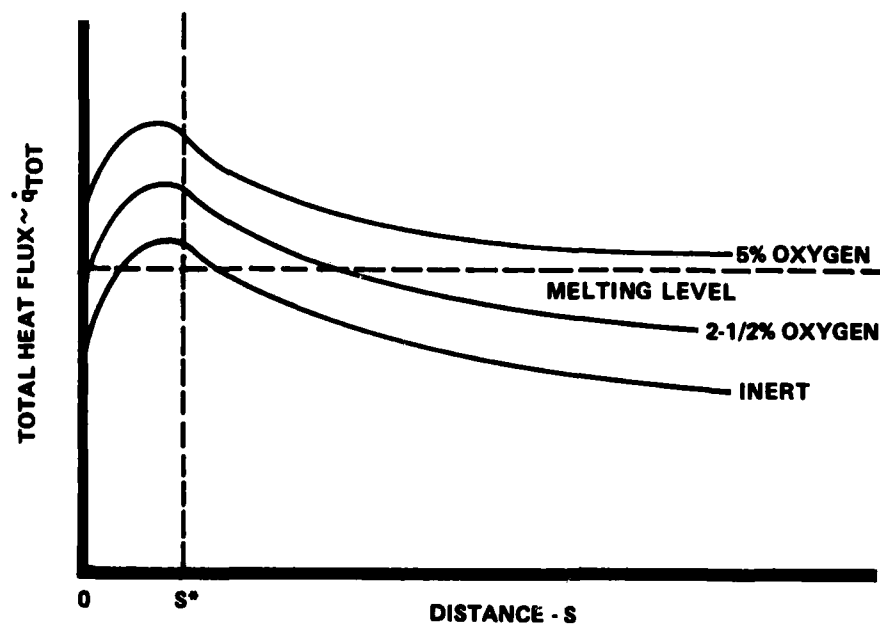
Figure 14 INFLUENCE OF OXIDATION ON SURFACE HEATING

43

5.3   Surface Features

The Scanning Electron Microscope (SEM) was used to examine the surface features of the samples tested during this program. Melt layers, oxide coatings, and cracking are among those features that were observed during this examination. The samples were sliced end to end to permit direct viewing of the surface. All samples were examined in this manner but several that are representative of the overall observations are discussed here.

Sample 1 from Run 32 was tested at a nominal pressure of 280 MPa in a nitrogen-argon environment. Internal diameter measurements indicate the sample experienced virtually no surface recession except near the leading edge. SEM photographs of the flow entrance, center, and flow exit regions of the sample are shown in Figure 15. The surface near the flow entrance has a grainy texture and an extremely fine check pattern. The surface roughness is probably related to original machining marks and grain boundaries in the steel. The center of the sample appears to exhibit a slightly thicker melt layer speckled with solidified droplets that originated farther upstream. The fine crack structure, which does not resemble cracking in a gun, also persists at this location. Finally, it is evident that no surface melting took place at the sample flow exit, as indicated by the presence of machining grooves beneath solidified spray.

Sample Nos. 2 and 8 were tested at nominal pressures of 280 MPa in an atmosphere containing 1.2 percent oxygen and 5 percent oxygen, respectively. These samples illustrate surface features that are characteristic of all tests conducted at high pressure in various concentrations of oxygen. The SEM photographs of Figures 16 and 17 at the entrance, center, and exit are similar inasmuch as particles protrude from what appears to be a melt layer. At lower magnification, this surface has a crust-like appearance as shown in Figure 18. The melt layer contains a fine microcrack pattern of much the same character as the test without oxygen. This also bears little resemblance to the cracking that has been observed in gun tubes.

A series of tests were conducted in an atmosphere containing a 2 1/2 percent concentration of oxygen for a range of peak pressures. The surface features illustrated in Figures 19, 20 and 21 show the progression of surface cracking from test conditions that represent the onset of melting erosion to those at the higher melting erosion conditions. The surface features at the sample inlet appear to be quite rough at the onset of erosion. This rough surface feature then gives way to what appears to be a molten sublayer with particles protruding at the higher pressures. The most significant aspect of this series of three figures is the crack patterns that are present at the center of the sample. The cracks that occurred during Run 34, in particular, are somewhat smaller in magnitude, but have the same general characteristics as those observed in guns. The flow exit region is covered with resolidified deposits for the low pressure test but this gives way to the general eroded melted layer with some resolidifed deposits at the higher pressures.

44
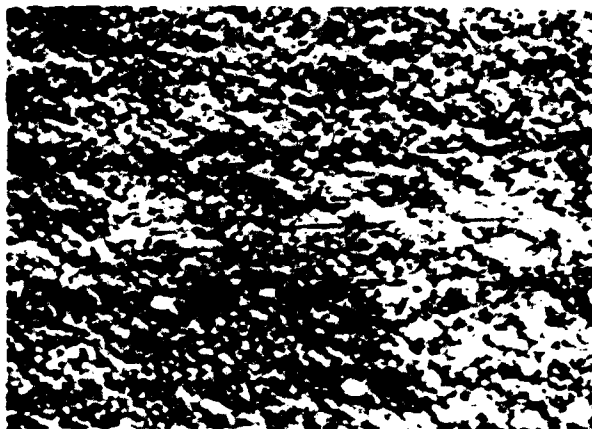
EXIT
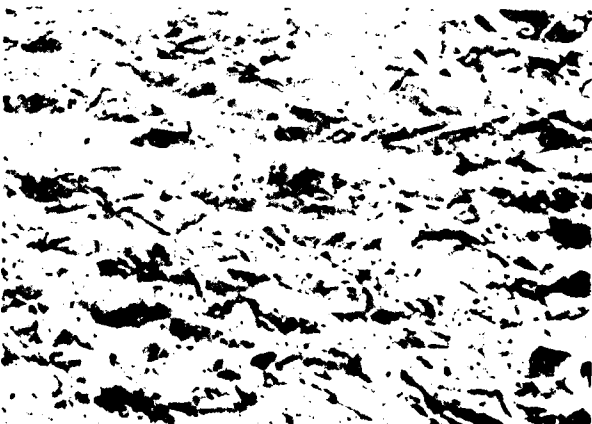
CENTER

FLOW

INLET

SAMPLE 1, RUN 32, 1000 MAGNIFICATION

Figure 15 SURFACE FEATURES OF A SAMPLE MADE FROM 4340 STEEL AND TESTED IN
AN INERT ATMOSPHERE AT 275 MPa

45
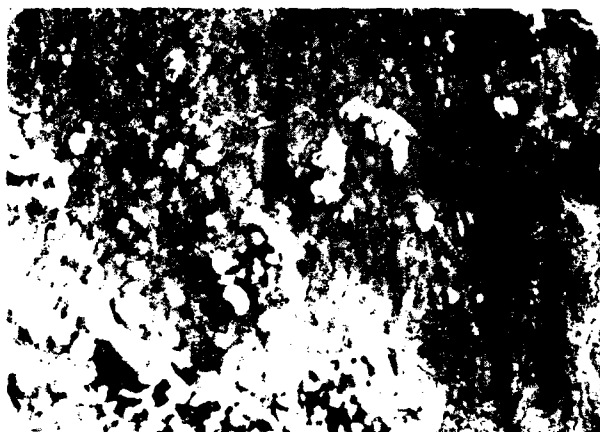
EXIT

CENTER

FLOW

INLET

SAMPLE 2, RUN 33, 1000 MAGNIFICATION

Figure 16   4340 STEEL SAMPLE SURFACE TESTED IN A 5 PERCENT OXYGEN
ATMOSPHERE TO 283 MPa, 3516°K

46

EXIT
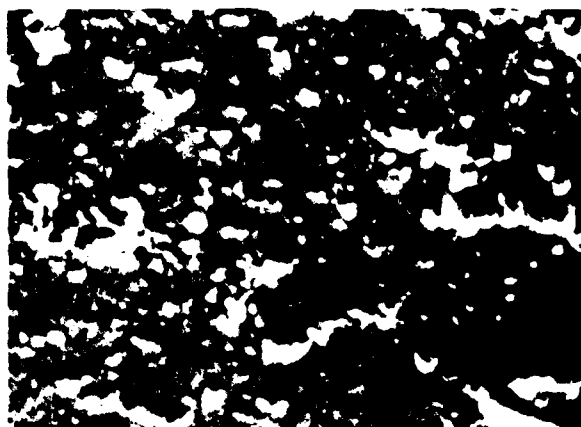
CENTER

FLOW

INLET

SAMPLE 8, RUN 42, 1000 MAGNIFICATION

Figure 17   SURFACE FEATURES OF A SAMPLE MADE FROM 4340 STEEL AND TESTED IN
AN ATMOSPHERE CONTAINING 1.2 PERCENT OXYGEN AT 275 MPa

47

FLOW

SAMPLE 2, RUN 33, 40 MAGNIFICATION

Figure 18   CRUST-LIKE CHARACTERISTIC OF THE OXIDE LAYER

EXIT

CENTER

FLOW ↑
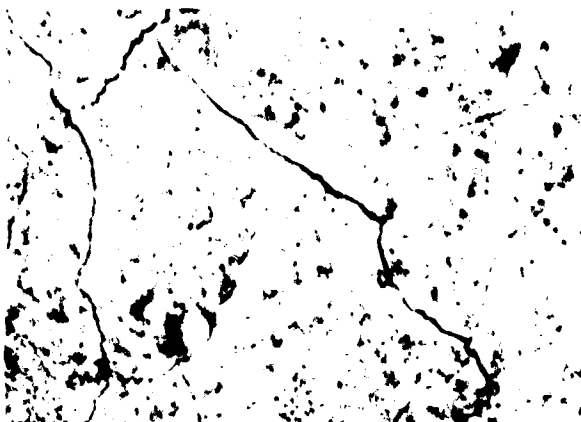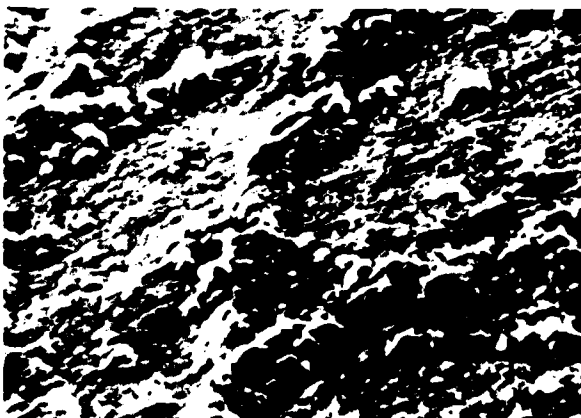
INLET

SAMPLE 4, RUN 34, 1000 MAGNIFICATION

Figure 19   SURFACE FEATURES OF A 4340 STEEL SAMPLE TESTED IN AN ATMOSPHERE
CONTAINING 2-1/2 PERCENT OXYGEN AT 175 MPa

EXIT
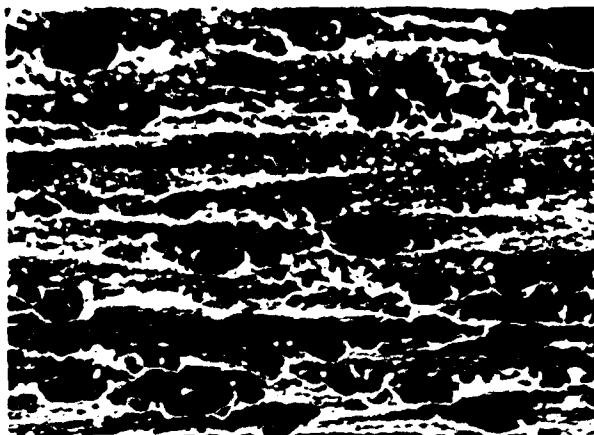
CENTER
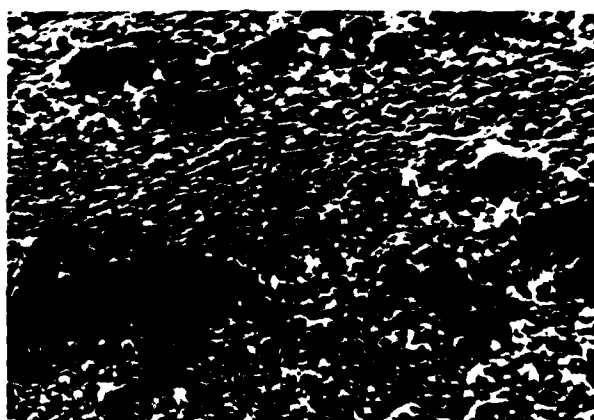
FLOW

INLET

SAMPLE 7, RUN 41, 1000 MAGNIFICATION

Figure 20 4340 STEEL SAMPLE SURFACE TESTED IN A 2.5 PERCENT OXYGEN
ATMOSPHERE TO 200 MPa, 3237°K

50

EXIT
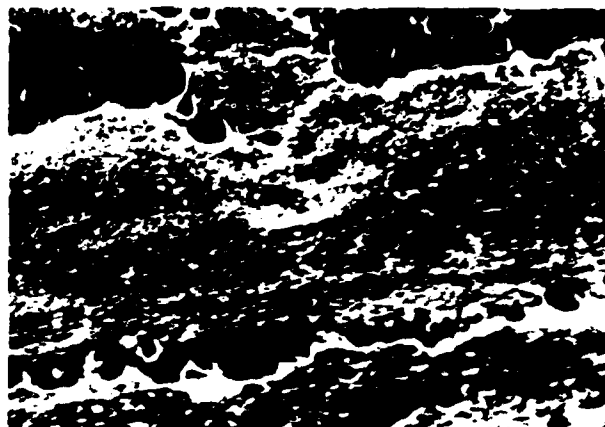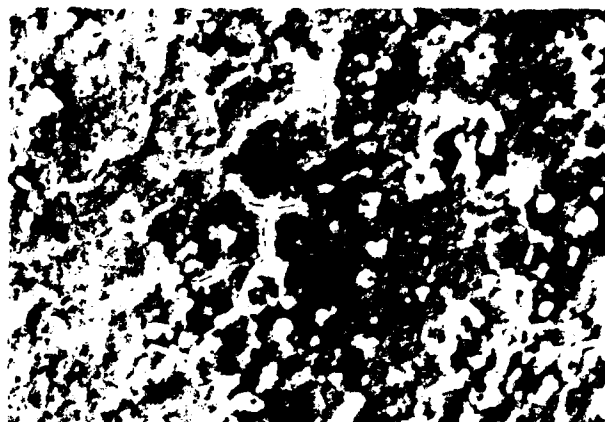
CENTER

FLOW

INLET
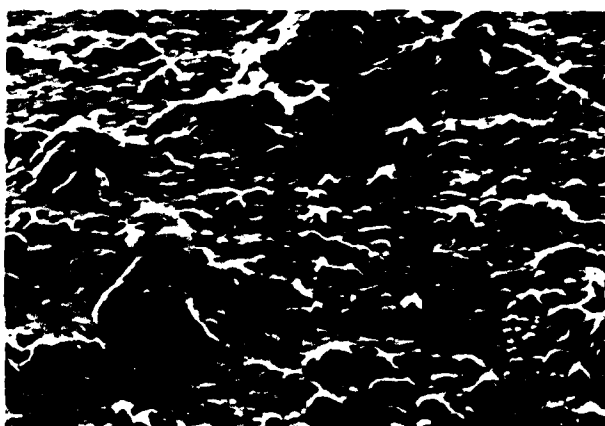
SAMPLE 6, RUN 40, 1000 MAGNIFICATION

Figure 21 4340 STEEL SAMPLE SURFACE TESTED IN A 2.5 PERCENT OXYGEN
ATMOSPHERE TO 232 MPa, 3372°K

51

It is interesting to note that the sample tested at low pressure experienced no weight loss and a surface buildup. All samples tested in oxygen at pressures from 170 to 230 MPa experienced surface buildup and cracking at the center. At higher pressures, this cracking feature seemed to diminish until a very fine crack structure was observed at pressures in the vicinity of 280 MPa. It is postulated that cracking may be associated with oxide thickness and perhaps melting of the oxide layer. At the higher pressures, melting and material removal occurred over the length of the sample but at the lower pressures the buildup was observed. This buildup, which is believed to be an oxide layer, appeared to crack upon cooling. The presence of an oxide or other form of brittle surface layer may, indeed, be related to initiation of cracking in gun barrels.

The surface features of samples tested in a 10 percent carbon dioxide gas mixture and experiencing, in one case, a high degree of erosion and, in the other case, virtually no erosion, are shown in Figures 22 and 23, respectively. Test sample No. 14 was tested during Run 48 in a gas mixture that contained 35 1/2 percent nitrogen. The final gas temperature was approximately $3300°K$. Sample No. 17 was tested during Run 51 in a mixture that contained only 5 percent nitrogen so that its gas temperature was $3800°K$. The peak pressures were 306 MPa during Run 48 and 285 MPa during Run 51.

During Run 51 the sample experienced large erosion over its entire length (Figure 22) and the SEM photographs of the surface give the appearance that the surface was scrubbed and eroded quite heavily. The cracks that are observed are very small microcracks. Other aspects of the structure appear to be protrusions or small particles that were engulfed in the melt layer.

Surface features were quite different for the sample tested during Run 48 (Figure 23) at the center and exit locations. The center in particular shows an interesting phenomenon. A rather thick region of melt covers most of the observed surface area. However, in the center of the picture is a region where the melt layer is either missing entirely or is extremely thin. The surface cracking is very small and practically insignificant in that region not covered by the melt. Cracking and surface checking are readily observed in the region covered by the thick melt layer. This observation appears to correlate with a similar observation during tests with oxygen.

Finally, Sample 26, tested during Run 60 in a gas mixture that consisted of 10 percent carbon dioxide and 5 percent hydrogen, exhibited rather severe cracking as shown in Figure 24. There was virtually no material removed during this test. A slight buildup was observed over a portion of the sample but the cracks observed here are quite similar to those observed previously during tests involving oxygen near the threshold of erosion when a surface buildup was recorded. The surface of this sample is somewhat smoother but otherwise quite similar to those tested in mixture involving oxygen and carbon dioxide without hydrogen.

EXIT
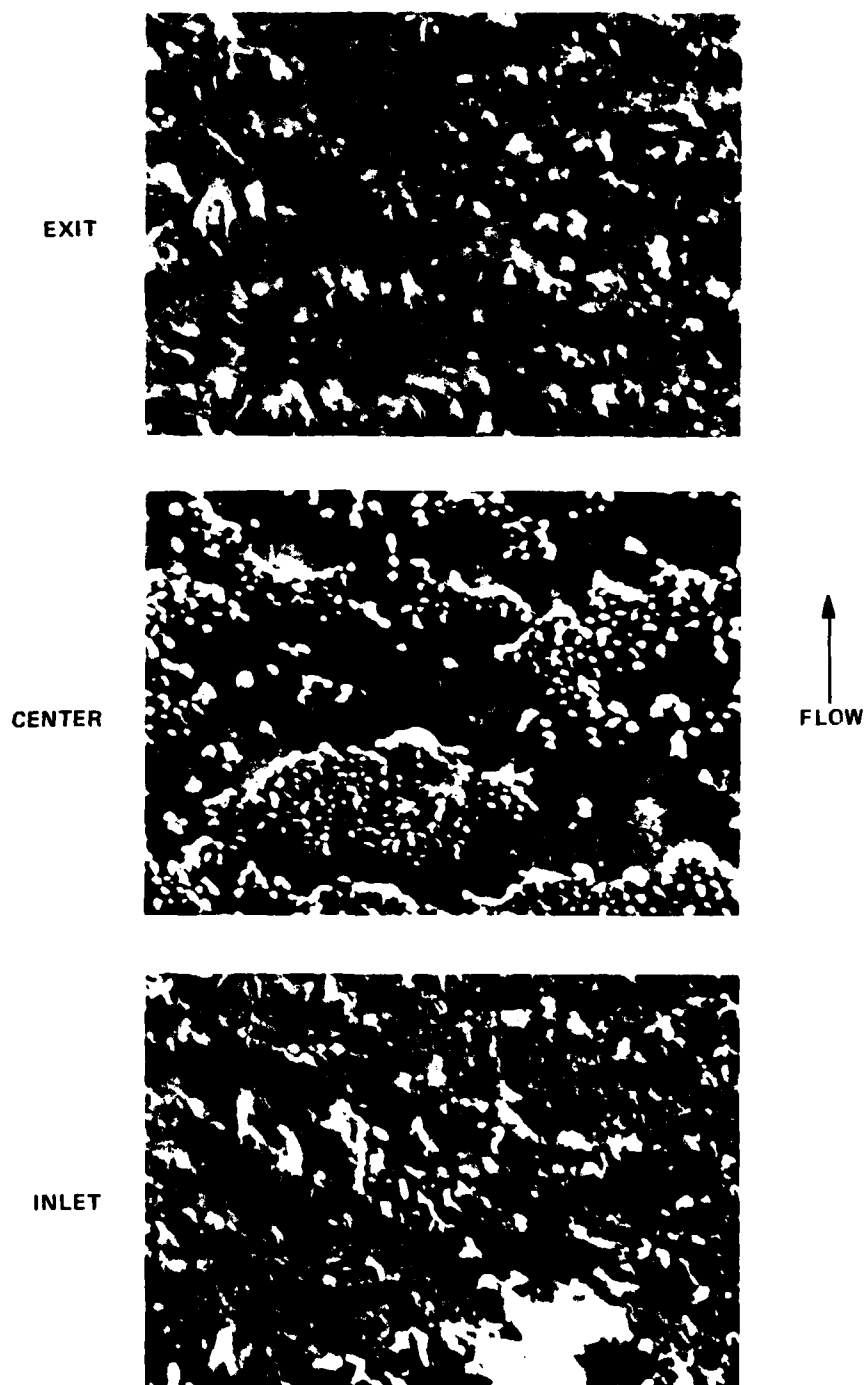
CENTER

FLOW

INLET

SAMPLE 17, RUN 51, 1000 MAGNIFICATION

Figure 22   4340 STEEL SAMPLE SURFACE TESTED IN A 10 PERCENT CARBON DIOXIDE
ATMOSPHERE TO 285 MPa, 3817ºK
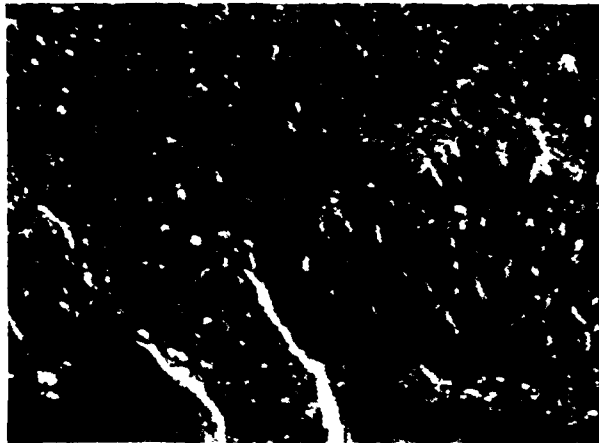
EXIT

CENTER

FLOW

INLET
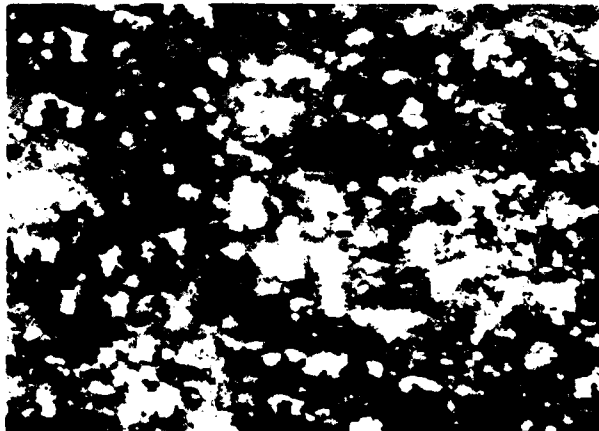
SAMPLE 14, RUN 48, 1000 MAGNIFICATION

Figure 23 SURFACE FEATURES OF A 4340 STEEL SAMPLE TESTED IN AN
ATMOSPHERE CONTAINING 10 PERCENT CARBON DIOXIDE AND
35-1/2 PERCENT NITROGEN AT 306 MPa

54

EXIT
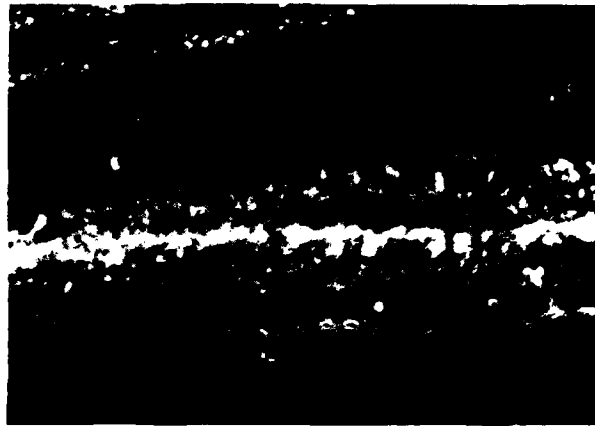
CENTER
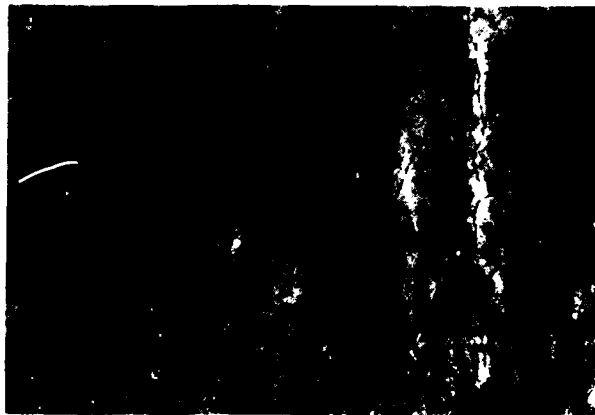
FLOW

INLET
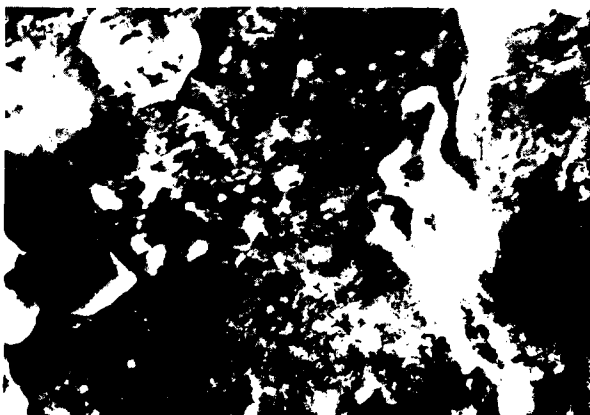
SAMPLE 26, RUN 60, 1000 MAGNIFICATION

Figure 24 4340 STEEL SAMPLE SURFACE TESTED IN A 10 PERCENT CARBON DIOXIDE
-5 PERCENT HYDROGEN ATMOSPHERE TO 210 MPa, 3316°K

5.4   Metallographic Examination

The test samples were sectioned, mounted, and polished so that the material might be examined in-depth at the location of the in-wall thermocouple. After polishing, each of the test samples was etched in a 2 percent Nital solution. This is the procedure normally used to observe the white layer on the surface of a gun barrel and the thermally altered layer, sometimes referred to as the martensite or hard layer that extends into the barrel material.

White layers in gun barrels have been the subject of extensive investigations and studies.[9] It has been stated[10] that white layers are formed primarily in reducing atmospheres containing carbon dioxide and carbon monoxide. During the current tests, however, white layers were observed in gas mixtures of oxygen, nitrogen, and argon in the absence of CO and CO_2. The white layers were observed during tests where there was a material buildup on the surface after the test as well as those where material was removed during the test. An example of a white layer formed in the presence of oxygen is shown in Figure 25.

White layers as distinct as those cited above were not observed during tests with carbon dioxide. An example of the thermally altered layer with a practically non-existent white layer is shown in Figure 26. In this figure, the white layer is more prominent than in any other photograph made with a carbon dioxide or carbon dioxide-hydrogen gas mixture. It is also noted that the white layer was not observed during a test with a gas mixture of nitrogen and argon as illustrated in Figure 27. This seems to indicate that, during these tests, the formation of oxide may have been the source of the white layer as opposed to a carbon enriched layer. The formation of this layer is not fully understood at this point and additional research is required to identify other causes for the formation of the white layers as they are observed in guns.

The thermally altered layer that extends beneath the white layer is caused by heating the material above the temperature required to form the austentitic reaction (~1150°K) and then quenching it sufficiently rapidly to form hard martensite. The thickness of this layer, which indicates the depth at which these conditions were satisfied, is illustrated in Figure 28 . Also shown are calculated temperature distributions into the sample for different times past the peak heating condition. In this curve, it is shown that the depth of the thermally altered layer corresponds approximately to the level of 1150°K and the point at which this level is maintained for an extended period of time as a result of the heating and quenching action.

---

9.   Kamdar, M., Campbell, A., and Brassard, T., "A Metallographic Study of White Layers in Gun Steel," U.S. Army ARRADCOM, Benet Weapons Laboratory Technical Report ARL CB-TR-78012, August 1978.

10. Kamdar, M., "On the Mechanism of the Formation of White Layers on Steel Surfaces," U.S. Army ARRADCOM, Benet Weapons Laboratory, presented at ARO-sponsored Workshop II on Mechanisms of Erosion in Hot Flowing Media, 9-12 October 1979.
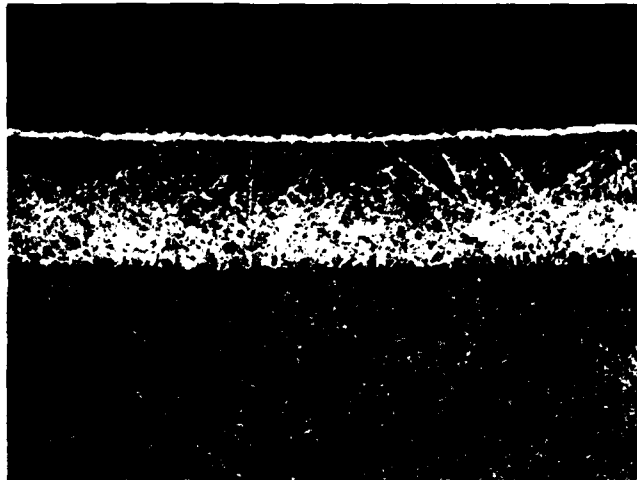
SAMPLE 11, RUN 45, 200 MAGNIFICATION

Figure 25 WHITE AND THERMALLY ALTERED LAYERS CREATED BY A TEST GAS
CONTAINING 2-1/2 PERCENT OXYGEN AND AT A PRESSURE OF 254 MPa

SAMPLE 20, RUN 54, 400 MAGNIFICATION

Figure 26 THERMALLY ALTERED LAYER CREATED BY A TEST GAS CONTAINING
10 PERCENT CARBON DIOXIDE AT A PRESSURE OF 308 MPa. NOTE THE
ABSENCE OF A PROMINENT WHITE LAYER

SAMPLE 1, RUN 32, 400 MAGNIFICATION

Figure 27 THERMALLY ALTERED LAYER CREATED BY A TEST GAS CONTAINING
45.5 PERCENT NITROGEN AT A PRESSURE OF 281 MPa. NOTE THE ABSENCE
OF A WHITE LAYER.

SPEC. 5 200X AT T.C.

0.0965 mm

$P_{MAX} = 280$ MPa
$T_{MAX} = 3700^{\circ}K$

PEAK + 2.4 msec

PEAK + 1 msec

PEAK SURF. TEMP.

TEMP $\sim {}^{\circ}K$

1665

1110

555

DEPTH – mm

0   0.025   0.05   0.075   0.1   0.125   0.15   0.175   0.2   0.225
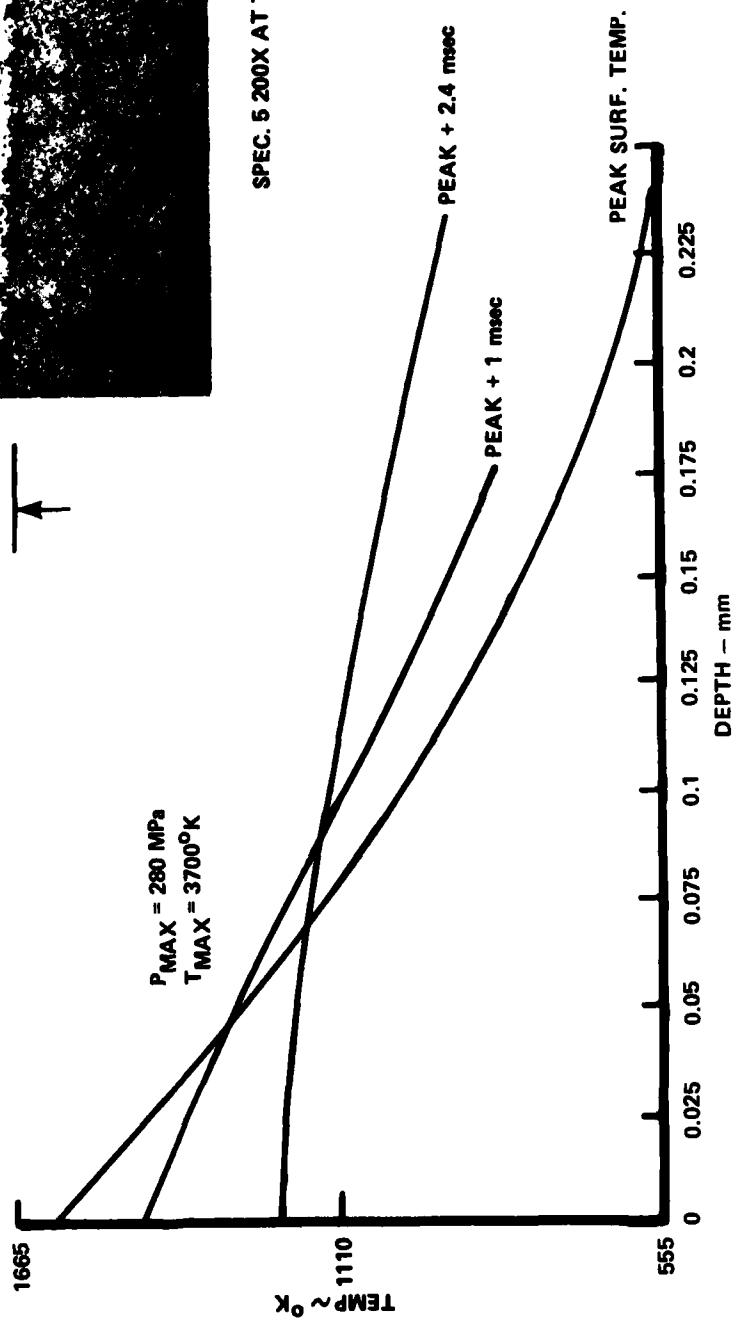
Figure 28 RELATIONSHIP BETWEEN THE HARD LAYER AND THE TEMPERATURE PROFILE

59

VI. CONCLUSIONS

This program is part of an ongoing effort to isolate the various phenomena that contribute to gun barrel erosion. Erosion of 4340 steel in an oxidizing atmosphere was the primary topic of investigation. This research led to the following conclusions and accomplishments:

1. Addition of small quantities of oxygen to the gas mixture was shown to increase the erosion of 4340 steel.

2. The increase in erosion was nearly linear with oxygen content which is indicative of diffusion controlled oxidation.

3. The addition of oxygen shifted the erosion threshold to less severe flow conditions.

4. An inert gas mixture produced no indication of surface melting at conditions comparable to the erosion threshold for a gas mixture containing 2 1/2 percent oxygen. This indicates that oxidation takes the form of a surface reaction rather than combustion of molten droplets.

5. Erosion in excess of that for an inert gas mixture was observed with gas mixtures containing carbon dioxide at sufficiently severe flow conditions and where the CO/CO_2 ratio was much less than 3.0.

6. The amount of erosion in the CO_2 atmosphere correlated with the calculated amount of oxygen at peak conditions assuming that the gas was in chemical equilibrium.

7. The correlation of erosion with equilibrium oxygen indicated that, in most cases, erosion was more severe in the gas containing carbon dioxide than that initially mixed with oxygen. The reason for the apparent increase in heating is not clear at present.

8. The erosion observed with carbon dioxide may be applicable to hot double base propellants such as M8.

9. Cracks were observed during virtually all tests except those with inert gases and were most prominent near the threshold of erosion where surface layers were thickest.

10. White layers were observed in an oxidizing atmosphere in contrast to the findings of Reference 10.

VII. REFERENCES

1. F.A. Vassallo, W.R. Brown, "Shock Tube Gun Melting Erosion Study," U.S. Army Ballistic Research Laboratory, ARRADCOM, Contract Report ARBRL-CR-00406, January 1979. (AD#A076219)

2. F.A. Vassallo, "Study of Wear and Erosion in the 60mm MC-AAAC Gun," Calspan Monthly Reports to ARRADCOM, Nos. 1 through 12, to 1 October 1978.

3. F.A. Vassallo, "Mathematical Models and Computer Routines Used in Evaluation of Caseless Ammunition Heat Transfer," Calspan Report No. GM-2948-Z-1, June 1971.

4. ASM Committee on Furnace Atmospheres, "Furnace Atmosphere and Carbon Control," ASM 1964, p. 2.

5. "Investigation of the Role of Carburization in Gun Barrel Erosion and Cracking," Bimonthly Progress Report No. 3, ARRADCOM Contract No. DAAK11-79-C-0049, November 1979.

6. Summerfield, et. al., "Erosion of Aluminum by High Pressure Propellant Gases," 10th JANNAF Combustion Meeting, CPIA Publication No. 243, August 1973.

7. Fisher and Cytron, "Influence of Combustion on Aluminum Cartridge Case Burnthrough," 10th JANNAF Combustion Meeting, CPIA Publication No. 243, August 1973.

8. Caveny, L., "Erosion of Steel by Combustion Gases," Presented at ARO sponsored Workshop II on Mechanisms of Erosion in Hot Flowing Media, 9-12 October 1979.

9. Kamdar, M., Campbell, A., and Brassard, T., "A Metallographic Study of White Layers in Gun Steel," U.S. Army ARRADCOM, Benet Weapons Laboratory Technical Report ARL CB-TR-78-12, August 1978.

10. Kamdar, M., "On the Mechanism of the Formation of White Layers on Steel Surfaces," U.S. Army ARRADCOM, Benet Weapons Laboratory, presented at ARO-sponsored Workshop II on Mechanisms of Erosion in Hot Flowing Media, 9-12 October 1979.

APPENDIX I

SHOCK TUBE GUN COMPUTER SIMULATION

Overview

The mathematical model described in this Appendix simulates the operation of the Shock Tube Gun. The simulation provides a complete description of the entire cycle of the Shock Tube Gun, beginning with release and subsequent acceleration of the piston by the high pressure driver gas. As the piston is accelerated through the driven tube, the simulation computes the increase in pressure and temperature of the test gas. In addition, the simulation evaluates the total temperature pressure and density in the plenum chamber and computes the flow through the test specimen. The heat flux to the specimen, the resulting temperature history at a location on the surface of the specimen and the temperature distribution normal to the surface are also calculated. Finally, the simulation calculates the travel of a projectile through the barrel.

The objective of this code is to provide a means for calculating test conditions for the purpose of establishing the initial driver pressure and gas mixture. Differences in the ballistic cycle of the Shock Tube Gun due to gas composition are reflected through differences in pressure and total heat input. A primary use of the code is to help distinguish between erosion due to melting and that due to chemical effects. This is done through computation of the convective heating to the sample without chemistry which provides a means for comparing tests within a test matrix on an equal basis as far as the inherent flow heating of the test gas. Thus, excess material removal from one gas mixture in comparison to another is likely due to chemical effects. This further allows estimates to be made of the effective heat input due to chemical effects. This can be done by comparing the heat input at the onset of erosion, or at points of equal erosion between inert and chemically active gases. The code enables the facility user to quantify levels of heating experienced.

The major assumption applied with formulating the code was that of quasi-steady operation. That is, pressure waves and other unsteady aspects of the event are not calculated. The pressure is assumed to be constant throughout the driver system and throughout the driven tube at any instant of time during the compression cycle.

The other limiting assumption that is currently employed in this code is that of a frozen gas composition whereby the initial gas composition is assumed to be maintained throughout the ballistic cycle. This assumption influences the resulting temperature and pressures to some extent in cases where chemical reactions and dissociation become important.

The individual gas constituents are assumed to be mixed uniformly. Furthermore, the parameters used by the Van der Waal equation of state for

an imperfect gas and the temperature dependency of specific heat are assumed to be satisfied through a linear averaging according to mole fraction.

The assumption of frozen gas constituency is an interim assumption that will be relieved when a chemical equilibrium gas code, also discussed in this appendix, can be combined with the STG model. At that time, the gas constituency will be assumed to be in thermal and chemical equilibrium at all times.

Model Description

Piston Motion

The piston motion is evaluated by applying a force balance on the piston. The accelerating force is applied by the high-pressure nitrogen driver, 500 to 700 psi, on the upstream side of the piston. The driven gas on the downstream side of the piston is initially at atmospheric pressure. It is assumed that no gas leaks past the piston. This is essentially verified, at least initially, by the maintenance of a perfect seal and the ability to evacuate the driven gas chamber. The nitrogen gas is represented by the ideal gas equation of state. The driver conditions are calculated from conservation of energy principles which are used to continually evaluate the amount of energy that is being transferred from the gas to the piston. As cited previously, this calculation is quasi-steady in that the unsteady expansion aspects are not considered and the pressure is assumed to be constant throughout the driver system.

The driver gas (nitrogen) properties are assumed to be constant over the range of temperature and pressure encountered during the compression cycle and are specified by:

Equation of state gas constant, $R = 55.0$ ft-lbf/lbm$°$R

Specific heat at constant volume, $c_v = 0.177$ Btu/lbm-$°$R

Specific heat at constant pressure, $c_p = 0.248$, and

Ratio of specific heats, $\gamma = 1.4$

The assumption of a perfect seal at the piston infers the existence of constant gas mass in the driver system during the cycle so that

$$P_D = \frac{m_D RT}{V} ,$$

where R and m are constants, the driver volume, V, is expressed in terms of piston travel and the initial volume by

$$V = V_o + A_T X_p ,$$

64

where A_T is the driver tube area.

Gas temperature is expressed in terms of internal energy where

$$E = c_V m_D T$$

and the energy change resulting from work expended through piston motion is:

$$\Delta E = p_D A_T \Delta x_p / 778. = c_V m_D \Delta T$$

The driver gas is initially at room temperature and it is assumed that the small temperature decrease during the cycle is not influenced by heat transfer.

Piston motion is evaluated by applying a force balance across the piston, taking into account the frictional drag,

$$F = A_t (p_D - p_T) - D$$

where p_D and p_T are the respective pressures of the driver and test gases, and D is the frictional drag of the piston which is expressed in terms of piston velocity by:

$$D = kV_p$$

Piston acceleration, velocity and travel follow:

$$a_p = \frac{F}{m}$$

$$\Delta V_p = a_p \Delta t$$

$$\Delta x_p = \frac{a_p}{2} \Delta t^2 + v_o \Delta t$$

Test Gas Compression

The compression of the test gas occurs as a result of piston motion. Energy that is added by virtue of the compression is calculated from the conservation of energy equation. The work done by the piston on the test gas during this compression is one term in this conservation of energy equation. Other terms include heat loss to the wall of the tube, which becomes important as the gas temperature rises. The other important equation is conservation of mass. The test chamber is not a closed chamber but contains

an exhaust port at the downstream end where the test sample is located. Thus, test gas is allowed to flow from the test chamber through the test sample. Therefore, the mass in the system is not constant by virtue of mass and energy flow from the driven tube and plenum chamber through the test sample. Terms in the conservation of energy and mass equations reflect this mass and energy loss.

The equation of state that applies to the test gas is the Van der Wall equation which includes terms to express the nonlinear relationship between pressure density and temperature. The terms for this equation are determined, as mentioned previously, by a linear averaging of the mole fraction of the test gas constituents.

The test gas specific heat is also assumed to be for non-perfect gas and is expressed in terms of a linear function of the gas temperature. The coefficients in this expression are also linear averages of the mole fraction of the test gas compositions. The test gas specific heat is expressed in terms of a secant function in which the product of the specific heat and the temperature yield the internal energy. This is contrary to a normal expression of specific heat whereby it is a tangent function so that the integral of the product of specific heat and temperature yield the internal energy. The technique used here provides rather simple yet effective means for evaluating the internal energy in a finite difference scheme with many time steps.

The Van der Waal equation of state used for the test gas is

$$p = \frac{RT}{v - \beta} + \frac{\alpha}{v^2}$$

where $\quad \dfrac{\alpha_i}{\beta_i} = \dfrac{27}{8} RT_{ci}, \quad \dfrac{\alpha_i}{\beta_i^2} = 27 p_{ci},$

v is the specific volume, and T_{ci} and p_{ci} are the critical temperature and pressure for the ith gas constituent. α and β are the average quantities based on the mole fraction of the ith constituent.

The specific heat at constant volume is defined by

$$c_v = ((c_{vo} + \Sigma_i X_{gi} \, c_v T_i (T - 460)^{e_i})T - \frac{\alpha \rho}{778}) \frac{1}{T_i}$$

where c_{vo} and $c_v T_i$ are the intercept and slope of the temperature-dependent specific heat, X_{gi} is the mole fraction of the ith constituent, and e_i is the temperature exponent in the curve fit relationship.

The test chamber mass balance is given by

$$m_T = m_{To} - \Delta m$$

66

where Δm is the mass flow through the test sample. Initially this flow is assumed to be negligible and the test chamber and barrel volumes are lumped together. When the projectile velocity exceeds 100 ft/sec, the calculation of flow through the test sample is initiated. This computation involves determination whether sonic or subsonic flow conditions exist within the test sample. The sonic static pressure is given by:

$$p^* = p_1 (1 + \frac{\gamma - 1}{2})^{-\gamma/(\gamma - 1)}$$

where p_1 is the test chamber pressure.

If p^* is greater than the barrel pressure, p_2, (downstream from the test sample) then sonic conditions exist and

$$\Delta m = p^* A_{12} (\frac{\gamma g}{RT^*})^{1/2} \Delta t,$$

where A_{12} is the test sample flow area, T^* is the sonic static temperature, and Δt is the computation time interval.

If subsonic conditions exist,

$$\Delta m = 8.02 A_{12} ((p_1 - p_2) \frac{p_1}{RT_1})^{1/2} \Delta t,$$

which is the equation for flow through a venturi in terms of the upstream and downstream line pressures.

The change in internal energy in the chamber over the calculation time interval is given by

$$\Delta E_1 = \frac{p_1 A_T \Delta x_p}{778} - c_V \Delta m T_1 \gamma$$

which represents the compression work due to the piston and the loss in enthalpy due to flow through the test sample. Heat transfer losses in the driven tube and chamber are not included in this analysis at present. The gas chamber temperature is defined by

$$T_1 = E_1 / c_V m_1$$

where E_1 is the current value of internal energy.

67

The Test Sample

The test sample is a straight channel with a rounded entrance. The flow through the channel is computed by either sonic or subconic conditions depending on the pressure at the inlet and outlet to the sample. The calculations provide the static flow conditions of pressure, temperature, and density in addition to the flow velocity over the surface of the sample. These conditions are in turn used in the equation that expresses turbulent heat flux to a flat plate. The heat flux is computed and then summed to yield a current level of total heat input. The heat flux to the surface is also applied to an unsteady heat conduction routine by which the surface temperature and the temperature distribution in the test sample are evaluated. These calculations are all performed within the same time step of the overall finite difference calculation.

The technique used to calculate heat flux to the test sample surface requires the flow velocity, density, and viscosity. The density and viscosity are evaluated on the basis of a reference temperature to take the temperature profile resulting from the boundary layer velocity distribution and sample surface temperature into account.

Mach number of flow through the test sample:

$$M = \left[\left(\left(\frac{p_1}{p_s} \right)^{\frac{\gamma - 1}{\gamma}} - 1 \right) \frac{2}{\gamma - 1} \right]^{1/2}$$

where p_s is the sonic static pressure if $M = 1$ or the downstream pressure, p_2 if the flow is subsonic.

Free stream static temperature:

$$T_e = T_1 (1 + (\frac{\gamma - 1}{2}) M^2)^{-1}$$

Free stream velocity:

$$U_e = [2gJ \gamma C_V (T_1 - T_e)]^{1/2}$$

Reference temperature:

$$T_{ref} = (T_e + T_{SAMP})/2 + \frac{0.11}{gJ} \frac{U_e^2}{c_V \gamma}$$

where T_{SAMP} is the test sample surface temperature.

Viscosity:

$$\mu = 7.0 \times 10^{-7} \, T_{ref}^{1.5} \, (T_{ref} + 198)^{-1}$$

Density:

$$\rho_{ref} = P_S \, (\beta P_S + RT_{ref})^{-1}$$

Turbulent flat plate heat flux at the location of the in-wall thermocouple:

$$Q = 0.052 (\rho_{ref} U_e)^{0.8} \mu^{0.2} \, c_v \gamma \, (T_1 - T_{SAMP})$$

The sample surface temperature is determined from the one-dimensional unsteady state heat conduction equation,

$$\frac{\partial T}{\partial t} = \alpha \frac{\partial^2 T}{\partial x^2}$$

with the surface boundary condition,

$$Q = K \frac{dT}{dX}$$

for X = 0, where Q is the heat flux to the sample surface. This equation does not consider the effects of cylindrical geometry.

A finite difference technique using a geometrical node grid spacing was incorporated into the Calspan code to solve the unsteady heat conduction equation. The general finite difference relationship is given by

$$\frac{\Delta T_i}{\Delta t} = \frac{2\alpha}{(F+1)\Delta x_{i-1}^2} \left(T_{i-1} - \frac{F+1}{F} T_i + \frac{1}{F} T_{i+1} \right)$$

where α is the thermal diffusivity
        T is the temperature rise
        t is the time interval
   Δx_{i-1} is the thickness of the i-1st grid, and
        F is the geometrical multiplier with the thickness of the ith grid being F times that of the i-1st grid.

The exposed surface boundary condition is satisfied by first determining a fictitious temperature in free space,

69

$$T_0 = 2q \frac{\Delta x_1}{K} + T_2$$

This temperature is then used to establish the surface temperature rise by

$$\frac{\Delta T_1}{\Delta t} = \frac{\alpha}{\Delta x_1{}^2} (T_0 - 2T_1 + T_2)$$

Barrel Flow

The flow through the barrel is expressed as an input of mass and energy to the volume between the test sample and the projectile. As mass and energy are accumulated, this is expressed in terms of pressure and temperature, which in turn provides the accelerating force for the projectile. In this calculation, the quasi-steady assumption of the previous calculation is relaxed by allowing pressure acting on the base of the projectile to be modified according to the Mach number of the flow at the base of the projectile. In this way, the unsteady expansion effects of the flow through the barrel is taken into account. The equation of state and the basic energy and mass conservation equations are the same as for the test gas in the driven tube. These equations are used to define "2" conditions in the barrel.

Projectile motion is calculated by an approximate technique that involves determination of the flow Mach number at the projectile base.

Specific enthalpy:

$$H_2 = \frac{E_2 \gamma}{M_g}$$

where M_g is the mass of gas contained in the barrel.

Static enthalpy at the projectile base:

$$H_{2_\infty} = 2.5 \times 10^4 H_2 - \frac{V_p{}^2}{2}$$

where V_p is the projectile velocity

Mach number:

$$M = V_p \{ (\gamma - 1) H_{2_\infty} \}^{-1/2}$$

The assumption is made that the pressure, p_2, is not the total pressure, but is a static pressure at the barrel origin.

It is further assumed that the difference in pressure between this location and the projectile base is equal to the difference between the pressure and the total pressure. This is expressed as a Mach number function:

$$\frac{P_{2_\infty}}{p_2^o} = \frac{p_2 - \Delta p}{p_2 + \Delta p} = \left(1 + \frac{\gamma-1}{2} M^2\right)^{-\gamma/\gamma-1}.$$

This allows the static pressure at the projectile base to be expressed in terms of the barrel origin pressure, p_2.

From this the projectile acceleration:

$$a_{pr} = 32.2 \, (p_{2_\infty} - p_r)/W_p$$

where p_r is the projectile resistance to motion, and W_p is the projectile weight, with $p_r = p_{r_o} + p_{r_x} X_{pr}$.

Projectile velocity change:

$$\Delta V_{pr} = a_{pr} \, \Delta t$$

Projectile displacement:

$$\Delta X_{pr} = V_{pr} \, \Delta t + a_{pr} \frac{\Delta t^2}{2}$$

71

```
C
C
C
C   LIST OF CONSTANTS AND VARIABLES USED IN THIS SHOCK TUBE GUN PROGRAM
C
C   DRIVER GAS PARAMETERS
C   PCH       INITIAL DRIVER PRESSURE   PSIA
C   VOL0      INITIAL VOLUME OF PROPELLING GAS - FT**3
C   T0        INITIAL PROPELLING GAS TEMPERATURE - DEG R
C   CVDVR     DRIVER GAS SPECIFIC HEAT - BTU/LBM-DEG R
C   RDVR      DRIVER GAS CONSTANT - FT-LBF/LBM-DEG R
C
C   PISTON PARAMETERS
C   AT        PISTON AREA - FT**2
C   KP1       DRAG RATE CONSTANT - LBF/FT
C   VELP      INITIAL PISTON VELOCITY - FT/SEC
C   WSHELL    PISTON WEIGHT - LBM
C   SHELRV    PISTON MASS DURING RETURN - LBM
C   XPMAX     MAX PISTON DISPLACEMENT - FT.
C
C   TEST GAS PARAMETERS
C   P20       INITIAL TEST GAS PRESSURE - PSIA
C   T20       INITIAL TEST GAS TEMPERATURE - DEG R
C   R2        TEST GAS CONSTANT - FT-LBF/LBM-DEG R
C   CV2       SPECIFIC HEAT OF TEST GAS- BTU/LBM-DEG R
C   CVT2      TEST GAS SPECIFIC HEAT
C   CVEXP     CURVE-FITTING EXPONENT
C   ALFA2     VANDERWAAL CONSTANT
C   BETA2     VANDERWAAL CONSTANT
C   GAM2      TEST GAS RATIO OF SPECIFIC HEATS
C
C   TEST VOLUME PARAMETERS
C   A2        TEST VOLUME AREA - FT**2
C   D3        DIAMETER OF TEST VOLUME EXIT - IN
C   CD2       FLOW COEFF. OF TEST VOLUME EXIT
C   VOL20     INITIAL VOLUME OF TEST GAS IN TUBE - FT**3
C   VOL2F     FINAL TEST VOLUME - FT**3
C
C   PROJECTILE PARAMETERS
C   BARL      BARREL LENGTH - FT
C   BORED     BORE DIAMETER-FT
C   PSTART    PRESSURE ABOVE WHICH PROJECTILE IS ALLOWED TO MOVE - LB/IN**2
C   RES0      Y-INTERCEPT OF PROJECTILE RESISTANCE FUNCTION - LBM
C   RESS      SLOPE OF PROJECTILE RESISTANCE FUNCTION - LBM/FT
C   RESC      CONSTANT RESISTANCE TERM AFTER FUNCTION L.T. RESC - LBM
C   VPROJ     INITIAL PROJECTILE VELOCITY - FT/SEC
C   VPROJ     PROJECTILE WEIGHT - LBM.
C   XPROJ     INITIAL PROJECTILE DISPLACEMENT - FT
C
C   TIME PARAMETERS
C   DELT      TIME INCREMENT - SEC
C   PRCI      NUMBER OF TIMES BETWEEN PRINT INTERVALS
C   TFO       LIMITING TIME - SEC
C
C
C
      READ (5,101) NUMBER
      DO 99 NM=1,NUMBER
      DIMENSION RG(9),CVG(9),CVTG(9),CVEXPG(9),ALFAG(9),BETAG(9),XG(9)
      DIMENSION G1(9),G2(9),G3(9),G4(9),G5(9)
      DIMENSION TNEW(40),TSAMP(40),DELX(40),DXNEW(40),DTEMP(40)
```

72

```
      REAL*4 M2,M20,M1,KP1
      DATA VOL0/31.5/,CVDVR/0.176/,RDVR/55.2/
      DATA AT/0.3068/,WSHELL/150.0/,SHELRV/150.0/,XPMAX/81.0/
      DATA A2/0.3068/,D3/0.5/,CD2/0.75/,VOL2F/0.00223/
      DATA BARL/15.0/,BORED/0.0984/,RESO/7200./,RESS/4320./,RESC/7200./
      DATA WPROJ/0.25/,VOL1F/0.082/,DOR12/0.5/
      JJ=1
      KK=1
      NN=0
      QFLUX=0.0
      UE=0.0
      R2=0.0
      CV2=0.0
      CVT2=0.0
      CVEXP=0.0
      ALFA2=0.0
      BETA2=0.0
      GAM2=0.0
      P20=14.7
      T20=530.0
      XPROJ=0.0
      VELP=0.0
      VPROJ=0.0
      VOL20=0.0
      DOR12=0.5
  100 FORMAT (8F10.5)
  101 FORMAT (I1)
  102 FORMAT (F5.2,5A3,6E10.3)
  103 FORMAT (12H1 INPUT DATA,T48,'TEST NO.',T59,I1)
  104 FORMAT (////T6,'TEST GAS MIXTURE BY MOLE FRACTION'/)
  105 FORMAT (/T6,F6.3,T17,5A3)
      READ (5,100) PCH,TO,KP1,PSTART,DELT,PRCI,TFO,FACTOR
      READ (5,101) NG
      WRITE (6,103) NM
      WRITE (6,104)
      DO 3 ID=1,NG
      READ (5,102) XG(ID),G1(ID),G2(ID),G3(ID),G4(ID),G5(ID),RG(ID),CVG(
     +ID),CVTG(ID),CVEXPG(ID),ALFAG(ID),BETAG(ID)
      WRITE (6,105) XG(ID),G1(ID),G2(ID),G3(ID),G4(ID),G5(ID)
      R2 = R2 + XG(ID)*RG(ID)
      CV2 = CV2 + XG(ID)*CVG(ID)
      ALFA2 = ALFA2 + XG(ID)*ALFAG(ID)
      BETA2 = BETA2 + XG(ID)*BETAG(ID)
    3 CONTINUE
      GAM2 = 1. + (R2/(778.*CV2))
      ABORE = 0.785* BORED**2
      CV=CVDVR
      DELTO=DELT
      DOR12=DOR12/12.0
      A12=0.7854*DOR12**2
      IPRC=IFIX(PRCI)
      IPRINT=0
      PCH=PCH*144.
      PCHP=PCH/144.
      P20=P20*144.0
      PARTIM = 0.
      PSTART=PSTART*144.
      QTOT=0.0
      RGAS=RDVR
      CP=RGAS/778.+CV
      GAM=CP/CV
```

73

```
      GM = PCH/(RGAS*T0)*VOL0
      E=GM*(CP-RGAS/778.)*T0
      TIME = 0.
      VMAX=XPMAX*AT
      XP=XPMAX
C  INITIAL CONDITIONS - UPSTREAM - FROM PISTON FACE TO TEST SAMPLE
      P1=P20
      VOL1=VOL1F+XP*A2
      T1=T20
      M1=P1*VOL1/R2/T1
      CVT2=0.0
      DO 1 J=1,NG
      CVT2=CVT2+XG(J)*CVTG(J)*(T1-460.0)**CVEXPG(J)
    1 CONTINUE
      E1=M1*(CV2+CVT2)*T1
      RHO1=M1/VOL1
      VV1=1.0/RHO1
C  INITIAL CONDITIONS - DOWNSTREAM - FROM TEST SAMPLE TO PROJECTILE BASE
      P2=P20
      VOL2=VOL2F+XPROJ*ABORE
      T2=T20
      M2=P2*VOL2/R2/T2
      CVT2=0.0
      DO 2 J=1,NG
      CVT2=CVT2+XG(J)*CVTG(J)*(T2-460.0)**CVEXPG(J)
    2 CONTINUE
      E2=M2*(CV2+CVT2)*T2
      RHO2=M2/VOL2
      VV2=1./RHO2
      WRITE (6,110)
  110 FORMAT  (///T6,'INITIAL CONDITIONS FOR TEST')
      WRITE(6,120)P20,PCH,AT,T20,T0,KP1,R2,RDVR,WSHELL,CV2,CVDVR,SHELRV,
     +CVT2,VOL0,XPMAX,CVEXP,PSTART,ALFA2,BARL,BETA2,A2,BORED,GAM2,D3,
     +DOR12,CD2,RES0,DELT,VOL20,RESS,PRCI,VOL2F,RESC,TF0,VOL1F,WPROJ
  120 FORMAT   (//T6,'P20 =',T17,F13.6,T31,'PSF' ,T48,'PCH =',T59,F13.6,
     +T73,'PSF' ,T90,'AT =',T101,F13.6,T115,'FT**2'//T6,'T20 =',T17,
     +F13.6,T31,'DEGR',T48,'T0 =',T59,F13.6,T73,'DEGR',T90,'KP1 =',T101,
     +F13.6,T115,'LBF/FT'//T6,'R2 =',T17,F13.6,T31,'FT-LBF/LBM-DEGR',
     +T48,'RDVR =',T59,F13.6,T73,'FT-LBF/LBM-DEGR',T90,'WSHELL =',T101,
     +F13.6,T115,'LBM'//T6,'CV2 =',T17,F13.6,T31,'BTU/LBM-DEGR',T48,
     +'CVDVR =',T59,F13.6,T73,'BTU/LBM-DEGR',T90,'SHELRV =',T101,F13.6,
     +T115,'LBM'//T6,'CVT2 =',T17,F13.6,T48,'VOL0 =',T59,F13.6,T73,
     +'FT**3',T90,'XPMAX =',T101,F13.6,T115,'FT'//T6,'CVEXP =',T17,
     +F13.6,T48,'PSTART =',T59,F13.6,T73,'PSF' //T6,'ALFA2 =',T17,F13.6,
     +T90,'BARL =',T101,F13.6,T115,'FT'//T6,'BETA2 =',T17,F13.6,T48,
     +'A2 =',T59,F13.6,T90,'BORED =',T101,F13.6,T115,'FT'//T6,'GAM2 =',
     +T17,F13.6,T48,'D3 =',T59,F13.6,T90,'DOR12 =',T101,F13.6,T115,'FT'/
     +/T48,'CD2 =',T59,F13.6,T90,'RES0 =',T101,F13.6,T115,'LBM'//T6,
     +'DELT =',T17,F13.6,T31,'SEC',T48,'VOL20 =',T59,F13.6,T73,'FT**3',
     +T90,'RESS =',T101,F13.6,T115,'LBM/FT'//T6,'PRCI =',T17,F13.6,T48,
     +'VOL2F =',T59,F13.6,T73,'FT**3',T90,'RESC =',T101,F13.6,T115,'LBM'
     +//T6,'TFO =',T17,F13.6,T31,'SEC',T48,'VOL1F =',T59,F13.6,T73,
     +'FT**3',T90,'WPROJ =',T101,F13.6,T115,'LBM'/////)
      DEPTH = 0.5/12.0
      XK = 19.3/3600.
      ALPHA = XK/57.6
      F=1.3
      DELX0=SQRT(ALPHA*DELT/0.25)
      SUMX=DELX0
      DELX(1)=DELX0
      DO 6 I=1,40
```

74

```fortran
      TSAMP(I)=T0
      TNEW(I)=T0
    6 CONTINUE
      DO 7 I=1,39
      DELX(I+1)=DELX(I)*F
      IF(SUMX.GE.DEPTH) GO TO 7
      SUMX=SUMX+DELX(I)
      KTEMP = I
    7 CONTINUE
      CONST1=ALPHA*2.0/(1.0+F)
      CONST2=(1.0+F)/F
      CONST3=1.0/F
      TZIP=QFLUX*2.0*DELX(1)/XK+TSAMP(2)
      NAMELIST/FIRST/DELX,KTEMP,TZIP
      WRITE (6,FIRST)
   10 CONTINUE
      T=T0
      RGAS=57.4+.333E-5*PCH
      CV=0.175+.183E-4*T
      CP=RGAS/778.+CV
      GAM=CP/CV
      IF(VELP.LT.-0.1) WSHELL=SHELRV
C COMPUTE THE DYNAMICS AND THERMODYNAMICS OF PISTON MOTION.
   24 XD=XPMAX-XP
      DRAG=KP1*ABS(VELP)
      FOVM=((PCH*AT-P1*A2)-DRAG)/WSHELL*32.17
   26 DVELP = FOVM * DELT
   28 VELP =VELP +DVELP
      IF(XP.LE.0.00001.AND.VELP.GT.0.0) VELP=0.0
      DXP=DELT*(VELP+FOVM*DELT/2.)
      XP=XP-DXP
      IF(XP.LE..00001) GO TO 99
      WORK = PCH * AT * DXP/778.
      E = E - WORK
   30 VOL=VOL0+AT*XD
      RHOCH = GM/VOL
      T = E/((CP-RGAS/778.)*GM)
      PCH = RHOCH*RGAS*T
C COMPUTE TEST GAS PROPERTIES.
      CVTX=0.0
      CVTY=0.0
      DO 31 J=1,NG
      CVTX=CVTX+XG(J)*CVTG(J)*(T2-460.0)**CVEXPG(J)
      CVTY=CVTY+XG(J)*CVTG(J)*(T1-460.0)**CVEXPG(J)
   31 CONTINUE
      CVY=((CV2+CVTY)*T1-ALFA2*RHO1/778.0)/T1
      CVX=((CV2+CVTX)*T2-ALFA2*RHO2/778.0)/T2
      RESIST = RESO + RESS * XPROJ
   32 IF(RESIST.LT.RESC) RESIST=RESC
      H2=E2*GAM2/M2
      H2INF=25000.*H2-VPROJ**2/2.
      XM2INF=VPROJ/SQRT((GAM2-1.0)*H2INF)
      FM=(1.0+(GAM2-1.0)/2.0*XM2INF**2)**(-GAM2/(GAM2-1.0))
      DELP=P2*(1.0-FM)/(1.0+FM)
   33 P20=P2+DELP
      P2INF=P2-DELP
      PFORCE = ABORE * (P2INF-RESIST)
      IF(PFORCE.LT.0.0) PFORCE=0.0
      IF(P2.LT.PSTART) PFORCE=0.0
      APROJ = PFORCE/WPROJ*32.17
      DXPROJ = VPROJ * DELT + APROJ * DELT**2/2.
```

```
35 XPROJ = XPROJ + DXPROJ
   IF(XPROJ.GE.BARL) GO TO 99
   V ⌐OJ = VPROJ + APROJ* DELT
   VOL1=VOL1F+XP*A2
   VOL2=VOL2F+XPROJ*ABORE
36 P1AVE=P1
   XM1=M1
   XM2=M2
   IPASS=0
   P1SAV=P1
   P2SAV=P2
37 CONTINUE
   IPASS=IPASS+1
   PSTAR=P1*(1.0+(GAM2-1.0)/2.0)**(-GAM2/(GAM2-1.0))
   TTOT=T1
   PS=PSTAR
   PTOT=P1
   IF(P20.GT.P1) GO TO 47
   IF(PSTAR.GE.P20) GO TO 38
   PS=P20
   DELTM1=8.02*A12*SQRT((P1-P20)*P1/R2/T1)*DELT
   GO TO 49
38 TSTAR=T1*2.0/(GAM2+1.0)
   DELTM1=PSTAR*A12*SQRT(GAM2*32.2/R2/TSTAR)*DELT
   GO TO 49
47 CONTINUE
   PSTAR=PSTAR*P20/P1
   TTOT=T2
   PS=PSTAR
   PTOT=P20
   IF(PSTAR.GE.P1) GO TO 48
   PS=P1
   DELTM1=-8.02*A12*SQRT((P20-P1)*P20/R2/T2)*DELT
   GO TO 49
48 TSTAR=T2*2.0/(GAM2+1.0)
   DELTM1=-PSTAR*A12*SQRT(GAM2*32.2/R2/TSTAR)*DELT
49 CONTINUE
   XM1=M1-DELTM1
   XM2=M2+DELTM1
   RHO1=XM1/VOL1
   RHO2=XM2/VOL2
   VV1=1.0/RHO1
   VV2=1./RHO2
   WORK=-ABORE*DXPROJ*P2INF/778.0-P2/288.*XPROJ*3.1416*BORED*DELT
C  P2/288. (P2 IS IN PSF) IS ASSUMED APPROXIMATELY EQUAL TO HEAT FLUX.
   IF(VPROJ.LT.100.) GO TO 58
   DELH=CVY*DELTM1*T1*GAM2
50 IF(DELTM1.LT.0.0) DELH= CVX*DELTM1*T2*GAM2
   EX=E2+WORK+DELH
   T2=EX/CVX/XM2
   PX=(R2*T2)/(VV2-BETA2)+ALFA2/VV2**2
   P2=(PX+P2SAV)/2.0
   EY=E1-DELH+P1AVE/778.0*A2*DXP
   T1=EY/CVV/XM1
   PY=(R2*T1)/(VV1-BETA2)+ALFA2/VV1**2
   P1=(PY+P1SAV)/2.0
54 DELP1=PY-P1
   P1AVE=P1+DELP1/2.0
   P20=P2+DELP
55 IF(IPASS.LT.3) GO TO 37
   E1=EY
```

```fortran
      E2=EX
      P1=PY
      P2=PX
      M1=XM1
      M2=XM2
      XMOR=SQRT(((PTOT/PS)**((GAM2-1.0)/GAM2)-1.0)*2.0/(GAM2-1.0))
      TE=TTOT/(1.0+(GAM2-1.0)/2.0*XMOR**2)
      UE=SQRT(5.0E4*CVY*GAM2*(TTOT-TE))
      TREF=(TE+TSAMP(1))/2.0+4.4E-6*UE**2/CVY/GAM2
      VIS=7.0E-7*TREF**1.5/(TREF+198.0)
      RHOREF=PS/(BETA2*PS+R2*TREF)
      QFLUX=0.052*(RHOREF*UE)**0.8*VIS**0.2*CVY*GAM2*(TTOT-TSAMP(1))
      IF(TSAMP(1).GT.3100.0) QFLUX=QFLUX*(TTOT-3100.0)/(TTOT-TSAMP(1))
      QFLUX = QFLUX*FACTOR
      TZIP=QFLUX*2.0*DELX(1)/XK+TSAMP(2)
      DTEMP(1)=ALPHA/(DELX(1)**2)*(TZIP-2.0*TSAMP(1)+TSAMP(2))
      DO 56 K=2,KTEMP
      DTEMP(K)=CONST1/(DELX(K-1)**2)*(TSAMP(K-1)-CONST2*TSAMP(K)+
     *   CONST3*TSAMP(K+1))
   56 CONTINUE
      DO 57 K=1,KTEMP
      TSAMP(K)=TSAMP(K)+DTEMP(K)*DELT
   57 CONTINUE
      TSAMP(KTEMP+1)=TSAMP(KTEMP-1)
      QTOT=QTOT+QFLUX*DELT
      IF(P20.GT.P1) UE=-UE
      GO TO 60
   58 CONTINUE
      VOL=VOL1+VOL2
      XMTOT=M1+M2
      ESUM=E1+E2+P1*A2*DXP/778.0 +WORK
      M1=XMTOT*VOL1/VOL
      M2=XMTOT*VOL2/VOL
      E1=ESUM*VOL1/VOL
      E2=ESUM*VOL2/VOL
      T1=ESUM/CVX/XMTOT
      T2=T1
      VVT=VOL/XMTOT
      P1=(R2*T1)/(VVT-BETA2)+ALFA2/VVT**2
      P2=P1
      RHO1=M1/VOL1
      RHO2=M2/VOL2
      VV1=1.0/RHO1
      VV2=1.0/RHO2
   60 CONTINUE
      IF (VOL1.GT.0.2*VMAX) GO TO 80
      IF(VOL1.LE.0.2*VMAX)DELT=0.1*DELTO
      IF(VOL1.LE.0.2*VMAX.AND.KK.EQ.1) GO TO 62
      IF(VOL1.LE.0.02*VMAX)DELT=0.01*DELTO
      IF(VOL1.LE.0.02*VMAX.AND.KK.EQ.2) GO TO 62
      GO TO 80
C    REVISE GRID SIZE DUE TO CHANGE IN TIME STEP.
   62 DELX0=SQRT(ALPHA*DELT/0.25)
      SUMX=DELX0
      DXNEW(1)=DELX0
      DO 64 I=2,40
      DXNEW(I)=DXNEW(I-1)*F
      IF(SUMX.GE.DEPTH) GO TO 64
      SUMX=SUMX+DXNEW(I)
      KNMAX = I
   64 CONTINUE
```

77

```
          XKOLD=DELX(1)
          XKNEW=0.0
          K=1
          KNEW=1
          A=(TZIP-TSAMP(2))/(2.0*DELX(K))
          B=(TSAMP(1)-TSAMP(2)-A*DELX(K))/DELX(K)**2
          TNEW(1)=TSAMP(1)
    66 KNEW=KNEW+1
          XKNEW=XKNEW+DXNEW(KNEW-1)
          TNEW(KNEW)=TSAMP(1)-(A*XKNEW+B*XKNEW**2)
          IF(XKNEW.LT.XKOLD)GO TO 66
    67 K=K+1
          XKOLD=XKOLD+DELX(K)
          A=(TSAMP(K-1)-TSAMP(K+1))/((F+1.0)*DELX(K-1))
          B=(TSAMP(K)-TSAMP(K+1)-A*DELX(K))/DELX(K)**2
    68 KNEW=KNEW+1
          XKNEW=XKNEW+DXNEW(KNEW-1)
          XDEL=XKNEW-XKOLD+DELX(K)
          TNEW(KNEW)=TSAMP(K)-(A*XDEL+B*XDEL**2)
          IF(XKNEW.LT.XKOLD.AND.KNEW+1.LE.KNMAX) GO TO 68
          IF(K+1.LE.KTEMP.AND.KNEW+1.LE.KNMAX) GO TO 67
          DO 70 I=1,KNMAX
          DELX(I)=DXNEW(I)
          TSAMP(I)=TNEW(I)
          TNEW(I)=T0
    70 CONTINUE
          KTEMP=KNMAX
          KK = KK+1
          NAMELIST/SECOND/DELX,KTEMP,TZIP,A,B
          WRITE (6,SECOND)
    80 CONTINUE
C  PRINT OUT COMPUTED RESULTS.
          IF (JJ.EQ.1) GO TO 88
    87 NN=1
          PARTIM=PARTIM+DELT
          IF(TIME.GT.TFO) GO TO 99
          IF( PRINT.LT.IPRC) GO TO 90
          GO TO 89
    88 WRITE (6,187)
   187 FORMAT (18H1 TABULATED OUTPUT)
          WRITE (6,188)
   188 FORMAT(///T6,'TIME',T20,'P1',T34,'T1',T48,'M1',T62,'VOL1',T76,'VEL
         +P',T90,'VPROJ',T104,'WORK',T118,'QFLUX'/T6,'PCH',T20,'P2',T34,'T2'
         +,T48,'M2',T62,'VOL2',T76,'XP',T90,'XPROJ',T104,'UE',T118,'QTOT'/
         +T4,'TSAMP(1)',T18,'TSAMP(2)',T32,'TSAMP(3)',T46,'TSAMP(4)',
         +T60,'TSAMP(5)',T74,'TSAMP(6)',T88,'TSAMP(7)',T102,'TSAMP(8)',
         +T116,'TSAMP(9)'//)
          JJ=JJ+1
    89 PCHP=PCH/144.
          P1P=P1/144.0
          P2P=P2/144.
          TIME=TIME+PARTIM
          PARTIM = 0.
          WRITE(6,190) TIME,P1P,T1,M1,VOL1,VELP,VPROJ,WORK,QFLUX,PCHP,P2P,T2
         +,M2,VOL2,XP,XPROJ,UE,QTOT,(TSAMP(I),I=1,9)
   190 FORMAT(9E14.6/9E14.6/9E14.6/)
          IF(NN.EQ.0) GO TO 87
          IPRINT = 0
    90 IPRINT=IPRINT+1
          GO TO 10
    99 CONTINUE


          STOP
          END
```

A sample printout of the STG program follows. Definitions of "Initial Condition" variables are given in the preceding program printout. However, some explanation of the "Tabulated Output" variables is required.

TIME	Time after piston release - seconds. TIME is initially zero and increases to a maximum value either when the projectile exits the barrel or when it equals a limiting value, i.e., TFO.
PCH	Driver gas pressure - psia. PCH is a prescribed maximum at TIME zero and decreases as the driver gas displaces the unlatched piston.
VOL1	Test gas volume included from piston face to test specimen inlet - ft^3. VOL1 is initially the entire volume of the driven tube but decreases to the volume of the test gas collection chamber when the piston has been fully displaced.
P1, T1, M1	Test gas pressure, temperature and mass associated with VOL1, measured in psia, °R and lbm, respectively.
VOL2	Test gas volume included from test specimen inlet to projectile base - ft^3. VOL2 has a minimum value of the test specimen bore volume at TIME zero and increases with projectile displacement to include the entire barrel volume.
P2, T2, M2	Test gas pressure, temperature and mass associated with VOL2, measured in psia, °R and lbm, respectively.
VELP, XP	Piston velocity and displacement - ft/sec, ft.
VPROJ, XPROJ	Projectile velocity and displacement - ft/sec, ft.
WORK	Work performed by driver gas on the driven piston, and by test gas on the projectile. During piston rebound, the program also computed negative work done on the piston by the test gas - ft-lbf.
UE	Test gas free stream velocity - ft/sec^2.
QFLUX	Test sample surface heat flux - Btu/ft^2-sec.
QTOT	Total integrated heat input to test sample surface - Btu/ft^2.
TSAMP	Test sample surface temperature - °R. TSAMP(1) is the computed temperature on the test sample surface. TSAMP(2) through TSAMP(9) are subsurface temperatures computed at depths printed in the nonlinear DELX array, which is amended when the time increment DELT is changed.

79

INPUT DATA   TEST NO. 1

TEST GAS MIXTURE BY MOLE FRACTION

  0.455   NITROGEN

  0.545   ARGON

INITIAL CONDITIONS FOR TEST

P20 =	2116.79980 PSF	PCH =	91872.0000 PSF	AT =	0.306800 FT**2
T20 =	530.000000 DEGR	TO =	535.000000 DEGR	KP1 =	6.000000 LBF/FT
R2 =	46.173813 FT-LBF/LBM-DEGR	RDVR =	55.199997 FT-LBF/LBM-DEGR	WSHELL =	150.000000 LBM
CV2 =	0.121737 BTU/LBM-DEGR	CVDVR =	0.176000 BTU/LBM-DEGR	SHELRV =	150.000000 LBM
CVT2 =	0.000669	VOLO =	31.500000 FT**3	XPMAX =	81.000000 FT
CVEXP =	0.0	PSTART =	7200.00000 PSF		
ALFA2 =	687.913330			BARL =	15.000000 FT
BETA2 =	0.017159	A2 =	0.306800	BORED =	0.098400 FT
GAM2 =	1.487521	D3 =	0.500000	DORI2 =	0.041667 FT
		CD2 =	0.750000	RESO =	7200.00000 LBM
DELT =	0.001000 SEC	VOL20 =	0.0 FT**3	RESS =	4320.00000 LBM/FT
PRC1 =	10.000000	VOL2F =	0.002230 FT**3	RESC =	7200.00000 LBM
TFO =	0.250000 SEC	VOL1F =	0.082000 FT**3	WPROJ =	0.250000 LBM

&FIRST
DELX= .610162970E-03, .793211395E-03, .103117409E-02; .134052646E-02, .174268196E-02, .226648500E-02, .294512860E-02,
.302866470E-02, .497726970E-02, .647043064E-02, .841155276E-02, .109360086E-01, .142154992E-01, .184801370E-01,
.240241624E-01, .312313922E-01, .406007841E-01, .527809868E-01, .686151981E-01, .891996622E-01, .115959466 ,
.150747180 , .195971191 , .254762352 , .331190825 , .430547774 , .559711764 , .727624834 ,
.945911705 , 1.22968388 , 1.59858799 , 2.07816315 , 2.70160961 , 3.51208973 , 4.56671388 ,
5.93542385 , 7.71604633 , 10.0308642 , 13.0401020 , 16.9621179 ,KTEMP=   12.TZIP= 535.000000
&END

TABULATED OUTPUT

TIME PCH TSAMP(1)	P1 P2 TSAMP(2)	T1 T2 TSAMP(3)	M1 M2 TSAMP(4)	VOL1 VOL2 TSAMP(5)	VELP XP TSAMP(6)	VPROJ XPROJ TSAMP(7)	WORK UE TSAMP(8)	QFLUX QTOT TSAMP(9)
0.0	0.147774E+02	0.530654E+03	0.215664E+01	0.249301E+02	0.590574E+01	0.0	0.0	0.0
0.635213E+03	0.147774E+02	0.530654E+03	0.192912E-03	0.223000E-02	0.809911E+02	0.0	0.0	0.0
0.535000E+03	0.535000E+03	0.535000E+03	0.535000E+03	0.535000E+03	0.535000E+03	0.535000E+03	0.535000E+03	0.535000E+03
0.110000E-01	0.148071E+02	0.531894E+03	0.215663E+01	0.248044E+02	0.641757E+02	0.0	0.0	0.0
0.632006E+03	0.148071E+02	0.531894E+03	0.193889E-03	0.223000E-02	0.805815E+02	0.0	0.0	0.0
0.535000E+03	0.535000E+03	0.535000E+03	0.535000E+03	0.535000E+03	0.535000E+03	0.535000E+03	0.535000E+03	0.535000E+03
0.210000E-01	0.151580E+02	0.534962E+03	0.215662E+01	0.245022E+02	0.121172E+03	0.0	0.0	0.0
0.623933E+03	0.151580E+02	0.534962E+03	0.196279E-03	0.223000E-02	0.795965E+02	0.0	0.0	0.0
0.535000E+03	0.535000E+03	0.535000E+03	0.535000E+03	0.535000E+03	0.535000E+03	0.535000E+03	0.535000E+03	0.535000E+03
0.310000E-01	0.155999E+02	0.539876E+03	0.215660E+01	0.240282E+02	0.176453E+03	0.0	0.0	0.0
0.611418E+03	0.155999E+02	0.539876E+03	0.200150E-03	0.223000E-02	0.780514E+02	0.0	0.0	0.0
0.535000E+03	0.535000E+03	0.535000E+03	0.535000E+03	0.535000E+03	0.535000E+03	0.535000E+03	0.535000E+03	0.535000E+03
0.409999E-01	0.162312E+02	0.546732E+03	0.215659E+01	0.233883E+02	0.229831E+03	0.0	0.0	0.0
0.596072E+03	0.162312E+02	0.546732E+03	0.205624E-03	0.223000E-02	0.759659E+02	0.0	0.0	0.0
0.535000E+03	0.535000E+03	0.535000E+03	0.535000E+03	0.535000E+03	0.535000E+03	0.535000E+03	0.535000E+03	0.535000E+03
0.509999E-01	0.170813E+02	0.555666E+03	0.215657E+01	0.225897E+02	0.280381E+03	0.0	0.0	0.0
0.575610E+03	0.170813E+02	0.555666E+03	0.212891E-03	0.223000E-02	0.733629E+02	0.0	0.0	0.0
0.535000E+03	0.535000E+03	0.535000E+03	0.535000E+03	0.535000E+03	0.535000E+03	0.535000E+03	0.535000E+03	0.535000E+03
0.609999E-01	0.181929E+02	0.566887E+03	0.215655E+01	0.216403E+02	0.328451E+03	0.0	0.0	0.0
0.553789E+03	0.181929E+02	0.566887E+03	0.222229E-03	0.223000E-02	0.702683E+02	0.0	0.0	0.0
0.535000E+03	0.535000E+03	0.535000E+03	0.535000E+03	0.535000E+03	0.535000E+03	0.535000E+03	0.535000E+03	0.535000E+03
0.709999E-01	0.196287E+02	0.580683E+03	0.215653E+01	0.205486E+02	0.373658E+03	0.0	0.0	0.0
0.530349E+03	0.196287E+02	0.580683E+03	0.234033E-03	0.223000E-02	0.667101E+02	0.0	0.0	0.0
0.535000E+03	0.535000E+03	0.535000E+03	0.535000E+03	0.535000E+03	0.535000E+03	0.535000E+03	0.535000E+03	0.535000E+03
0.809999E-01	0.214799E+02	0.597483E+03	0.215650E+01	0.193237E+02	0.415882E+03	0.0	0.0	0.0
0.505568E+03	0.214799E+02	0.597483E+03	0.248065E-03	0.223000E-02	0.627176E+02	0.0	0.0	0.0
0.535000E+03	0.535000E+03	0.535000E+03	0.535000E+03	0.535000E+03	0.535000E+03	0.535000E+03	0.535000E+03	0.535000E+03

0.909997E-01 0.230821E+02 0.617762E+03 0.216647E+01 0.179749E+02 0.465062E+03 0.0   0.0   0.0
0.481234E+03 0.230821E+02 0.617762E+02 0.267636E-03 0.223000E-02 0.683212E+02 0.0   0.0   0.0
0.535000E+03 0.535000E+03 0.535000E+03 0.535000E+03 0.535000E+03 0.535000E+03 0.535000E+03 0.535000E+03 0.535000E+03

0.101000E+00 0.270424E+02 0.642361E+03 0.215644E+01 0.165116E+02 0.491130E+03 0.0   0.0   0.0
0.456634E+03 0.270424E+02 0.642361E+02 0.291241E-03 0.223000E-02 0.536615E+02 0.0   0.0   0.0
0.535000E+03 0.535000E+03 0.535000E+03 0.535000E+03 0.535000E+03 0.535000E+03 0.535000E+03 0.535000E+03 0.535000E+03

0.111000E+00 0.312899E+02 0.672402E+03 0.216639E+01 0.149433E+02 0.524123E+03 0.0   0.0   0.0
0.432651E+03 0.312899E+02 0.672402E+02 0.321801E-03 0.223000E-02 0.404396E+02 0.0   0.0   0.0
0.535000E+03 0.535000E+03 0.535000E+03 0.535000E+03 0.535000E+03 0.535000E+03 0.535000E+03 0.535000E+03 0.535000E+03

0.121000E+00 0.371735E+02 0.709542E+03 0.216634E+01 0.132795E+02 0.563986E+03 0.0   0.0   0.0
0.409275E+03 0.371735E+02 0.709542E+02 0.362111E-03 0.223000E-02 0.430165E+02 0.0   0.0   0.0
0.535000E+03 0.535000E+03 0.535000E+03 0.535000E+03 0.535000E+03 0.535000E+03 0.535000E+03 0.535000E+03 0.535000E+03

0.130999E+00 0.456704E+02 0.756374E+03 0.215627E+01 0.115299E+02 0.580661E+03 0.0   0.0   0.0
0.387012E+03 0.456704E+02 0.756374E+02 0.417044E-03 0.223000E-02 0.373138E+02 0.0   0.0   0.0
0.535000E+03 0.535000E+03 0.535000E+03 0.535000E+03 0.535000E+03 0.535000E+03 0.535000E+03 0.535000E+03 0.535000E+03

0.140999E+00 0.586750E+02 0.817162E+03 0.215616E+01 0.970460E+01 0.603973E+03 0.296248E+01 -0.246052E-03 0.0
0.365900E+03 0.586750E+02 0.817162E+03 0.504741E-03 0.227177E-02 0.313644E+02 0.549585E-02 0.0   0.0
0.535000E+03 0.535000E+03 0.535000E+03 0.535000E+03 0.535000E+03 0.535000E+03 0.535000E+03 0.535000E+03 0.535000E+03

0.160999E+00 0.803075E+02 0.899489E+03 0.215677E+01 0.781459E+01 0.623507E+03 0.267041E+02 -0.416372E-02 0.0
0.346029E+03 0.803075E+02 0.899489E+03 0.884129E-03 0.320494E-02 0.262040E+02 0.128268E+00 0.0   0.0
0.535000E+03 0.535000E+03 0.535000E+03 0.535000E+03 0.535000E+03 0.535000E+03 0.535000E+03 0.535000E+03 0.535000E+03

0.160999E+00 0.121175E+03 0.101843E+04 0.215411E+01 0.587309E+01 0.638250E+03 0.779630E+02 -0.231366E-01 0.0
0.327459E+03 0.121175E+03 0.101843E+04 0.263904E-02 0.692260E-02 0.180756E+02 0.617382E+00 0.0   0.0
0.535000E+03 0.535000E+03 0.535000E+03 0.535000E+03 0.535000E+03 0.535000E+03 0.535000E+03 0.535000E+03 0.535000E+03

&SECOND
DELX= .192950465E-03, .250036437E-03, .326085836E-03, .423911260E-03, .551084289E-03, .716408947E-03, .931330957E-03,
   .121072936E-02, .157394703E-02, .204612990E-02, .265986717E-02, .345796608E-02, .449533761E-02, .584393367E-02,
   .769710744E-02, .987623269E-02, .406007841E-01, .627809868E-01, .686161981E-01, .891996622E-01, .115959466   ,
   .150747180   , .196971191   , .254762362   , .331190826   , .430647774   , .659711754   , .727624834   ,
   .945911706   , 1.22968388   , 1.59850799   , 2.07816316   , 2.70160961   , 3.51208973   , 4.56571388   ,
   5.93542385   , 7.71604633   , 10.0308642   , 13.0401020   , 16.9521179   , KTEMP=   16, TZIP= 657.743164   , A=
   .0   , B= .0
&END
0.165599E+00 0.162474E+03 0.111238E+04 0.215214E+01 0.478985E+01 0.643436E+03 0.117539E+03 -0.444277E-02 0.105857E+03
0.316720E+03 0.129506E+03 0.979003E+03 0.449806E-02 0.110474E-01 0.153460E+02 0.116007E+01 0.862816E+03 0.282641E+00
0.545294E+03 0.541943E+03 0.538840E+03 0.536449E+03 0.535316E+03 0.535147E+03 0.535115E+03 0.534996E+03 0.535041E+03

0.166599E+00 0.172628E+03 0.113291E+04 0.215160E+01 0.469233E+01 0.644019E+03 0.123036E+03 -0.496014E-02 0.117468E+03
0.315026E+03 0.133937E+03 0.980013E+03 0.503087E-02 0.119647E-01 0.147012E+02 0.128074E+01 0.920227E+03 0.394815E+00
0.547830E+03 0.544081E+03 0.540820E+03 0.537660E+03 0.535036E+03 0.535883E+03 0.536225E+03 0.535013E+03 0.535036E+03

0.167599E+00 0.183908E+03 0.115472E+04 0.215101E+01 0.439466E+01 0.644483E+03 0.130269E+03 -0.554197E-02 0.130003E+03
0.313345E+03 0.138970E+03 0.983460E+03 0.561900E-02 0.129302E-01 0.140669E+02 0.140777E+01 0.978129E+03 0.519129E+00
0.550610E+03 0.546338E+03 0.542301E+03 0.538911E+03 0.536716E+03 0.535883E+03 0.536291E+03 0.535034E+03 0.535033E+03

0.168699E+00 0.196496E+03 0.117793E+04 0.215036E+01 0.419560E+01 0.644819E+03 0.136890E+03 -0.619503E-02 0.144043E+03
0.311690E+03 0.144675E+03 0.989009E+03 0.626642E-02 0.139464E-01 0.134122E+02 0.164133E+01 0.102961E+04 0.656672E+00
0.553373E+03 0.548731E+03 0.544183E+03 0.540236E+03 0.537446E+03 0.536048E+03 0.536360E+03 0.535060E+03 0.535031E+03

0.169599E+00 0.210614E+03 0.120270E+04 0.214964E+01 0.399099E+01 0.645014E+03 0.143762E+03 -0.692902E-02 0.159614E+03
0.310028E+03 0.150772E+03 0.996628E+03 0.697085E-02 0.150117E-01 0.127672E+02 0.168163E+01 0.108443E+04 0.809232E+00
0.556467E+03 0.551297E+03 0.546187E+03 0.541647E+03 0.538284E+03 0.536262E+03 0.536437E+03 0.535084E+03 0.535031E+03

0.170699E+00 0.226632E+03 0.122921E+04 0.214886E+01 0.380109E+01 0.646051E+03 0.160912E+03 -0.776655E-02 0.177129E+03
0.308391E+03 0.157618E+03 0.100600E+04 0.776215E-02 0.161313E-01 0.121222E+02 0.182893E+01 0.114059E+04 0.978304E+00
0.559806E+03 0.554066E+03 0.548340E+03 0.543167E+03 0.539164E+03 0.536694E+03 0.535547E+03 0.535114E+03 0.535032E+03

0.171599E+00 0.244691E+03 0.125769E+04 0.214799E+01 0.360321E+01 0.644914E+03 0.168434E+03 -0.869356E-02 0.196966E+03
0.306770E+03 0.165196E+03 0.101750E+04 0.862546E-02 0.173067E-01 0.114772E+02 0.198356E+01 0.119861E+04 0.116613E+01
0.563476E+03 0.557085E+03 0.550674E+03 0.544816E+03 0.540156E+03 0.537150E+03 0.536690E+03 0.535150E+03 0.535034E+03

0.172599E+00 0.265212E+03 0.128838E+04 0.214703E+01 0.340540E+01 0.644580E+03 0.166396E+03 -0.976021E-02 0.219581E+03
0.306163E+03 0.173617E+03 0.103116E+04 0.967830E-02 0.185408E-01 0.108325E+02 0.214593E+01 0.126864E+04 0.137528E+01
0.567532E+03 0.560402E+03 0.553227E+03 0.546617E+03 0.541262E+03 0.537686E+03 0.535871E+03 0.535195E+03 0.535039E+03

0.173599E+00 0.288932E+03 0.132159E+04 0.214597E+01 0.320774E+01 0.644023E+03 0.174880E+03 -0.109819E-01 0.245547E+03
0.303572E+03 0.183020E+03 0.104717E+04 0.106320E-01 0.198374E-01 0.101882E+02 0.231652E+01 0.132144E+04 0.160893E+01
0.572062E+03 0.564076E+03 0.556039E+03 0.548596E+03 0.542490E+03 0.538302E+03 0.536093E+03 0.535251E+03 0.535046E+03

0.174599E+00 0.316439E+03 0.135768E+04 0.214480E+01 0.301029E+01 0.643211E+03 0.184022E+03 -0.123912E-01 0.275586E+03
0.301996E+03 0.193600E+03 0.106879E+04 0.118036E-01 0.212010E-01 0.954464E+01 0.249692E+01 0.138744E+04 0.187052E+01
0.677131E+03 0.568101E+03 0.559160E+03 0.550784E+03 0.543881E+03 0.539003E+03 0.536368E+03 0.535320E+03 0.535055E+03

0.175599E+00 0.348032E+03 0.139706E+04 0.214349E+01 0.282310E+01 0.642106E+03 0.193932E+03 -0.140296E-01 0.310625E+03
0.300437E+03 0.205620E+03 0.108734E+04 0.131080E-01 0.226360E-01 0.890206E+01 0.268482E+01 0.145720E+04 0.21647
0.582082E+03 0.572801E+03 0.562661E+03 0.553216E+03 0.545384E+03 0.539793E+03 0.536669E+03 0.535404E+03 0.535068E+03

0.176599E+00 0.386699E+03 0.144034E+04 0.214202E+01 0.261641E+01 0.640660E+03 0.204785E+03 -0.159519E-01 0.351875E+03
0.298894E+03 0.219119E+03 0.111224E+04 0.145684E-01 0.241514E-01 0.826079E+01 0.288408E+01 0.153142E+04 0.243766E+01
0.589453E+03 0.578044E+03 0.566683E+03 0.555937E+03 0.547062E+03 0.540662E+03 0.537030E+03 0.535505E+03 0.535084E+03

0.177599E+00 0.432247E+03 0.148015E+04 0.214038E+01 0.242010E+01 0.638809E+03 0.216784E+03 -0.182302E-01 0.409947E+03
0.297370E+03 0.234744E+03 0.114104E+04 0.162128E-01 0.257827E-01 0.762120E+01 0.309476E+01 0.161096E+04 0.287579E+01
0.697029E+03 0.584047E+03 0.571048E+03 0.559001E+03 0.548942E+03 0.541661E+03 0.537445E+03 0.535624E+03 0.535105E+03

0.178599E+00 0.487480E+03 0.154134E+04 0.213861E+01 0.222461E+01 0.636475E+03 0.230188E+03 -0.209622E-01 0.459993E+03
0.295863E+03 0.252073E+03 0.117441E+04 0.180756E-01 0.274803E-01 0.698374E+01 0.331811E+01 0.169683E+04 0.330827E+01
0.606880E+03 0.590903E+03 0.576161E+03 0.562247E+03 0.551069E+03 0.542805E+03 0.537910E+03 0.535765E+03 0.535130E+03

0.179599E+00 0.555707E+03 0.160117E+04 0.213683E+01 0.202906E+01 0.633566E+03 0.244938E+03 -0.233410E-01 0.535208E+03
0.294375E+03 0.262673E+03 0.119901E+04 0.197834E-01 0.292864E-01 0.634096E+01 0.366560E+01 0.176524E+04 0.380774E+01
0.616349E+03 0.599115E+03 0.582070E+03 0.566454E+03 0.553479E+03 0.544072E+03 0.538458E+03 0.535930E+03 0.535161E+03

81

```
0.180599E+00  0.641450E+03  0.166904E+04  0.213513E+01  0.183613E+01  0.629909E+03  0.259447E+03 -0.266437E-01  0.632499E+03
0.292900E+03  0.270016E+03  0.120311E+04  0.214430E-01  0.311719E-01  0.571752E+01  0.380774E+01  0.179617E+04  0.439447E+01
0.629203E+03  0.608918E+03  0.589069E+03  0.571059E+03  0.556227E+03  0.645506E+03  0.539070E+03  0.536122E+03  0.535199E+03

0.181599E+00  0.751546E+03  0.174685E+04  0.213321E+01  0.164369E+01  0.625345E+03  0.274312E+03 -0.285096E-01  0.768508E+03
0.291463E+03  0.283006E+03  0.122860E+04  0.233670E-01  0.332000E-01  0.609028E+01  0.407457E+01  0.184235E+04  0.509347E+01
0.648136E+03  0.620916E+03  0.597485E+03  0.576489E+03  0.569399E+03  0.547137E+03  0.539766E+03  0.536344E+03  0.535245E+03

0.182599E+00  0.896691E+03  0.183729E+04  0.213098E+01  0.145296E+01  0.619591E+03  0.289994E+03 -0.321646E-01  0.925820E+03
0.290042E+03  0.300323E+03  0.126705E+04  0.255864E-01  0.353439E-01  0.446826E+01  0.435662E+01  0.189512E+04  0.593990E+01
0.665287E+03  0.635072E+03  0.607792E+03  0.582998E+03  0.563113E+03  0.549009E+03  0.540558E+03  0.536599E+03  0.535299E+03

0.183599E+00  0.109442E+04  0.194418E+04  0.212837E+01  0.126407E+01  0.612250E+03  0.307239E+03 -0.369531E-01  0.115478E+04
0.288640E+03  0.324478E+03  0.132162E+04  0.281933E-01  0.376123E-01  0.385291E+01  0.465507E+01  0.195633E+04  0.698541E+01
0.691421E+03  0.654960E+03  0.620677E+03  0.590944E+03  0.567529E+03  0.651180E+03  0.541463E+03  0.536892E+03  0.535362E+03

0.184599E+00  0.137511E+04  0.207317E+04  0.212523E+01  0.107792E+01  0.602711E+03  0.327070E+03 -0.434308E-01  0.148001E+04
0.287204E+03  0.358204E+03  0.139658E+04  0.313245E-01  0.400209E-01  0.572872E+01  0.497196E+01  0.202865E+04  0.830911E+01
0.726393E+03  0.679984E+03  0.637193E+03  0.600856E+03  0.572872E+03  0.563730E+03  0.542506E+03  0.537228E+03  0.535436E+03

0.185599E+00  0.179538E+04  0.223303E+04  0.212136E+01  0.895257E+00  0.589979E+03  0.351011E+03 -0.525581E-01  0.196437E+04
0.285955E+03  0.406151E+03  0.149901E+04  0.351966E-01  0.428947E-01  0.266077E+01  0.531058E+01  0.211620E+04  0.100386E+02
0.775091E+03  0.714028E+03  0.659034E+03  0.613649E+03  0.579479E+03  0.556774E+03  0.543716E+03  0.537615E+03  0.535523E+03

0.186599E+00  0.247111E+04  0.243017E+04  0.211637E+01  0.717346E+00  0.572311E+03  0.381376E+03 -0.661407E-01  0.273126E+04
0.284670E+03  0.476075E+03  0.164099E+04  0.401780E-01  0.453730E-01  0.207008E+01  0.567611E+01  0.222553E+04  0.123936E+02
0.846511E+03  0.762521E+03  0.689090E+03  0.630354E+03  0.587064E+03  0.560477E+03  0.545137E+03  0.538061E+03  0.535624E+03

0.187599E+00  0.367063E+04  0.271409E+04  0.210959E+01  0.546266E+00  0.646339E+03  0.422122E+03 -0.879701E-01  0.404949E+04
0.283443E+03  0.587845E+03  0.184474E+04  0.469553E-01  0.484183E-01  0.151326E+01  0.607676E+01  0.236798E+04  0.157863E+02
0.958039E+03  0.836023E+03  0.732741E+03  0.653596E+03  0.598873E+03  0.565093E+03  0.546832E+03  0.538580E+03  0.535741E+03
&SECOND
DELX=  .610162970E-04,  .793211366E-04,  .103117403E-03,  .134052534E-03,  .174268178E-03,  .226548495E-03,  .294512835E-03,
       .382066245E-03,  .497725792E-03,  .647043111E-03,  .841155415E-03,  .109350123E-02,  .142155075E-02,  .184801477E-02,
       .240241759E-02,  .312314089E-02,  .406007841E-02,  .527809560E-02,  .686151907E-02,  .891996920E-02,  .115959495E-01,
       .150747180    ,  .195971191    ,  .254762352    ,  .331190825    ,  .430547774    ,  .559711754    ,  .727624834    ,
       .945911705    ,  1.22960308    ,  1.59858799    ,  2.07816315    ,  2.70160961    ,  3.51208973    ,  4.56571388    ,
       5.93542385    ,  7.71604633    ,  10.0308542    ,  13.0401020    ,  16.9521179    ,  .KTEMP=           21.TZIP=  1188.80737    ,A=
       .0            ,B=   .0
&END
0.187879E+00  0.435734E+04  0.283775E+04  0.210637E+01  0.485287E+00  0.533311E+03  0.441198E+03 -0.101358E-01  0.480287E+04
0.282932E+03  0.644020E+03  0.194021E+04  0.501674E-01  0.496316E-01  0.131449E+01  0.623639E+01  0.243272E+04  0.174456E+02
0.101768E+04  0.966114E+03  0.907734E+03  0.844359E+03  0.780467E+03  0.720348E+03  0.663222E+03  0.616758E+03  0.589869E+03

0.187979E+00  0.458050E+04  0.287526E+04  0.210541E+01  0.468997E+00  0.529287E+03  0.446901E+03 -0.105111E-01  0.503841E+04
0.282816E+03  0.667717E+03  0.196910E+04  0.511252E-01  0.499690E-01  0.126140E+01  0.628078E+01  0.245156E+04  0.179396E+02
0.103510E+04  0.981227E+03  0.920553E+03  0.855102E+03  0.788441E+03  0.724969E+03  0.666618E+03  0.619139E+03  0.590251E+03

0.188079E+00  0.482207E+04  0.291427E+04  0.210441E+01  0.452836E+00  0.525045E+03  0.452837E+03 -0.109119E-01  0.528972E+04
0.282701E+03  0.681427E+03  0.199950E+04  0.521262E-01  0.503109E-01  0.120872E+01  0.632577E+01  0.247107E+04  0.184571E+02
0.105414E+04  0.997578E+03  0.934199E+03  0.866051E+03  0.796570E+03  0.730133E+03  0.670112E+03  0.621481E+03  0.590741E+03

0.188179E+00  0.508409E+04  0.295487E+04  0.210335E+01  0.436807E+00  0.520565E+03  0.459021E+03 -0.113407E-01  0.555917E+04
0.282586E+03  0.701480E+03  0.203126E+04  0.531735E-01  0.506574E-01  0.115640E+01  0.637135E+01  0.249130E+04  0.190006E+02
0.107443E+04  0.101505E+04  0.948672E+03  0.877482E+03  0.808000E+03  0.735701E+03  0.673742E+03  0.623808E+03  0.591327E+03

0.188279E+00  0.536891E+04  0.299717E+04  0.210225E+01  0.420921E+00  0.515829E+03  0.465471E+03 -0.118004E-01  0.584891E+04
0.282473E+03  0.722847E+03  0.206456E+04  0.542709E-01  0.510007E-01  0.110470E+01  0.641757E+01  0.251229E+04  0.195722E+02
0.109609E+04  0.103366E+04  0.964021E+03  0.889514E+03  0.813826E+03  0.741619E+03  0.677525E+03  0.626141E+03  0.592002E+03

0.188379E+00  0.567920E+04  0.304128E+04  0.210110E+01  0.405186E+00  0.510812E+03  0.472205E+03 -0.122942E-01  0.616107E+04
0.282361E+03  0.745664E+03  0.209952E+04  0.554224E-01  0.513650E-01  0.105341E+01  0.646445E+01  0.253409E+04  0.201740E+02
0.111918E+04  0.105347E+04  0.980312E+03  0.902227E+03  0.823115E+03  0.747873E+03  0.681475E+03  0.628498E+03  0.592756E+03

0.188479E+00  0.601801E+04  0.308730E+04  0.209988E+01  0.389610E+00  0.505490E+03  0.479242E+03 -0.128255E-01  0.649795E+04
0.282250E+03  0.770036E+03  0.213623E+04  0.566326E-01  0.517265E-01  0.100264E+01  0.651201E+01  0.255673E+04  0.208083E+02
0.114302E+04  0.107457E+04  0.997624E+03  0.915688E+03  0.832916E+03  0.754468E+03  0.685598E+03  0.630895E+03  0.593583E+03

0.188579E+00  0.638984E+04  0.313539E+04  0.209860E+01  0.374205E+00  0.499834E+03  0.486607E+03 -0.133986E-01  0.686204E+04
0.282140E+03  0.796156E+03  0.217484E+04  0.579063E-01  0.520936E-01  0.952420E+00  0.656030E+01  0.258028E+04  0.214778E+02
0.117015E+04  0.109708E+04  0.101604E+04  0.929969E+03  0.843275E+03  0.761418E+03  0.689906E+03  0.633347E+03  0.594481E+03

0.188679E+00  0.679573E+04  0.318565E+04  0.209726E+01  0.358980E+00  0.493812E+03  0.494322E+03 -0.140181E-01  0.725615E+04
0.282032E+03  0.824198E+03  0.221651E+04  0.592493E-01  0.524663E-01  0.902803E+00  0.660934E+01  0.260480E+04  0.221054E+02
0.119832E+04  0.112112E+04  0.103567E+04  0.946138E+03  0.854241E+03  0.768748E+03  0.694412E+03  0.635866E+03  0.595445E+03

0.188779E+00  0.724334E+04  0.323828E+04  0.209593E+01  0.343947E+00  0.487388E+03  0.502416E+03 -0.146894E-01  0.768337E+04
0.281925E+03  0.854357E+03  0.225840E+04  0.606678E-01  0.528450E-01  0.853803E+00  0.665917E+01  0.263033E+04  0.229341E+02
0.122862E+04  0.114684E+04  0.105662E+04  0.961276E+03  0.868863E+03  0.776477E+03  0.699128E+03  0.638464E+03  0.596473E+03

0.188878E+00  0.773700E+04  0.329334E+04  0.209433E+01  0.329119E+00  0.480522E+03  0.510918E+03 -0.154188E-01  0.814712E+04
0.281820E+03  0.886075E+03  0.230367E+04  0.621807E-01  0.532301E-01  0.805472E+00  0.670982E+01  0.265694E+04  0.237276E+02
0.126092E+04  0.117430E+04  0.107900E+04  0.978469E+03  0.878197E+03  0.784461E+03  0.704070E+03  0.641152E+03  0.597555E+03

0.188978E+00  0.828289E+04  0.335109E+04  0.209273E+01  0.314510E+00  0.473168E+03  0.519864E+03 -0.162133E-01  0.865118E+04
0.281716E+03  0.922006E+03  0.235182E+04  0.637599E-01  0.536217E-01  0.757857E+00  0.676135E+01  0.268471E+04  0.245696E+02
0.129576E+04  0.120393E+04  0.110295E+04  0.996811E+03  0.891302E+03  0.793271E+03  0.709254E+03  0.643940E+03  0.598720E+03

0.189078E+00  0.888815E+04  0.341165E+04  0.209104E+01  0.300137E+00  0.465272E+03  0.829288E+03 -0.170811E-01  0.919970E+04
0.281614E+03  0.960089E+03  0.240217E+04  0.654503E-01  0.540204E-01  0.711009E+00  0.681380E+01  0.271369E+04  0.254644E+02
0.133323E+04  0.123660E+04  0.112862E+04  0.101641E+04  0.905247E+03  0.802403E+03  0.714700E+03  0.646839E+03  0.599939E+03

0.189178E+00  0.956100E+04  0.347522E+04  0.208923E+01  0.286018E+00  0.456776E+03  0.539235E+03 -0.180317E-01  0.979720E+04
0.281514E+03  0.100137E+04  0.245584E+04  0.672499E-01  0.544264E-01  0.664986E+00  0.686722E+01  0.274395E+04  0.264168E+02
0.137363E+04  0.126994E+04  0.115617E+04  0.103737E+04  0.920104E+03  0.812084E+03  0.720429E+03  0.649860E+03  0.601221E+03

0.189278E+00  0.103109E+05  0.354197E+04  0.208731E+01  0.272171E+00  0.447611E+03  0.549750E+03 -0.190762E-01  0.104485E+05
0.281416E+03  0.104634E+04  0.251277E+04  0.691702E-01  0.548402E-01  0.619852E+00  0.692166E+01  0.277557E+04  0.274318E+02
0.141723E+04  0.130863E+04  0.118579E+04  0.105983E+04  0.938987E+03  0.822355E+03  0.726462E+03  0.653014E+03  0.602569E+03
```

82

```
0.189370E+00  0.111469E+05  0.361209E+04  0.200525E+01  0.280018E+00  0.437700E+03  0.560086E+03 -0.202274E-01  0.111589E+05
0.201320E+03  0.109542E+04  0.267324E+04  0.712239E-01  0.552222E-01  0.675679E+00  0.697719E+01  0.280061E+04  0.201616E+02
0.144434E+04  0.134633E+04  0.121760E+04  0.100393E+04  0.982894E+03  0.833269E+03  0.732026E+03  0.656313E+03  0.603984E+03

0.189470E+00  0.120872E+05  0.368074E+04  0.200305E+01  0.243305E+00  0.426955E+03  0.572702E+03 -0.215004E-01  0.119335E+05
0.201226E+03  0.114912E+04  0.263763E+04  0.734267E-01  0.556029E-01  0.512646E+00  0.703385E+01  0.284313E+04  0.296730E+02
0.151630E+04  0.139919E+04  0.126200E+04  0.110063E+04  0.971010E+03  0.844082E+03  0.739549E+03  0.659768E+03  0.605460E+03

0.189570E+00  0.131400E+05  0.376307E+04  0.200065E+01  0.232499E+00  0.415274E+03  0.586264E+03 -0.229126E-01  0.127770E+05
0.201134E+03  0.120004E+04  0.270598E+04  0.767914E-01  0.561329E-01  0.490543E+00  0.709174E+01  0.287919E+04  0.309121E+02
0.157044E+04  0.143552E+04  0.128906E+04  0.113768E+04  0.990436E+03  0.857257E+03  0.746660E+03  0.663392E+03  0.607026E+03

0.189670E+00  0.143230E+05  0.384421E+04  0.207012E+01  0.219990E+00  0.402543E+03  0.598640E+03 -0.244845E-01  0.136963E+05
0.201046E+03  0.127285E+04  0.277007E+04  0.783397E-01  0.566920E-01  0.449770E+00  0.715092E+01  0.291681E+04  0.322391E+02
0.163015E+04  0.148664E+04  0.132806E+04  0.116760E+04  0.101127E+04  0.870461E+03  0.754196E+03  0.667199E+03  0.600654E+03

0.189770E+00  0.156533E+05  0.392921E+04  0.207536E+01  0.207092E+00  0.388631E+03  0.612936E+03 -0.262401E-01  0.146943E+05
0.200960E+03  0.134431E+04  0.205655E+04  0.810913E-01  0.570431E-01  0.410340E+00  0.721149E+01  0.295601E+04  0.336635E+02
0.169470E+04  0.153985E+04  0.137722E+04  0.120002E+04  0.103366E+04  0.884572E+03  0.762106E+03  0.671206E+03  0.610372E+03

0.189870E+00  0.171492E+05  0.401804E+04  0.207230E+01  0.196246E+00  0.373391E+03  0.626230E+03 -0.282070E-01  0.157731E+05
0.200877E+03  0.142330E+04  0.293932E+04  0.840692E-01  0.576147E-01  0.372379E+00  0.727363E+01  0.299676E+04  0.351916E+02
0.176469E+04  0.169848E+04  0.141999E+04  0.123491E+04  0.106771E+04  0.899669E+03  0.770691E+03  0.675427E+03  0.612169E+03

0.189970E+00  0.188204E+05  0.411055E+04  0.206915E+01  0.186664E+00  0.356659E+03  0.644633E+03 -0.306173E-01  0.169320E+05
0.200798E+03  0.151075E+04  0.302749E+04  0.872906E-01  0.579903E-01  0.338031E+00  0.733716E+01  0.303696E+04  0.368319E+02
0.184018E+04  0.166182E+04  0.146946E+04  0.127266E+04  0.109351E+04  0.915844E+03  0.779716E+03  0.679881E+03  0.614056E+03

0.190070E+00  0.207072E+05  0.420639E+04  0.206563E+01  0.174486E+00  0.338254E+03  0.662267E+03 -0.329078E-01  0.181689E+05
0.200723E+03  0.160773E+04  0.312120E+04  0.900071E-01  0.584049E-01  0.301484E+00  0.740249E+01  0.308244E+04  0.365925E+02
0.192146E+04  0.173013E+04  0.152391E+04  0.131317E+04  0.111161E+04  0.933192E+03  0.789347E+03  0.684588E+03  0.616037E+03

0.190170E+00  0.227967E+05  0.430496E+04  0.206181E+01  0.164477E+00  0.317982E+03  0.681269E+03 -0.357199E-01  0.194705E+05
0.200652E+03  0.171533E+04  0.322002E+04  0.946235E-01  0.590084E-01  0.260029E+00  0.746965E+01  0.312692E+04  0.404904E+02
0.200859E+04  0.180354E+04  0.158256E+04  0.135696E+04  0.114198E+04  0.951814E+03  0.799621E+03  0.689568E+03  0.618119E+03

0.190270E+00  0.250984E+05  0.440532E+04  0.205765E+01  0.155126E+00  0.295642E+03  0.701788E+03 -0.388992E-01  0.208180E+05
0.200585E+03  0.183463E+04  0.332600E+04  0.987772E-01  0.596309E-01  0.230352E+00  0.753879E+01  0.317198E+04  0.426012E+02
0.210140E+04  0.188206E+04  0.164563E+04  0.140400E+04  0.117389E+04  0.971816E+03  0.810595E+03  0.694845E+03  0.620308E+03

0.190370E+00  0.276979E+05  0.450607E+04  0.205313E+01  0.146803E+00  0.271039E+03  0.723991E+03 -0.424930E-01  0.221790E+05
0.200524E+03  0.196666E+04  0.343678E+04  0.103296E+00  0.600728E-01  0.210245E+00  0.761006E+01  0.321699E+04  0.446579E+02
0.219936E+04  0.196547E+04  0.171280E+04  0.148464E+04  0.120067E+04  0.993303E+03  0.822329E+03  0.700443E+03  0.622613E+03

0.190470E+00  0.302553E+05  0.460626E+04  0.204822E+01  0.138679E+00  0.243999E+03  0.748063E+03 -0.466623E-01  0.235095E+05
0.200469E+03  0.211218E+04  0.355231E+04  0.108204E+00  0.606310E-01  0.184742E+00  0.768364E+01  0.326111E+04  0.469494E+02
0.230148E+04  0.205321E+04  0.178417E+04  0.150867E+04  0.124600E+04  0.101630E+04  0.834685E+03  0.706390E+03  0.625041E+03

0.190570E+00  0.329968E+05  0.470029E+04  0.204291E+01  0.131731E+00  0.214402E+03  0.774157E+03 -0.511182E-01  0.247443E+05
0.200419E+03  0.227150E+04  0.367161E+04  0.113614E+00  0.612102E-01  0.162097E+00  0.775973E+01  0.330322E+04  0.493695E+02
0.240620E+04  0.214433E+04  0.185918E+04  0.156604E+04  0.126652E+04  0.104113E+04  0.848326E+03  0.712715E+03  0.627602E+03

0.190670E+00  0.357055E+05  0.470790E+04  0.203719E+01  0.125739E+00  0.182214E+03  0.802485E+03 -0.562237E-01  0.258054E+05
0.200376E+03  0.244424E+04  0.379310E+04  0.119229E+00  0.618092E-01  0.142666E+03  0.783053E+01  0.334196E+04  0.519038E+02
0.251125E+04  0.223733E+04  0.193703E+04  0.162645E+04  0.132642E+04  0.108784E+04  0.862716E+03  0.719447E+03  0.630304E+03

0.190770E+00  0.382197E+05  0.486455E+04  0.203109E+01  0.120701E+00  0.147533E+03  0.833207E+03 -0.618013E-01  0.266033E+05
0.200340E+03  0.262899E+04  0.391462E+04  0.128328E+00  0.624306E-01  0.126406E+00  0.792029E+01  0.337671E+04  0.545307E+02
0.261372E+04  0.233019E+04  0.201651E+04  0.168936E+04  0.137337E+04  0.109694E+04  0.878113E+03  0.726619E+03  0.633160E+03

0.190870E+00  0.403431E+05  0.492611E+04  0.202464E+01  0.116929E+00  0.110625E+03  0.866461E+03 -0.680729E-01  0.270490E+05
0.200312E+03  0.282312E+04  0.403352E+04  0.131707E+00  0.630763E-01  0.113860E+00  0.800525E+01  0.340281E+04  0.572187E+02
0.271013E+04  0.242035E+04  0.209600E+04  0.176396E+04  0.142049E+04  0.112601E+04  0.894567E+03  0.734263E+03  0.636181E+03

0.190970E+00  0.418715E+05  0.496879E+04  0.201793E+01  0.114243E+00  0.719476E+02  0.902341E+03 -0.747429E-01  0.270700E+05
0.200292E+03  0.302264E+04  0.414677E+04  0.138473E+00  0.637484E-01  0.105095E+00  0.809367E+01  0.342166E+04  0.599284E+02
0.279676E+04  0.250490E+04  0.217392E+04  0.181911E+04  0.146938E+04  0.118779E+04  0.912114E+03  0.742412E+03  0.639379E+03

0.191077E+00  0.426339E+05  0.499973E+04  0.201105E+01  0.112767E+00  0.321430E+02  0.940874E+03 -0.817951E-01  0.266791E+05
0.200280E+03  0.322236E+04  0.425135E+04  0.145346E+00  0.644497E-01  0.100282E+00  0.818580E+01  0.343101E+04  0.626140E+02
0.287016E+04  0.258090E+04  0.224685E+04  0.180348E+04  0.151932E+04  0.119112E+04  0.930767E+03  0.751096E+03  0.647765E+03

0.191177E+00  0.425359E+05  0.498733E+04  0.200413E+01  0.112520E+00 -0.801542E+01  0.982006E+03 -0.890965E-01  0.257323E+05
0.200277E+03  0.341643E+04  0.434458E+04  0.152267E+00  0.651792E-01 -0.994778E-01  0.828192E+01  0.343019E+04  0.652319E+02
0.292768E+04  0.264572E+04  0.231379E+04  0.194654E+04  0.156914E+04  0.122576E+04  0.950514E+03  0.760341E+03  0.646356E+03

0.191277E+00  0.415071E+05  0.496175E+04  0.199720E+01  0.113490E+00 -0.477146E+02  0.102560E+04 -0.964907E-01  0.244408E+05
0.200282E+03  0.359896E+04  0.442462E+04  0.159113E+00  0.659420E-01 -0.102668E+00  0.838227E+01  0.341924E+04  0.677369E+02
0.296788E+04  0.269749E+04  0.237238E+04  0.200375E+04  0.161939E+04  0.126134E+04  0.971306E+03  0.770168E+03  0.650162E+03

0.191377E+00  0.398900E+05  0.491479E+04  0.199062E+01  0.115674E+00 -0.861923E+02  0.107144E+04 -0.103016E+00  0.228494E+05
0.200296E+03  0.376484E+04  0.449015E+04  0.166760E+00  0.667390E-01 -0.109761E+00  0.848710E+01  0.339890E+04  0.700954E+02
0.299068E+04  0.273829E+04  0.242120E+04  0.205673E+04  0.166761E+04  0.129747E+04  0.993055E+03  0.780691E+03  0.554199E+03

0.191477E+00  0.376494E+05  0.484955E+04  0.199425E+01  0.118999E+00 -0.122820E+03  0.111925E+04 -0.110922E+00  0.210714E+05
0.200318E+03  0.391026E+04  0.454145E+04  0.172136E+00  0.678712E-01 -0.120958E+00  0.859662E+01  0.337046E+04  0.722835E+02
0.299728E+04  0.275924E+04  0.245974E+04  0.210339E+04  0.171330E+04  0.133364E+04  0.101563E+04  0.791611E+03  0.658478E+03

0.191577E+00  0.350461E+05  0.479094E+04  0.197261E+01  0.123408E+00 -0.157165E+03  0.116870E+04 -0.117603E+00  0.192172E+05
0.200340E+03  0.403299E+04  0.457910E+04  0.179149E+00  0.684006E-01 -0.134956E+00  0.871100E+01  0.333555E+04  0.742889E+02
0.298978E+04  0.277031E+04  0.248774E+04  0.214305E+04  0.175880E+04  0.136935E+04  0.103887E+04  0.803219E+03  0.663012E+03

0.191677E+00  0.322073E+05  0.467964E+04  0.197261E+01  0.128010E+00 -0.108940E+03  0.121945E+04 -0.124008E+00  0.171789E+05
0.200306E+03  0.413226E+04  0.460439E+04  0.183767E+00  0.693406E-01 -0.152601E+00  0.883039E+01  0.329584E+04  0.761099E+02
0.297071E+04  0.277009E+04  0.250684E+04  0.217848E+04  0.179451E+04  0.140410E+04  0.106257E+04  0.815392E+03  0.667810E+03

0.191777E+00  0.298222E+05  0.468260E+04  0.196739E+01  0.135160E+00 -0.218117E+03  0.127116E+04 -0.129032E+00  0.156734E+05
0.200427E+03  0.420866E+04  0.461898E+04  0.188974E+00  0.702946E-01 -0.173267E+00  0.895491E+01  0.325290E+04  0.774930E+02
0.294270E+04  0.276042E+04  0.251600E+04  0.220072E+04  0.182004E+04  0.143742E+04  0.108652E+04  0.826092E+03  0.672879E+03

0.191877E+00  0.268624E+05  0.448105E+04  0.196259E+01  0.142346E+00 -0.244707E+03  0.132350E+04 -0.135122E+00  0.139929E+05
0.200477E+03  0.426323E+04  0.462407E+04  0.193774E+00  0.712800E-01 -0.196695E+00  0.908464E+01  0.320000E+04  0.792207E+02
0.290817E+04  0.274322E+04  0.251644E+04  0.221927E+04  0.188008E+04  0.146892E+04  0.111047E+04  0.841269E+03  0.678225E+11
```

```
0.191977E+00  0.243766E+05  0.437989E+04  0.105817E+01  0.150304E+00 -0.268860E+03  0.137615E+04 -0.139862E+00  0.125083E+05
0.280631E+03  0.429011E+04  0.462157E+04  0.198185E+00  0.723065E-01  0.222633E+00  0.921961E+01  0.316246E+04  0.805371E+02
0.266910E+04  0.272026E+04  0.281141E+04  0.223170E+04  0.188406E+04  0.149832E+04  0.113420E+04  0.854858E+03  0.683R48E+03

0.192077E+00  0.220967E+05  0.427856E+04  0.195412E+01  0.158960E+00 -0.290726E+03  0.142885E+04 -0.144055E+00  0.111758E+05
0.280591E+03  0.431530E+04  0.461260E+04  0.202231E+00  0.733724E-01  0.250840E+00  0.935986E+01  0.311688E+04  0.817133E+02
0.282741E+04  0.269309E+04  0.260113E+04  0.223074E+04  0.190608E+04  0.152541E+04  0.118751E+04  0.868788E+03  0.689746E+03

0.192177E+00  0.200337E+05  0.417920E+04  0.195041E+01  0.168249E+00 -0.310536E+03  0.148135E+04 -0.147714E+00  0.999117E+04
0.280665E+03  0.431694E+04  0.459859E+04  0.205943E+00  0.744784E-01  0.281125E+00  0.950635E+01  0.307192E+04  0.827645E+02
0.278417E+04  0.266290E+04  0.248873E+04  0.224113E+04  0.192204E+04  0.165007E+04  0.118019E+04  0.882981E+03  0.695915E+03

0.192277E+00  0.181862E+05  0.408271E+04  0.194700E+01  0.178111E+00 -0.328488E+03  0.153344E+04 -0.150859E+00  0.894464E+04
0.280723E+03  0.430507E+04  0.458027E+04  0.209350E+00  0.756242E-01  0.313270E+00  0.965610E+01  0.302801E+04  0.837048E+02
0.274043E+04  0.263099E+04  0.246916E+04  0.223958E+04  0.193526E+04  0.157226E+04  0.120209E+04  0.897352E+03  0.702344E+03

0.192377E+00  0.165373E+05  0.398965E+04  0.194386E+01  0.188493E+00 -0.344777E+03  0.158494E+04 -0.153515E+00  0.802355E+04
0.280794E+03  0.428164E+04  0.456866E+04  0.212481E+00  0.768092E-01  0.347109E+00  0.981202E+01  0.298542E+04  0.845476E+02
0.269689E+04  0.259790E+04  0.244923E+04  0.223477E+04  0.194511E+04  0.159203E+04  0.122306E+04  0.911817E+03  0.709021E+03

0.192477E+00  0.150726E+05  0.390034E+04  0.194097E+01  0.199347E+00 -0.359585E+03  0.163568E+04 -0.155708E+00  0.721429E+04
0.280870E+03  0.424037E+04  0.453410E+04  0.215364E+00  0.780333E-01  0.382486E+00  0.997306E+01  0.294431E+04  0.853045E+02
0.265406E+04  0.256435E+04  0.242762E+04  0.222730E+04  0.195196E+04  0.160944E+04  0.124302E+04  0.926294E+03  0.715930E+03

0.192577E+00  0.137723E+05  0.381493E+04  0.193831E+01  0.210630E+00 -0.373080E+03  0.168556E+04 -0.157470E+00  0.650353E+04
0.280948E+03  0.420602E+04  0.450746E+04  0.218024E+00  0.792955E-01  0.419264E+00  0.101391E+02  0.290477E+04  0.659860E+02
0.261228E+04  0.253079E+04  0.240485E+04  0.221767E+04  0.195617E+04  0.162462E+04  0.126188E+04  0.940704E+03  0.723052E+03

0.192677E+00  0.126181E+05  0.373341E+04  0.193584E+01  0.222306E+00 -0.385407E+03  0.173445E+04 -0.158829E+00  0.587886E+04
0.281029E+03  0.415837E+04  0.447908E+04  0.220486E+00  0.805953E-01  0.457321E+00  0.103101E+02  0.286682E+04  0.866012E+02
0.257175E+04  0.249755E+04  0.238137E+04  0.220634E+04  0.195810E+04  0.163769E+04  0.127960E+04  0.954975E+03  0.730366E+03

0.192777E+00  0.116924E+05  0.365573E+04  0.193356E+01  0.234340E+00 -0.396699E+03  0.178227E+04 -0.159814E+00  0.53251E+04
0.281112E+03  0.410422E+04  0.444935E+04  0.222767E+00  0.819318E-01  0.496547E+00  0.104860E+02  0.283046E+04  0.871582E+02
0.253261E+04  0.246487E+04  0.235750E+04  0.219368E+04  0.195806E+04  0.164882E+04  0.129617E+04  0.969040E+03  0.737851E+03

0.192877E+00  0.106796E+05  0.358177E+04  0.193143E+01  0.246704E+00 -0.407069E+03  0.182896E+04 -0.160456E+00  0.404434E+04
0.281198E+03  0.404544E+04  0.441656E+04  0.224888E+00  0.833042E-01  0.536846E+00  0.106665E+02  0.279565E+04  0.876630E+02
0.249493E+04  0.243293E+04  0.233350E+04  0.218000E+04  0.195633E+04  0.165816E+04  0.131158E+04  0.982841E+03  0.745482E+03

0.192977E+00  0.986559E+04  0.351136E+04  0.192945E+01  0.259371E+00 -0.416619E+03  0.187445E+04 -0.160782E+00  0.441585E+04
0.281786E+03  0.398293E+04  0.43R696E+04  0.226865E+00  0.847117E-01  0.578132E+00  0.108517E+02  0.276233E+04  0.881242E+02
0.245872E+04  0.240183E+04  0.230958E+04  0.216557E+04  0.195316E+04  0.166586E+04  0.132584E+04  0.996328E+03  0.753235E+03

0.193077E+00  0.913791E+04  0.344434E+04  0.192760E+01  0.272317E+00 -0.425436E+03  0.191870E+04 -0.160821E+00  0.403621E+04
0.281377E+03  0.391750E+04  0.435476E+04  0.228711E+00  0.861533E-01  0.620328E+00  0.110414E+02  0.273045E+04  0.885445E+02
0.242397E+04  0.237165E+04  0.228588E+04  0.215060E+04  0.194878E+04  0.167208E+04  0.133899E+04  0.100946E+04  0.761082E+03

0.193177E+00  0.848578E+04  0.338052E+04  0.192587E+01  0.285521E+00 -0.433597E+03  0.196169E+04 -0.160598E+00  0.369834E+04
0.281469E+03  0.384981E+04  0.432212E+04  0.230440E+00  0.876281E-01  0.663366E+00  0.112354E+02  0.269993E+04  0.889292E+02
0.239066E+04  0.234241E+04  0.226251E+04  0.213526E+04  0.194339E+04  0.167696E+04  0.135107E+04  0.102220E+04  0.76900.E+03

0.193277E+00  0.789662E+04  0.331936E+04  0.192374E+01  0.298964E+00 -0.441170E+03  0.200344E+04 -0.160495E+00  0.341467E+04
0.281562E+03  0.378967E+04  0.428981E+04  0.232565E+00  0.891350E-01  0.707184E+00  0.114337E+02  0.258434E+04  0.89282.9E+02
0.235894E+04  0.231421E+04  0.223958E+04  0.211970E+04  0.193714E+04  0.168063E+04  0.136211E+04  0.103452E+04  0.776978E+03

0.193376E+00  0.736591E+04  0.326104E+04  0.192168E+01  0.312630E+00 -0.448211E+03  0.204402E+04 -0.160233E+00  0.3153/3E+04
0.281658E+03  0.372826E+04  0.425723E+04  0.234617E+00  0.906733E-01  0.751728E+00  0.116360E+02  0.244290E+04  0.896098E+02
0.232864E+04  0.228711E+04  0.221721E+04  0.210405E+04  0.193020E+04  0.168323E+04  0.137216E+04  0.104640E+04  0.784974E+03

0.193476E+00  0.688697E+04  0.320547E+04  0.191982E+01  0.326503E+00 -0.454772E+03  0.208340E+04 -0.159690E+00  0.290822E+04
0.281755E+03  0.366381E+04  0.422438E+04  0.236477E+00  0.922419E-01  0.796946E+00  0.118424E+02  0.230424E+04  0.899115E+02
0.229946E+04  0.226090E+04  0.219538E+04  0.208841E+04  0.192270E+04  0.168486E+04  0.138129E+04  0.105782E+04  0.792973E+03

0.193576E+00  0.645380E+04  0.315248E+04  0.191813E+01  0.340540E+00 -0.460900E+03  0.212154E+04 -0.158898E+00  0.267720E+04
0.281053E+03  0.369704E+04  0.419141E+04  0.238162E+00  0.938399E-01  0.842794E+00  0.120527E+02  0.216788E+04  0.901895E+02
0.227125E+04  0.223549E+04  0.217404E+04  0.207284E+04  0.191475E+04  0.168565E+04  0.138953E+04  0.106878E+04  0.800955E+03

0.193676E+00  0.606088E+04  0.310190E+04  0.191660E+01  0.354816E+00 -0.466635E+03  0.215843E+04 -0.157884E+00  0.245958E+04
0.281952E+03  0.352854E+04  0.415840E+04  0.239685E+00  0.954666E-01  0.889231E+00  0.122667E+02  0.203335E+04  0.904450E+02
0.224391E+04  0.221077E+04  0.215314E+04  0.205734E+04  0.190642E+04  0.168567E+04  0.139696E+04  0.107928E+04  0.008900E+03

0.193776E+00  0.570352E+04  0.305357E+04  0.191522E+01  0.369232E+00 -0.472015E+03  0.219406E+04 -0.156673E+00  0.225409E+04
0.282054E+03  0.348804E+04  0.412548E+04  0.241058E+00  0.971207E-01  0.936219E+00  0.124843E+02  0.190006E+04  0.906799E+02
0.221736E+04  0.218671E+04  0.213267E+04  0.204194E+04  0.189778E+04  0.168502E+04  0.140361E+04  0.108930E+04  0.816791E+03

0.193876E+00  0.537765E+04  0.300736E+04  0.191398E+01  0.383807E+00 -0.477070E+03  0.222843E+04 -0.155290E+00  0.20593E+04
0.282186E+03  0.338837E+04  0.409271E+04  0.242294E+00  0.988015E-01  0.983727E+00  0.127054E+02  0.176738E+04  0.908941E+02
0.219155E+04  0.216324E+04  0.211258E+04  0.202664E+04  0.188889E+04  0.168377E+04  0.140954E+04  0.109686E+04  0.824609E+03

0.193976E+00  0.507979E+04  0.296312E+04  0.191287E+01  0.398531E+00 -0.481829E+03  0.226155E+04 -0.153756E+00  0.187412E+04
0.282269E+03  0.331760E+04  0.406014E+04  0.243400E+00  0.100608E+00  0.103172E+01  0.129299E+02  0.163458E+04  0.910897E+02
0.216640E+04  0.214031E+04  0.209286E+04  0.201145E+04  0.187977E+04  0.168199E+04  0.141481E+04  0.110796E+04  0.832342E+03

0.194076E+00  0.480686E+04  0.292075E+04  0.191188E+01  0.413395E+00 -0.486317E+03  0.229341E+04 -0.152092E+00  0.169673E+04
0.282362E+03  0.324653E+04  0.402793E+04  0.244386E+00  0.102239E+00  0.108017E+01  0.131577E+02  0.150074E+04  0.912672E+02
0.214186E+04  0.211789E+04  0.207349E+04  0.199637E+04  0.187048E+04  0.167971E+04  0.141944E+04  0.111660E+04  0.839974E+03

0.194176E+00  0.455620E+04  0.288012E+04  0.191100E+01  0.428393E+00 -0.490557E+03  0.232404E+04 -0.150313E+00  0.152552E+04
0.282468E+03  0.317573E+04  0.399503E+04  0.245258E+00  0.103994E+00  0.112905E+01  0.133886E+02  0.136467E+04  0.914273E+02
0.211705E+04  0.209893E+04  0.205444E+04  0.198141E+04  0.186102E+04  0.167701E+04  0.142349E+04  0.112481E+04  0.847495E+03

0.194276E+00  0.432550E+04  0.284113E+04  0.191024E+01  0.443516E+00 -0.494569E+03  0.235346E+04 -0.148438E+00  0.13583E+04
0.282602E+03  0.303540E+04  0.393205E+04  0.246677E+00  0.107571E+00  0.122803E+01  0.138592E+02  0.107866E+04  0.916972E+02
0.207113E+04  0.205314E+04  0.201716E+04  0.195180E+04  0.184173E+04  0.167044E+04  0.142999E+04  0.113993E+04  0.862159E+03

0.194476E+00  0.391604E+04  0.276770E+04  0.190902E+01  0.474114E+00 -0.501977E+03  0.240870E+04 -0.144448E+00  0.102370E+04
0.282790E+03  0.296616E+04  0.390193E+04  0.247230E+00  0.109392E+00  0.127808E+01  0.140987E+02  0.922470E+03  0.910007E+02
0.204020E+04  0.203217E+04  0.199886E+04  0.193714E+04  0.183192E+04  0.166665E+04  0.143252E+04  0.114688E+04  0.869287E+03

0.194576E+00  0.373394E+04  0.273300E+04  0.190857E+01  0.489577E+00 -0.505404E+03  0.243457E+04 -0.142355E+00  0.844188E+03
0.282699E+03  0.289763E+04  0.367141E+04  0.247678E+00  0.111232E+00  0.132848E+01  0.143409E+02  0.749041E+03  0.918997E+02
0.702532E+04  0.201133E+04  0.198069E+04  0.192263E+04  0.182201E+04  0.166257E+04  0.143459E+04  0.116343E+04  0.876769E+03
```

84

APPENDIX II

ISENTROPIC EQUILIBRIUM COMBUSTION CODE

Adiabatic Compression Program

An existing equilibrium combustion program has been modified to calculate the properties of a gas mixture at various points on an isentrope. The program uses a list of thermal properties of possible constituents of the mixture. The program writes output containing the composition and thermal properties of the gas mixture at the input pressures.

Input to the program consists of "REACTANT" cards specifying the composition at the initial point on the isentrope and a namelist, "&INPT2," which specifies the temperature and pressure at the initial point and a schedule of other pressures (up to 26 pressures including the initial value). OMIT cards may be used if desired to exclude certain species from consideration as mixture constituents.

The program operates as follows:

(1)   The initial mixture as specified by the reactant cards and the mixture ratio specified by &INPT2 is analyzed to determine which chemical elements are present. The number of gram-atoms of each element is calculated as well as the mixture molecular weight and mixture total enthalpy (Subroutine REAC).

(2)   The taped thermal data is searched (SEARCH) and the names and thermal properties of possible compounds which could be formed from the available atoms are extracted. This list is then compared to the OMIT cards and the net list of species to be considered is printed.

(3)   Subroutine EQLBRM then varies the composition seeking to minimize the Gibbs free energy of the mixture subject to the constraint that the numbers of atoms of the different elements do not vary.

In this process, species with molefractions of less than 10^{-7} at any iteration are dropped from consideration. Occasionally, the constraint equations

$$\Sigma_j \ a_{ij} \ n_j = b_i$$

where a_{ij} is the number of atoms of type i in species j, become linearly dependent. In this case, the program will print the message "SINGULAR MATRIX" and then calculate the thermal properties of the input mixture at the specified pressure and temperature (Subroutine HCALC). Sometimes the mixture free energy will have a very broad minimum or will possess two minima

85
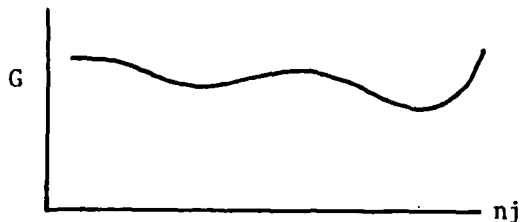
as in the sketch. If this is the situation, the program will print the message

> "35 ITERATIONS DID NOT SATISFY CONVERGENCE REQUIREMENTS FOR THE POINT _____"

and then calculate the thermal properties of the input mixture.

(4)   One way or the other, the program will obtain the entropy at point #1. This entropy will then be held constant (SP=.TRUE.). EQLBRM will calculate the equilibrium composition at an estimated temperature and the new pressure, calculate the mixture entropy, and compare it to the entropy at point #1. If the two entropies do not agree, the temperature estimate is changed and a new equilibrium calculated.

(5)   If, at any point, the equilibrium calculation fails, the control program THERMP will call subroutine FRØZEN to obtain the thermal properties corresponding to the fixed entropy, the new pressure and the composition at the previous point.

(6)   After 13 points have been calculated, the program will print the results. Then it will complete and output the remainder of the pressure schedule.

(7)   After completing the pressure schedule, the program will look for a new mixture ratio MIX.

```
REACTANTS
AR  1.0...      0.0         0.0         0.0      00  0.0        0.5460  M      0.0   G    298.150  F    0.0
N   2.0000      0.0         0.0         0.0      00  0.0        0.4560  M      0.0   G    298.150  F    0.0
OMIT    C(S)
NAMELISTS
&INPT2
KASE=       2,T= 300.000000   .    .0              .    .0              .    .0              .    .0              .    .0
    .0          .    .0              .    .0              .    .0              .    .0              .    .0
    .0          .    .0              .    .0              .    .0              .    .0              .    .0
    .0          .    .0              .    .0              .    .0              .    .0              .    .0
    .0          .    .0              .    .0              .    .0              .    .0              .    .0
    .0          .    .0              .    .0              .    .0         .P= 14.6999998    .    25.0000000   .    45.0000000   .
134.000000  .   446.000000  .   1340.00000  .   2233.00000  .   4466.00000  .   6699.00000  .   8932.00000  .
11165.0000  .   13398.0000  .   15631.0000  .   17864.0000  .   20097.0000  .   22330.0000  .   24563.0000  .
26796.0000  .   29029.0000  .   31262.0000  .   33495.0000  .   35728.0000  .   37961.0000  .   40194.0000  .
42427.0000  .   44660.0000  ,PSIA=T,MMHG=F,NSQM=F,V=   .0   .    .0   .    .0   .    .0   .
    .0          .    .0              .    .0              .    .0              .    .0              .    .0
    .0          .    .0         ,RHO=  14.6999998    .    25.0000000   .    45.0000000   .    134.000000   .    446.000000   .
1340.00000  .   2233.00000  .   4466.00000  .   6699.00000  .   8932.00000  .   11165.0000  .   13398.0000  .
15631.0000  .   17864.0000  .   20097.0000  .   22330.0000  .   24563.0000  .   26796.0000  .   29029.0000  .
31262.0000  .   33495.0000  .   35728.0000  .   37961.0000  .   40194.0000  .   42427.0000  .   44660.0000  .ERATIO=F,OF=
..FPCT=F,FA=F,MIX=   .0          .    .0              .    .0              .    .0              .    .0
    .0          .    .0              .    .0              .    .0              .    .0              .    .0
    .0          .    .0         ,TP=T,HP=F,SP=F,TV=F,UV=F,SV=F,RKT=T,SHOCK=F,DETH=F,OTTO=F,CR=   .0         ,SO=   .0
SO=    .0         ,IONS=F,IDEBUG=        0,TRACE=   .0         ,SIUNIT=F,EUNITS=F,TRNSPT=F,FROZN=F,PUNCH=F,NODATA=F,DIF=F
&END

NO INPT2 VALUE GIVEN FOR OF, EQRAT, FA, OR FPCT

SPECIES BEING CONSIDERED IN THIS SYSTEM
  L 5/66  AR              J 3/77  N              J 3/77  N2              J12/70  N3

OF =   0  0
                    EFFECTIVE FUEL       EFFECTIVE OXIDANT        MIXTURE
ENTHALPY               HPP(2)                 HPP(1)               HSUB0
(KG-MOL)(D G K)/KG     0.0                    0.0                  0.0

KG-ATOMS/K,            BOP(I,2)               BOP(I,1)             BO(I)
    AR             0.15788972E-01             0.0              0.15788972E-01
    N              0.26363246E-01             0.0              0.26363246E-01

PT      AR       N
 1   -19.217  -11.910   11.000
 2   -18.699  -11.646    1.000
 3   -18.223  -11.438    1.000
 4   -17.561  -11.196    2.000
 5   -16.955  -11.023    2.000
 6   -16.485  -10.942    2.000
 7   -16.285  -10.924    2.000
 8   -16.025  -10.916    2.000
 9   -15.877  -10.916    1.000
10   -15.776  -10.923    1.000
11   -15.699  -10.929    1.000
12   -15.636  -10.936    1.000
13   -15.584  -10.942    1.000


                    THERMODYNAMIC EQUILIBRIUM PROPERTIES AT ASSIGNED

                              ENTROPY AND PRESSURE

CASE NO.      2                                                    MOLES      ENERGY    STATE    TEMP      DENSITY
                                                                              CAL/MOL            DEG K     G/CC
        CHEMICAL FORMULA
FUEL    AR 1.00000                                                 0.54500     0.0       G      298.15     0.0
FUEL    N  2.00000                                                 0.45500     0.0       G      298.15     0.0

        O/F=  0.0        PERCENT FUEL=100.0000    EQUIVALENCE RATIO=  0.0      REACTANT DENSITY=  0.0


THERMODYNAMIC PROPERTIES


P, ATM        1.0003   1.7011   3.0621   9.1181   30.340   91.181   151.95   303.89   455.84   607.78   759.73   911.68   1063.62
T, DEG K       300      369      430      631      933      1318     1842     1902     2149     2341     2501     2640     2764
RHO, G/CC   1.4026-3 1.9932-3 2.9414-3 6.0027-3 1.3688-2 2.9106-2 4.1456-2 6.7204-2 8.9227-2 1.0921-1 1.2777-1 1.4625-1 1.6190-1
H, CAL/G       0.3     10.4     23.8     57.0     110.5    181.1    223.1    291.6    339.0    376.0    407.1    434.0    458.0
S, CAL/(G)(K)  1.2279   1.2279   1.2280   1.2279   1.2279   1.2279   1.2279   1.2279   1.2280   1.2280   1.2279   1.2279   1.2279

M, MOL WT      34.518   34.518   34.518   34.518   34.518   34.518   34.518   34.518   34.518   34.518   34.518   34.518   34.518
(DLV/DLP)T    -1.00000 -1.00000 -1.00000 -1.00000 -1.00000 -1.00000 -1.00000 -1.00000 -1.00000 -1.00000 -1.00000 -1.00000 -1.00000
(DLV/DLT)P     1.0000   1.0000   1.0000   1.0000   1.0000   1.0000   1.0000   1.0000   1.0000   1.0000   1.0000   1.0000   1.0000
CP, CAL/(G)(K) 0.1702   0.1703   0.1709   0.1739   0.1802   0.1861   0.1885   0.1913   0.1926   0.1934   0.1939   0.1943   0.1946
GAMMA (S)      1.5111   1.5106   1.5080   1.4949   1.4694   1.4479   1.4396   1.4305   1.4263   1.4239   1.4223   1.4211   1.4202
SON VEL,M/SEC  330.4    361.4    398.8    476.5    574.5    678.0    731.2    809.6    859.3    896.0    925.7    950.7    972.3


MOLE FRACTIONS


AR      0.54500  0.54500  0.54500  0.54500  0.54500  0.54500  0.54500  0.54500  0.54500  0.54500  0.54500  0.54500  0.54500
N2      0.45500  0.45500  0.45500  0.45500  0.45500  0.45500  0.45500  0.45500  0.45500  0.45500  0.45500  0.45500  0.45500

ADDITIONAL PRODUCTS WHICH WERE CONSIDERED BUT WHOSE MOLE FRACTIONS WERE LESS THAN  0.50000E-05 FOR ALL ASSIGNED CONDITIONS

    N          N3
```

```
PT   ...      N
 1  -15.539  -10.948  7.000
 2  -15.499  -10.953  1.000
 3  -15.463  -10.958  1.000
 4  -15.432  -10.963  1.000
 5  -15.403  -10.968  1.000
 6  -15.376  -10.973  1.000
 7  -15.352  -10.977  1.000
 8  -15.329  -10.981  2.000
 9  -15.308  -10.985  1.000
10  -15.288  -10.989  1.000
11  -15.269  -10.993  1.000
12  -15.252  -10.996  1.000
13  -15.235  -11.000  1.000
```

THERMODYNAMIC EQUILIBRIUM PROPERTIES AT ASSIGNED

ENTROPY AND PRESSURE

CASE NO.   2

	CHEMICAL FORMULA	MOLES	ENERGY CAL/MOL	STATE	TEMP DEG K	DENSITY G/CC
FUEL	AR 1.00000	0.54500	0.0	G	298.15	0.0
FUEL	N 2.00000	0.45500	0.0	G	298.15	0.0

O/F= 0.0   PERCENT FUEL=100.0000   EQUIVALENCE RATIO= 0.0   REACTANT DENSITY= 0.0

THERMODYNAMIC PROPERTIES

```
P, ATM          1215.57  1367.51  1519.46  1671.41  1823.36  1975.30  2127.24  2279.19  2431.14  2583.08  2735.03  2886.97  3038.92
T, DEG K           2875     2977     3070     3158     3240     3317     3390     3460     3526     3589     3650     3708     3765
RHO, G/CC       1.7768-1 1.9327-1 2.0817-1 2.2264-1 2.3674-1 2.5049-1 2.6394-1 2.7712-1 2.9004-1 3.0273-1 3.1521-1 3.2749-1 3.3950-1
H, CAL/G           479.6    499.6    517.8    534.9    550.9    566.0    580.3    593.9    606.9    619.3    631.3    642.7    653.7
S, CAL/(G)(K)     1.2279   1.2279   1.2279   1.2279   1.2279   1.2279   1.2279   1.2279   1.2279   1.2279   1.2279   1.2279   1.2279

M, MOL WT         34.518   34.518   34.518   34.518   34.518   34.518   34.518   34.518   34.518   34.518   34.518   34.518   34.518
(DLV/DLP)T       -1.00000 -1.00000 -1.00000 -1.00000 -1.00000 -1.00000 -1.00000 -1.00001 -1.00000 -1.00000 -1.00000 -1.00000 -1.00000
(DLV/DLT)P        1.0000   1.0000   1.0000   1.0000   1.0000   1.0000   1.0000   1.0000   1.0000   1.0000   1.0000   1.0001   1.0001
CP, CAL/(G)(K)    0.1948   0.1950   0.1952   0.1954   0.1955   0.1956   0.1958   0.1959   0.1960   0.1961   0.1963   0.1964   0.1965
GAMMA (S)         1.4194   1.4188   1.4183   1.4178   1.4174   1.4169   1.4166   1.4162   1.4158   1.4155   1.4152   1.4148   1.4145
SON VEL,M/SEC      991.4   1008.6   1024.2   1038.5   1051.7   1064.0   1075.5   1086.4   1096.6   1106.2   1115.4   1124.2   1132.5
```

MOLE FRACTIONS

```
AR   0.54500  0.54500  0.54500  0.54500  0.54500  0.54500  0.54500  0.54500  0.54500  0.54500  0.54500  0.54500  0.54500
N    0.00000  0.00000  0.00000  0.00000  0.00000  0.00000  0.00000  0.00000  0.00000  0.00000  0.00001  0.00001  0.00001
N2   0.45500  0.45500  0.45500  0.45500  0.45500  0.45500  0.45500  0.45500  0.45500  0.45500  0.45500  0.45500  0.45499
```

ADDITIONAL PRODUCTS WHICH WERE CONSIDERED BUT WHOSE MOLE FRACTIONS WERE LESS THAN 0.50000E-05 FOR ALL ASSIGNED CONDITIONS

N3

DISTRIBUTION LIST

No. of Copies	Organization	No. of Copies	Organization
2	Commander Defense Technical Info Center ATTN: DDC-DDA Cameron Station Alexandria, VA 22314	5	Commander US Army Armament Research & Development Command ATTN: FC & SCWSL, D. Gyorog H. Kahn B. Brodman S. Cytron T. Hung Dover, NJ 07801
1	Director of Defense Research & Engineering ATTN: R. Thorkildsen The Pentagon Washington, DC 20301		
1	Defense Advanced Research Projects Agency ATTN: Dir, Materials Div 1400 Wilson Boulevard Arlington, VA 22209	6	Commander US Army Armament Research & Development Command ATTN: DRDAR-LC, J. Frasier H. Fair J. Lannon A. Bracuti A. Moss R. Walker Dover, NJ 07801
1	HQDA (DAMA-ARZ) Washington, DC 20301		
1	HQDA (DAMA-CSM) Washington, DC 20301	6	Commander US Army Armament Research & Development Command ATTN: DRDAR-LC, J. Picard D. Costa E. Barrieres R. Corn K. Rubin J. Houle Dover, NJ 07801
1	HQDA (DAMA-WSW) Washington, DC 20301		
1	Commander US Army Materiel Development & Readiness Command ATTN: DRCDMD-ST 5001 Eisenhower Avenue Alexandria, VA 22333		
2	Commander US Army Armament Research & Development Command ATTN: DRDAR-TSS (2 cys) Dover, NJ 07801	5	Commander US Army Armament Research & Development Command ATTN: DRDAR-LC, D. Katz E. Wurzel K. Russell D. Downs R.L. Trask Dover, NJ 07801
1	Commander US Army Armament Research & Development Command ATTN: DRDAR-QA, J.Rutkowski Dover, NJ 07801		

DISTRIBUTION LIST

No. of Copies	Organization	No. of Copies	Organization
4	Director US Army ARRADCOM Benet Weapons Laboratory ATTN: I. Ahmad 　　　T. Davidson 　　　J. Zweig 　　　G. Friar Watervliet, NY 12189	1	Commander Applied Technology Laboratory US Army Research & Technology 　　Laboratories (AVRADCOM) ATTN: R.A. Langsworthy Fort Eustis, VA 23604
5	Director US Army ARRADCOM Benet Weapons Laboratory ATTN: J. Busuttil 　　　W. Austin 　　　R. Montgomery 　　　R. Billington 　　　J. Santini Watervliet, NY 12189	1	Commander US Army Communications Research 　& Development Command ATTN: DRDCO-PPA-SA Fort Monmouth, NJ 07703
		1	Commander US Army Electronics Research 　& Development Command Technical Support Activity ATTN: DELSD-L Fort Monmouth, NJ 07703
1	Director US Army ARRADCOM Benet Weapons Laboratory ATTN: DRDAR-LCB-TL Watervliet, NY 12189	2	Commander US Army Missile Command ATTN: DRDMI-R 　　　DRDMI-YDL Redstone Arsenal, AL 35809
1	Commander US Army Armament Materiel 　Readiness Command ATTN: DRSAR-LEP-L, Tech Lib Rock Island, IL 61299	1	Commander US Army Tank Automotive Research 　& Development Command ATTN: DRDTA-UL Warren, MI 48090
1	Commander US Army Aviation Research 　& Development Command ATTN: DRSAV-E P.O. Box 209 St. Louis, MO 63166	1	Project Manager Cannon Artillery Weapons Systems ATTN: DRCPM-CAW US Army Armament Research & 　Development Command Dover, NJ 07801
1	Director US Army Air Mobility Research 　& Development Laboratory Ames Research Center Moffett Field, CA 94035	1	Project Manager - XM1 Tank Main Armament Dev Div Dover, NJ 07801
		1	Project Manager - ARGADS Dover, NJ 07801

90

DISTRIBUTION LIST

No. of Copies	Organization	No. of Copies	Organization
1	Project Manager, M60 Tanks US Army Tank & Automotive Cmd 28150 Dequindre Road Warren, MI 48090	1	Commander US Army Armor Center ATTN: ATZK-XM1 Fort Knox, KY 40121
1	Project Manager - XM1 Tank US Army Tank&Automotive Cmd 28150 Dequindre Road Warren, MI 48090	1	President US Army Maintenance Mgmt Ctr Lexington, KY 40507
2	Project Manager - M110E2 ATTN: J. Turkeltaub S. Smith Rock Island, IL 61299	1	President US Army Armor & Engineer Bd Fort Knox, KY 40121
2	Director US Army Materials & Mechanics Research Center ATTN: J.W. Johnson K. Shepard Watertown, MA 02172	1	Commander US Army Field Artillery School ATTN: J. Porter Fort Sill, OK 73503
3	Director US Army Research Office ATTN: P. Parrish E. Saibel D. Squire P.O. Box 12211 Research Triangle Park, NC 27709	5	Commander Naval Surface Weapons Center ATTN: M. Shamblen J. O'Brasky C. Smith L. Russell T.W. Smith Dahlgren, VA 22448
1	Director US Army TRADOC Systems Analysis Activity ATTN: ATAA-SL, Tech Lib White Sands Missile Range NM 88002	2	Commander Naval Ordnance Station ATTN: L. Dickinson S. Mitchell Indian Head, MD 20640
1	Commander US Army Air Defense Center ATTN: ATSA-SM-L Fort Bliss, TX 79916	1	Commander Naval Ordnance Station Louisville ATTN: F. Blume Louisville, KY 40202
		1	AFOSR/NA ATTN: L. Caveny, Bldg 410
		1	AFATL (D. Uhrig) Eglin AFB, FL 32542

DISTRIBUTION LIST

No. of Copies	Organization	No. of Copies	Organization
1	Lawrence Livermore Laboratory ATTN: J. Kury P.O. Box 808 Livermore, CA 94550	1	Purdue University School of Mechanical Engineering ATTN: J.R. Osborn W. Lafayette, IN 47909
1	National Bureau of Standards Materials Division ATTN: A.W. Ruff Washington, DC 20234	1	SRI International Materials Research Center 333 Ravenswood Avenue Menlo Park, CA 94025
1	National Science Foundation Materials Division Washington, DC 20550	1	University of Illinois Dept of Aeronautics and Aerospace Engineering ATTN: H. Krier Urbana, IL 61803

1   Battelle Columbus Laboratory
      ATTN: G. Wolken
      505 King Avenue
      Columbus, OH 43201

Aberdeen Proving Ground

2   Calspan Corporation
      ATTN: E.B. Fisher
          C.C. Morphy
      P.O. Box 400
      Buffalo, NY 14225

Dir, USAMSAA
   ATTN: DRXSY-D
         DRXSY-MP, H. Cohen
         D. Barnhardt, RAM Div
         G. Alexander, RAM Div
         Air Warfare Div
         Ground Warfare Div
         RAM Division

2   Calspan Corporation
      ATTN: G. Sterbutzel
          F. Vassallo
      P.O. Box 235
      Buffalo, NY 14221

Cdr, USATECOM
   ATTN: DRSTE-FA
         DRSTE-AR
         DRSTE-AD
         DRSTE-TO-F

1   Director
      Chemical Propulsion Info Agcy
      Johns Hopkins University
      ATTN: T. Christian
      Johns Hopkins Road
      Laurel, MD 20810

Dir, USAMTD, Bldg 400
   ATTN: D. Tag,
         H. Graves
         C. Lavery
         L. Barnhard
         K. Jones
         R. Moody, Bldg 525

2   Princeton University
      Forrestal Campus Library
      ATTN: Tech Lib
         B. Royce
      P.O. Box 710
      Princeton, NJ 08540

Dir, Wpns Sys Concepts Team
   Bldg E3516, EA
   ATTN: DRDAR-ACW

USER EVALUATION OF REPORT

Please take a few minutes to answer the questions below; tear out this sheet and return it to Director, US Army Ballistic Research Laboratory, ARRADCOM, ATTN: DRDAR-TSB, Aberdeen Proving Ground, Maryland 21005. Your comments will provide us with information for improving future reports.

1. BRL Report Number_____

2. Does this report satisfy a need? (Comment on purpose, related project, or other area of interest for which report will be used.)

_____

_____

_____

3. How, specifically, is the report being used? (Information source, design data or procedure, management procedure, source of ideas, etc.)_____

_____

_____

4. Has the information in this report led to any quantitative savings as far as man-hours/contract dollars saved, operating costs avoided, efficiencies achieved, etc.? If so, please elaborate.

_____

_____

5. General Comments (Indicate what you think should be changed to make this report and future reports of this type more responsive to your needs, more usable, improve readability, etc.)_____

_____

_____

_____

6. If you would like to be contacted by the personnel who prepared this report to raise specific questions or discuss the topic, please fill in the following information.

Name:_____

Telephone Number:_____

Organization Address:_____

_____

_____